# C1 Chemistry for the Production of Ultra-Clean Liquid Transportation Fuels and Hydrogen

**Consortium for Fossil Fuel Science**
University of Kentucky
West Virginia University
University of Pittsburgh
University of Utah
Auburn University

*Consortium for
Fossil Fuel
Science*

**C1 Chemistry for Production of Ultra-Clean Liquid Transportation Fuels and Hydrogen**

U.S. Department of Energy (Fossil Energy) Contract No. DE-FC26-02NT41594

***Contact:*** Gerald P. Huffman, Director, Consortium for Fossil Fuel Science, University of Kentucky, Suite 107 Whalen Building, 533 S. Limestone St., Lexington, KY 40506-0043
(859) 257-4027; FAX: (859)257-7215; **huffman@engr.uky.edu**

# Abstract

Faculty and students from five universities – the University of Kentucky, University of Pittsburgh, University of Utah, West Virginia University, and Auburn University - are collaborating in a research program to develop C1 chemistry processes to produce ultra-clean liquid transportation fuels and hydrogen, the zero-emissions transportation fuel of the future. The feedstocks contain one carbon atom per molecular unit. They include synthesis gas (syngas), a mixture of carbon monoxide and hydrogen produced by coal gasification or reforming of natural gas, methane, methanol, carbon dioxide, and carbon monoxide. An important objective is to develop C1 technology for the production of liquid transportation fuel and hydrogen from domestically plentiful resources such as coal, coalbed methane, and natural gas. An Industrial Advisory Board with representatives from Chevron-Texaco, Eastman Chemical, Conoco-Phillips, the Air Force Research Laboratory, the U.S. Army National Automotive Center (Tank & Automotive Command – TACOM), and Tier Associates provides guidance on the practicality of the research. The current report presents results obtained in this research program during the six months of the subject contract from October 1, 2002 through March 31, 2003. The results are presented in thirteen detailed reports on research projects headed by various faculty members at each of the five CFFS Universities. Additionally, an Executive Summary has been prepared that summarizes the principal results of all of these projects during the six-month reporting period.

# Table of Contents

# Executive Summary

Prepared by Gerald P. Huffman, Director, Consortium for Fossil Fuel Science
(859) 257-4027; huffman@engr.uky.edu

## Introduction

The Consortium for Fossil Fuel Science (CFFS), a five university research consortium, is conducting a program of basic research aimed at developing innovative and economical technology for producing clean liquid transportation fuels and hydrogen from coal, natural gas, and other hydrocarbons by C1 chemistry. The research program is made up of thirteen separate but coordinated research projects being conducted at the five CFFS universities, all contributing towards achieving the goal of producing clean, economical transportation fuel from domestic resources. The current report briefly summarizes progress made toward those goals during the first six months of the second year of this research contract. This Executive Summary briefly summarizes the principal results obtained during this period. The appended individual project reports provide more details and contain all the required elements of DOE research contract reports: an introduction, experimental procedures, results and discussion, conclusions, and references. Lists of all publications and presentations resulting from this research contract during this period are also given in these project reports.

## Results

### Liquid fuels

There are active interactions between the components of hybrid catalysts consisting of Pt-promoted tungstated zirconia and sulfated zirconia (PtWZr/SZr) in converting a long-chain paraffin. Using PtWZr/SZr hybrid catalysts, an appropriate balance of hydroisomerization and hydrocracking functions can be achieved to significantly increase yields of middle distillates, including jet and diesel fuels. The component ratio of hybrid catalysts affects the Pt dispersions and surface areas, which may relate to catalytic performance. $H_2$ pressure is an important factor in affecting the reactivities and selectivities of the hybrid catalyst systems.

Acetylene is incorporated into Fischer-Tropsch (F-T) reactions much more effectively than are higher acetylenes, consistent with the reported special role of $C_2$ species in chain initiation. Acetylene initiates F-T more readily than ethene. Incorporation of acetylene reaches 69% with an iron catalyst and 59% with cobalt; this compares to less than 10% incorporation of ethene for iron and 10-30% for cobalt in the literature[2-7]. With iron catalysts, addition of acetylene resulted in a significant increase of hydrocarbons as well as oxygenated products. Formation of oxygenates might follow different pathways for iron and cobalt catalyst.

Significant deviations of the hydrocarbon distributions from the ASF model are observed when the FTS reaction is conducted in a near-critical and supercritical hexane (SCH) medium over an alumina supported cobalt catalyst. Rather than a single chain growth probability ($\alpha$-value) for the product distribution as in the standard ASF model, three distinct chain growth probabilities are required to represent the product distributions obtained in the SCH environment. The extent to which the middle distillate compounds incorporate in the chain growth and hence

deviate from standard ASF is strongly related to the physical properties of the reaction mixture (gas-like properties vs. liquid-like properties) under the specified reaction temperature and pressure.

Cobalt and ruthenium catalysts supported on silica aerogel are active towards the production of hydrocarbons via Fischer-Tropsch synthesis. The silica aerogel support has high surface area and is mesoporous. In loadings less than 10%, cobalt exists as discrete 50-70 nm metal particles suspended within the silica aerogel support and the interconnected, 3D network of mesopores allows for very fast mass transport. Hydrocarbons as large as $C_{15}$ were produced and the product distribution was centered around $C_9$-$C_{10}$ for both catalysts at 265 $^o$C.

Metal pentadienyl complexes have been shown to be very effective for the incorporation of Fe and Ru into aerogels; furthermore, high catalytic activities have been obtained in some cases. A suitable Co source has also been identified. In contrast, metallocene sources are less effective for simple incorporation. However, the strong reducing nature of cobaltocene has opened up the possibility of a redox-targeting approach for directing the incorporation of a second metal to existing metal oxide in the support. Early results indicate significantly enhanced reactivities in accord with expectations.

Molybdenum-promoted AC-supported iron catalysts have been investigated for F-T synthesis of liquid hydrocarbons. The three catalysts investigated had the following compositions (weight %): 15.7% Fe/0.8% Cu/0.9% K/AC, with 0, 6, or 12 % Mo. The AC-supported iron catalyst shows high initial activity, but its deactivation rate is also high. Catalyst stability is improved significantly after addition of molybdenum into the Fe/AC catalysts, but activity is suppressed dramatically, especially when Mo loading is over 6%. Also, methane and oxygenate selectivities on the Mo-Fe/AC catalysts are increased compared with the Fe/AC catalyst.

A hybrid catalyst system consisting of a methanol synthesis catalyst C-79 and MTO catalyst SAPO-34 was employed for syngas conversion to light olefins. The experimental results demonstrate that CO conversions and C2-C4 light olefins selectivity can be significantly increased by employing the hybrid catalyst system as compared to either catalyst alone.


Hydrogen

It has been shown that efficient production of pure hydrogen can be achieved by dehydrogenation of cyclohexane or methylcyclohexane with catalysts consisting of 0.1-1.0 wt.% Pt supported on stacked-cone carbon nanotubes (SC-CNT). The SC-CNT were produced by catalytic dehydrogenation of propane. The catalysts exhibited 100 % selectivity for conversion of cyclohexane to hydrogen and benzene and methylcyclohexane to hydrogen and toluene. A 0.25 wt.% Pt/ SC-CNT catalyst had approximately the same activity as a commercial 1 wt.% Pt/$Al_2O_3$ catalyst. High resolution TEM showed the dispersion of the Pt catalyst particles on the SC-CNT support to be very high after 6.5 hours of reaction, with particle sizes ~ 1 to 2 nm. A 0.1wt% Pt/SC-CNT exhibited the highest efficiency (turnover-number (TON)) for hydrogen production per metal atom.

A preliminary experiment on the aqueous-phase reforming of ethylene glycol using a 1 wt.% Pt-99 wt.% $Al_2O_3$ catalyst in a batch system has shown that significant amounts of hydrogen are produced, with very low production of carbon monoxide.

New apparatus for the production of hydrogen by reforming of lower alcohols in supercritical water has been assembled and is working correctly. Depending on operating conditions, 3-4 moles of hydrogen are typically produced per mole of methanol or ethanol.

## Structure and reaction mechanisms of C1 catalysts

$^{29}$Si and $^{13}$C solid state NMR methods were used to investigate several metal-loaded silica aerogel F-T catalysts. The results are as follows:

1. No distinct differences in the $^{29}$Si NMR spectra are observed among the cobalt, ferrocene and ruthenocene loaded silica aerogel samples. Although the loading of metal compounds results in less distinct spectral lines from the Q sub-units, the silica tetrahedral sub-units do not collapse.

2. The metal-loading has significant influence on the $^{29}$Si spin lattice relaxation time.

3. The ferrocene or ruthenocene molecules exhibit a fast tumbling motion in the silica aerogel support, based on the $^{13}$C NMR data. Their behavior indicates that rapid exchange exists within the aerogel structure on a time scale equivalent to that observed in liquid and gaseous states.

Variable temperature magnetometry and electron magnetic resonance (EMR) were use to characterize the structures of Co on several supports and Ni-SAPO catalysts. Co(0), CoO, and $Co_3O_4$ are easily detected by their characteristic magnetic signatures. The results show that reduction follows the sequence $Co_3O_4 \rightarrow CoO \rightarrow Co(0)$ and that reduction to Co(0) is often not complete. This is clearly important for FT synthesis. For the Ni-SAPO, the electronic state of Ni was found to be Ni(I) for the lightly doped samples, whereas for higher dopings, both Ni(I) and Ni(0) states were observed.

Mössbauer and XAFS spectroscopy have been used to characterize various catalysts developed by CFFS researchers for use in C1 or hydrogen reactions, as summarized below.

1. Mössbauer spectroscopy results confirm the importance of hercynite ($FeAl_2O_4$) in determining the activity of Fe-based alloy dehydrogenation catalysts. With increasing time on stream at 700 ºC, the amount of hercynite and the hydrogen production decrease, while the cementite ($Fe_3C$) content increases proportionately. This suggests that the reduction of hercynite and formation of cementite cause the detachment of the catalyst particles from the support.

2. Pt nanoparticles supported on stacked cone carbon nanotubes (SC-CNT) are excellent catalysts for the dehydrogenation of cyclohexane to benzene. However, XAFS spectroscopy indicates that a relatively small percentage of the Pt in the nanoparticles is metallic. Secondary components, which could be due to Pt-O or Pt-C surface interactions, dominate the spectra.

3. Preliminary measurements indicate that both XAFS and Mössbauer spectroscopies will be useful for understanding the formation of novel catalysts that involve the placement of iron and other metal pentadienyl or cyclopentadienyl compounds inside silica aerogels.

## Conclusions

Excellent progress was made towards the goals of the CFFS C1 chemistry program during the first six months of the current contract year. Some significant findings are listed below.

<u>Liquid fuels</u>

➢ Acetylene is incorporated into Fischer-Tropsch (F-T) reactions much more effectively than higher acetylenes, resulting in a significant increase of hydrocarbons and oxygenated products.

➢ Significant deviations of hydrocarbon distributions from the ASF model are observed when the F-T reaction is conducted in near-critical and supercritical hexane (SCH). These deviations can be controlled by variation of pressure and temperature.

➢ Cobalt and ruthenium catalysts supported on silica aerogel yielded hydrocarbons as large as $C_{15}$ with a product distribution was centered around $C_9$-$C_{10}$. Metal pentadienyl complexes were shown to be very effective for the incorporation of Fe and Ru into aerogels.

➢ The addition of 6% Mo to activated carbon-supported iron F-T catalysts significantly improves their stability.

➢ A hybrid catalyst system consisting of a methanol synthesis catalyst C-79 and MTO catalyst SAPO-34 was developed for syngas conversion to light olefins.

<u>Hydrogen</u>

➢ Efficient production of pure hydrogen was achieved by dehydrogenation of cyclohexane to benzene and methylcyclohexane to toluene using catalysts consisting of 0.1-1.0 wt.% Pt supported on stacked-cone carbon nanotubes (SC-CNT).

➢ Aqueous reforming of ethylene glycol using a 1 wt.% Pt-99 wt.% $Al_2O_3$ catalyst produced large amounts of hydrogen with very low production of carbon monoxide.

➢ Reforming of methanol and ethanol in supercritical water to produce hydrogen was demonstrated.

**Structure and reaction mechanisms of C1 catalysts**
➢ Ferrocene or ruthenocene molecules exhibit a fast tumbling motion in the silica aerogel support, based on the $^{13}C$ NMR data.
➢ Magnetometry and electron magnetic resonance (EMR) follow the sequence $Co_3O_4 \rightarrow CoO \rightarrow Co(0)$ and demonstrate that reduction to Co(0) is often not complete.
➢ Mössbauer and XAFS spectroscopy established that reduction of hercynite and formation of cementite cause the detachment of Fe-alloy catalyst particles from the alumina support.
➢ XAFS spectroscopy indicates that a relatively small percentage of the Pt in 1-2 nm particles on stacked-cone CNT is completely metallic. Pt surface interactions dominate the spectra.

# Acetylene as a Probe in Fisher-Tropsch Mechanism Studies

L. Hou, Y. Zhang, J. Tierney and I. Wender

Chemical Engineering Department, University of Pittsburgh

## Introduction

The Fischer-Tropsch (F-T) synthesis converts syngas (CO/H$_2$), which can be produced from natural gas, coal and biomass, into long chain hydrocarbons. The hydrocarbons can be further processed to produce gasoline, jet/diesel, lubricants and chemicals. Diesel fuels from F-T synthesis are sulfur-free and can be used as blending agents for diesel from petroleum. Iron and cobalt are the only major F-T synthesis catalysts in industrial use; both catalysts yield products consistent with ASF polymerization kinetics. Cobalt catalysts produce mainly saturated hydrocarbons and a negligible amount of oxygenates, while iron catalysts generally yield more olefins and oxygenated products. It is generally agreed that F-T synthesis is a stepwise growth of hydrocarbon chains by addition of monomeric units[1]. However, it is still under debate in terms of the chain initiation and chain termination steps and the formation of oxygenates is less well understood. Many researchers have investigated the role of secondary olefin reactions by addition of olefins, especially ethylene, to the syngas feed during the F-T synthesis[2-10]. It has been shown that ethylene is incorporated into higher F-T products. Kose[11,12] has reported that the adsorption of acetylene and ethylene results in formation of the same surface species on both Ni and Rh.

The use of acetylenic compounds as probes to study F-T synthesis should provide important clues as to the mechanistic details. There is no report on incorporation of acetylenes into F-T synthesis with cobalt and precipitated iron catalysts. The only work with acetylene was done by Russian scientists who introduced acetylene, labeled with ^{14}C into F-T synthesis on fused iron catalyst to obtain higher alcohols[13]. Their results showed that incorporation of acetylene into alcohols and C$_{3+}$ hydrocarbons was higher than obtained by addition of ^{14}C labeled ethylene; acetylene initiated but did not propagate chain growth. In our previous studies, we focused on the addition of substituted acetylenes, such 1-hexyne and phenylacetylenes, to cobalt catalyzed F-T reactions. We found that alkynes are incorporated more easily than alkenes and proposed surface-bound acetylenes as chain initiators. Another interesting finding is that alkynes could be incorporated into F-T synthesis yielding oxygenated products, mostly aldehydes and alcohols with one carbon more than the added alkynes.

The objective of this study is to investigate the mechanism of the F-T synthesis with acetylene as a probe molecule, with consideration of the possible differences in the pathways that occur with cobalt and iron catalysts. To develop a better understanding of the mechanism of formation of oxygenated products from CO hydrogenation on iron and cobalt, our studies with acetylene are carried out under pressures which promote formation of oxygenates. This work will lead to the possibility of modifying the F-T synthesis to increase the amounts of oxygenated products. The addition of oxygenates to diesel fuel from petroleum can significantly lower particle matter (PM) emissions.

## Experimental

<u>Catalyst preparation</u>

The supported Co catalysts were prepared by incipient-wetness impregnation of cobalt nitrate and ruthenium nitrate on alumina. The alumina was calcined at $500^oC$ for 10 hours before impregnation. The catalyst with a composition of Co (10 wt%), Ru (0.5 wt%) and $Al_2O_3$ (89.5wt %) was dried in air at $110^oC$ for 10 hours, followed by calcination at $300^oC$ for 5 hours. Before reaction, catalysts were activated in flowing hydrogen at $350^oC$ for 10 hours. The iron catalyst was obtained from Dr. Burt Davis of the University of Kentucky. It had been prepared by a precipitation method with a composition of 100Fe/4.4Si/1.25K.

<u>Experimental set-up</u>

The F-T reaction was carried out in a computer controlled fixed bed reactor. The reactor is stainless-steel with i.d. 3/8 inches. Acetylene was introduced from a tank of premixed gas containing (mol): 1% acetylene, 10% Ar, 44.01% CO, 44.99% $H_2$. A thermocouple was inserted into the middle of the catalyst bed in the reactor.  The reactor was loaded with 2.5 gram of a Co or Fe catalyst. Co catalysts were activated by $H_2$ at a rate of 50 ml/min, with a temperature program ramping from room temperature to $350^oC$ at $1^oC$ /min, holding at $350^oC$ for 10 hours. Fe catalysts were activated similarly but kept at $350^oC$ for 5 hours and $450^oC$ for 2 hours. After reduction, the temperature of the reactor was lowered to the reaction temperature. The F-T reaction was started by gradually increasing the CO and $H_2$ flow rate to avoid a temperature surge due to active sites present in the fresh catalysts. Liquid products were collected by a cold trap in an ice-water bath and analyzed by a GC-MS.  Wax products were collected by a hot trap at about $200^oC$.  A stream of effluent gas was removed between the hot trap and the cold trap and went through three sampling valves controlled by a computer and analyzed by two online GCs (HP6890 and HP5890).

Since the gas mixture contains acetylene, special safety precautions were taken. The reactor was surrounded on one side by a wall and on three sides by a safety shield made of impact resistant 0.5 inch-thick polycarbonate. Copper, which reacts with acetylene to form explosive acetylides, was not present in the reaction system.

## Results and Discussion

<u>Relative rate of acetylene and 1-hexyne incorporation</u>

Under F-T conditions, the following reactions of acetylene may occur: hydrogenation to ethene and ethane, dimerization to $C_4$ hydrocarbons or incorporation into F-T products. Hydrogenolysis is not important under our synthesis conditions, since a large increase of methane has not been observed. Table 1 shows that acetylene is more readily incorporated into F-T products than is 1-hexyne. Incorporation of olefins of different chain lengths into F-T synthesis has been studied in several papers. Schulz et al.[2] noted that incorporation of ethylene is more than an order of magnitude higher than propylene, which shows the special role of the two-carbon entity. Such a chain initiator can be produced by adsorption of acetylenic probes, a much easier route than coupling of two adsorbed surface methylidynes. Coupling of two CH groups has been shown to produce acetylenic structures[14].

Effect of acetylene on cobalt or iron catalyzed F-T synthesis

F-T synthesis was conducted under 700 psi, 180°C on both cobalt and iron catalysts. F-T product distributions without and with acetylene addition over these two catalysts are shown in Table 2. Addition of acetylene to the cobalt and iron catalyzed F-T synthesis results in about 3 times increase in catalyst efficiency ( defined as the yield of the products per gram catalyst ). The iron catalyst shows greater hydrogenation ability, while dimerization is a preferred reaction for cobalt. Iron catalysts produced greater yields of oxygenated compounds than cobalt catalysts. While significant enhancements of hydrocarbon products have been observed for both cobalt and iron, influences of acetylene on oxygenates are different for these two catalysts. With iron catalysts, addition of acetylene results in an increase in oxygenates as well as hydrocarbons, an indication that oxygenate formation involves growing hydrocarbon chains. The oxygenated product distributions without and with acetylene in Table 1 are plotted as log(Wn/n) against n in Figure 1. (Wn: weight fraction, n: carbon number). The data are approximated by two straight lines. Figure 1 indicates that, with iron catalysts, oxygenates under either normal F-T synthesis or F-T synthesis with acetylene follow ASF distribution, just as with hydrocarbons. For cobalt catalysts, amounts of oxygenated products are negligible without acetylene addition. With acetylene, the distribution of oxygenates is different from that of typical F-T products; they may be formed via hydroformylation of olefins. The decrease of $\alpha$ value for total F-T products upon acetylene addition shown in Table 2 indicates that the increase in rates of chain initiation are higher than the increase in rates of chain growth, indicating that acetylene serves mainly as a chain initiator.

Effect of operating variables on acetylene incorporation

Conversions of acetylene under F-T conditions with cobalt and iron catalysts are shown in Table 3. It shows that dimerization is dependent on the catalyst and inert to reaction conditions. Hydrogenation and incorporation are competitive reactions. The differences between selectivity of acetylene conversions over iron at 100 psi and 700 psi are within experimental error. Increases in temperature from 180°C to 260°C slightly increase the rate of hydrogenation; as a result, incorporation decreases. However, under our conditions, incorporation is the most important reaction on both catalysts, which contrasts with ethene addition. Hydrogenation of ethene has been found to be the predominant conversion on both iron and cobalt catalysts[18-20]. Albert[21] studied ethylene and acetylene chemisorptions on Co(0001) and observed that an acetylene monolayer blocks all surface sites for subsequent CO chemisorptions, while an ethylene monolayer allows the coadsorption of 25% of a CO monolayer. Since acetylene is more strongly adsorbed on catalysts than ethene and CO, it initiates F-T reactions more rapidly than does ethene.

## Conclusions

Acetylene is incorporated into F-T reactions much more effectively than are higher acetylenes, consistent with the reported special role of $C_2$ species in chain initiation. Acetylene initiates F-T more readily than ethene. Incorporation of acetylene reaches 69% with an iron catalyst and 59% with cobalt; this compares to less than 10% incorporation of ethene for iron and 10~30% for cobalt in the literature[2-7]. With iron catalysts, addition of acetylene resulted in a significant increase of hydrocarbons as well as oxygenated products. Formation of oxygenates might follow different pathways for iron and cobalt catalyst.

## Papers Presented or Published

1.  Y. Zhang, L. Hou, J. W. Tierney and I. Wender, "Acetylenes as Probes in the Fischer-Tropsch Reactions", ACS Annual Meeting, September, 2003, New York.
2.  Y. Zhang, L. Hou, J. W. Tierney and I. Wender, "Fischer-Tropsch Mechanism Studies Using

Acetylenic Molecules as Probes", Topics in Catalysis, submitted in January, 2004


## Future Work

We will study the effect of operating variables, such as temperature, pressure, $H_2$/CO ratios and space velocity in F-T reactions with acetylene. We expect catalyst activity and selectivity will differ at various conditions. The response of selectivity to hydrocarbons and oxygenates to reaction conditions could provide information on the mechanism of their formation. Since sulfur is a well known poison to CO hydrogenation, thiophene will be added into acetylene incorporated F-T reactions to investigate the nature of the incorporation. Loktev et al. [13] studied the effect of acetylene on CO hydrogenation on a fused iron catalyst. They focused on alcohol synthesis and operated at very high pressure and low temperature. We will investigate effect of acetylene on a fused iron catalyst under somewhat comparable reaction conditions with precipitated iron and cobalt catalysts.

## References

1.  F. Fischer and H. Tropsch, Brennstoff-Chemie, **1926**, 7, 97.
2.  Schulz, H. and M. Claeys, Applied Catalysis, **1999**, 186(1-2), 71-90.
3.  B.H. Davis, Catalysis Today, **2003**, 84(1-2), 83-98.
4.  J. H. Boelee, J. M. G. Cüsters and K. Van Der Wiele, Applied Catalysis, **1989**, 53, 1-13.
5.  Robert T. Hanlon and Charles N. Satterfield, Energy & Fuels, **1988**, 2, 196.
6.  A.A. Adesina, Applied Catalysis, **1996**, 138, 345.
7.  Ya. T. Eidus, Russian Chemical Reviews, **1967**, 36, 338.
8.  P.M. Maitlis, et al., Applied Catalysis, **1999**, 186(1-2), 363.
9.  H. Schulz, B.R.Rao, M. Elstner, Erdöl und Kohle, **1970**, 22, 651.
10. Li-Min Tau, Hossein A. Dabbagh., and Burtron H. Davis, Energy & Fuels, **1990**, 4, 94.
11. Rickmer Kose, Wendy A. Brown and David A. King, Chemical Physics Letters, **1999**, 311, 109.
12. W. A. Brown, R. Kose and D. A. King, Journal of Molecular Catalysis, **1999**, 141, 21.
13. S.M. Loktev, Journal of Catalysis, **1982**, 17, 225.
14. L.R. Beanan and J.B. Keister, Organometallics, **1985**, 4(10),1713.
15. Mark E. Dry, Catalysis Today, **1990**, 183
16. B. H. Davis, Fuel Processing Technology, **2001**, 71, 157
17. G. Henrici-Olive, S. Olive, Journal of Molecular Catalysis, **1984**, 24, 7
18. M. L.Turner, N. Marsih, B. E. Mann, R. Quyoum, H. C. Long, P. M. Maitlis, Journal of the American Chemical Society, **2002**, 124(35), 10456.
19. J. Patzlaff, Y. Liu, C. Graffmann, J. Gaube, Catalysis Today, **2002**, 71(3-4), 381.

20. J. Patzlaff,  Y. Liu, C. Graffmann, J. Gaube, Applied Catalysis, **1999**, 186(1- 2), 109.
21. Mark R. Albert  and Larry G. Sneddon, Surface Science, **1984**, 147, 127

Table 1.  Selectivity of 1-hexyne / $C_2H_2$ F-T reactions on a cobalt catalyst

| Selectivity (%) | Hydrogenation | Dimerization | Incorporation |
|---|---|---|---|
| 1-Hexyne[1] | 47 | 35 | 18 |
| $C_2H_2$[2] | 11 | 37 | 51 |

[1] 10Co/90Al, 150°C, 100psi, $H_2$/CO=2
[2] 10Co/0.5Ru/89.5Al, 150°C, atmospheric pressure, $H_2$/CO=2

Table 2. Yields (mg/g.h) of F-T products with acetylene on cobalt and iron catalysts

|  | Co[1] | | Fe[2] | |
|---|---|---|---|---|
|  | without acetylene | with acetylene | without acetylene | with acetylene |
| $C_1$ | 3.31 | 4.06 | 1.68 | 1.37 |
| $C_2$ | 0.76 | 4.83 | 1.68 | 15.97 |
| $C_3$ | 3.46 | 8.04 | 2.95 | 7.65 |
| $C_4$ | 3.51 | 24.74 | 3.11 | 9.93 |
| $C_5$ | 2.98 | 10.53 | 2.32 | 7.53 |
| $C_6$ | 3.05 | 6.84 | 1.75 | 5.09 |
| $C_{7+}$ | 10.42 | 18.45 | 9.00 | 17.46 |
| $C_3$ oxygenates | 0.09 | 0.77 | 0.85 | 3.87 |
| $C_4$ oxygenates | 0.05 | 0.52 | 1.27 | 2.78 |
| $C_5$ oxygenates | 0.00 | 0.84 | 1.10 | 2.51 |
| $C_6$ oxygenates | 0.00 | 0.13 | 0.77 | 1.92 |
| $S_{hydrogenation}$ (%) | - | 8.6 | - | 27.9 |
| $S_{dimerization}$ (%) | - | 32.4 | - | 4.4 |
| $S_{incorporation}$ (%) | - | 59.0 | - | 67.7 |
| $\alpha$ | 0.75 | 0.61 | 0.72 | 0.61 |
| Catalyst Efficiency(mg/g.h) | 11 | 31 | 9 | 26 |

[1] 10Co/0.5Ru/89.5Al, 180°C, 700psi, $H_2$/CO=2, 1% acetylene
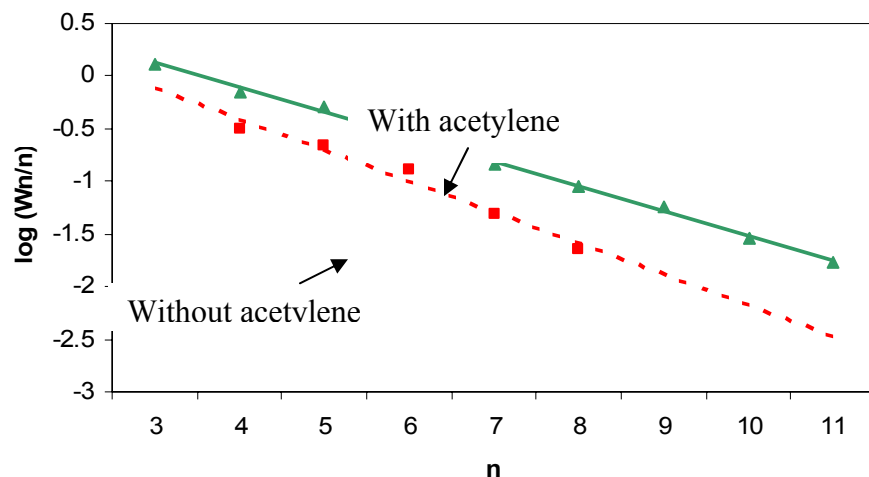[2] 100Fe/4.4Si/1.25K, 180°C, 700psi, $H_2$/CO=1, 1% acetylene

Figure 1. Chain length distributions of oxygenated products without/with acetylene addition: 100Fe/4.4Si/1.25K, T=180$^{\circ}$C, P=700psi, H$_2$/CO=1, 1% acetylene

Table 3. Effect of operation variables on acetylene incorporation

| | Co [1] | | Fe [2] | | |
|---|---|---|---|---|---|
| T ($^{o}$C) | 180 | 180 | 180 | 180 | 260 |
| P ( psi ) | 700 | 700 | 100 | 700 | 700 |
| H$_2$/CO | 1 | 2 | 1 | 1 | 1 |
| Hydrogenation (%) | 9 | 14 | 26 | 28 | 34 |
| Dimerization (%) | 32 | 33 | 5 | 4 | 4 |
| Incorporation (%) | 59 | 53 | 69 | 68 | 62 |

[1] 10Co/89.5Al/0.5Ru, 180C, 700psi, 1% acetylene
[2] 100Fe/4.4Si/1.25K, H$_2$/CO=1, 1% acetylene

14

# Diesel and Jet Fuel from Fischer-Tropsch Wax

Z. Zhou, Y. Zhang, J. Tierney and I. Wender
Chemical Engineering Department, University of Pittsburgh

## Introduction

The Fischer-Tropsch (F-T) synthesis is inherently a very good way to produce high quality, environmentally clean transportation fuels, especially diesel and jet fuels. Traditional transportation fuels made from petroleum contain environmentally undesirable elements, such as sulfur, nitrogen, aromatics and metals. Consumption of transportation fuels is increasing and stringent regulations for cleaner and high quality products are being applied. Since premium fuel products can be produced with the F-T process, they have been used as blending agents to upgrade transportation fuels made from petroleum. Because of the sequential chain-growth mechanism involved in F-T reactions, it is not possible to obtain paraffin fractions with a specific carbon-chain range.[1,2] F-T products are always mixtures of light and heavy hydrocarbons and some oxygenates, which includes light gases, naphtha and jet and diesel fuel fractions. More than half of the F-T products are high molecular weight hydrocarbon materials, termed F-T waxes. These F-T waxes must be cracked and isomerized to obtain desired transportation fuels.

Previous applications of the F-T synthesis by Sasol and by Shell used proprietary catalysts to convert F-T waxes to the desired fuel fractions such as diesel fuels. It is generally recognized that the catalysts used in F-T wax cracking and isomerization contain a metal, such as Pt, on a support, such as a zeolite. [3] The zeolite-based catalysts have low reactivities and operate at about 350-500°C, to obtain acceptable conversions.[4-9] In the present work, we aim at obtaining a readily available, active catalyst system which can be configured to convert F-T waxes into clean high octane gasoline, high cetane diesel or jet fuel under mild conditions. The catalyst systems we have studied were based on anion-modified zirconia catalysts which have demonstrated high reactivities in the conversion of the long-chain paraffins in F-T waxes. Sulfated zirconia and tungstated zirconia are two anion-modified zirconia catalysts studied by researchers. [10-15] The acidity of sulfated zirconia (SZr) catalysts was attributed to the electron-withdrawing function of the $SO_4^{2-}$ group leading to an electron-deficiency on zirconium atoms.



**Lewis acid**          **Bronsted acid**
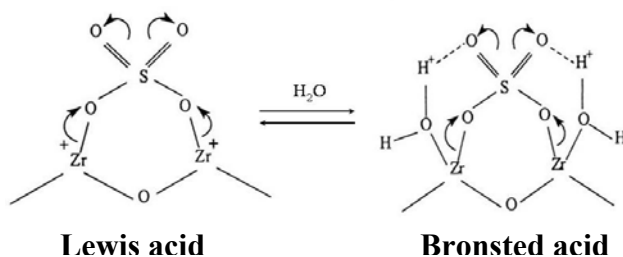
The electron-deficient zirconium centers behave as Lewis acid sites; these change to Bronsted acid sites by addition of water molecules. Later, it was found that acid sites with similar structures can also be generated by supporting tungstate on zirconia. Tungstated zirconia is a milder cracking catalyst and more appropriate for production of middle distillate fuels from long-chain paraffins, perhaps because of a higher hydrogen transfer rate over the surface of tungstated zirconia. [11] While sulfated zirconia and tungstated zirconia have been studied individually for

years, there are few reported studies on combinations of these two types of catalysts, which we called the hybrid catalysts.

We have reported the feasibility of synthesizing hybrid catalysts consisting of Pt-promoted tungstated zirconia (PtWZr) and a mordenite component with an improved performance in converting long-chain paraffins, such as n-$C_{24}$, into transportation fuel products.[16] That result demonstrated a promising method of combining functions of different catalysts. Since our last report, we studied hybrid catalysts consisting PtWZr and sulfated zirconia (SZr) to convert long-chain paraffins in F-T waxes, using n-$C_{36}$ as a model compound, into middle distillate fuels (jet and diesel). Hydrogen pressure was studied since it is a key factor that affects product distributions. Catalyst characterization tests were also carried out.

**Experimental**

Catalysts preparation:
Pt/$WO_3$/$ZrO_2$, noted as PtWZr, was prepared by incipient wetness impregnation of tungstated zirconia (12.5 wt%W) from Magnesium Elektron, Ltd. (MEL) with Pt$(NH_3)_4Cl_2 \cdot H_2O$ (Strem Chemicals) to achieve a desired Pt loading of 0.5 wt%. These were then calcined at 600°C in air. $SO_4$/$ZrO_2$ (9 wt% $SO_4$), noted as SZr, was obtained from Magnesium Elektron, Inc (MEI). Hybrid zirconia catalysts were prepared via mechanical mixing PtWZr with SZr followed by calcination at 550ºC for 3 hours. Hybrid catalysts with various weight ratios of PtWZr and SZr were prepared.

Experimental procedures:
Catalytic tests were carried out in a 27 ml autoclave reaction system. We used n-$C_{36}$ as a model compound for an F-T wax. In a typical reaction, 0.2 g of the catalyst was activated at 500°C and then loaded into the reactor, which was pre-dried overnight beforehand. AF-Ter loading the catalyst, the reactant, typically 0.8 g, was charged. The initial hydrogen pressure was set at room temperature before heating the reactor to the desired temperature in a fluidized sand bath. The reaction temperature was set to 200°C. The reactor was shaken horizontally at 180 rpm during reaction to mix the contents. A computer was used to record the reaction pressure, temperature and time during the run. The reaction was ended at the desired time by quickly cooling the reactor with ice water. Products in the gas phase were discharged into a collector and analyzed using an HP-6890 gas chromatography with an HP Porapak Q 80/100 packed column and TCD detector. Liquid products in the reactor were collected in vials. When waxy products remained in the reactor, appropriate amounts of $CS_2$ were used to dissolve them for analysis. Liquid samples were injected into an HP-5890 gas chromatograph (GC), with HP-1 Cross-linked Methyl Silicon Gum, 25m × 0.2mm × 0.33μm column and FID detector. We used GC analysis results of the reaction products to calculate conversions and selectivities. Conversion is the weight percent of the converted reactant in the original reactant fed to the reactor. Selectivity is the weight percent of a product in the total products. Yield can be obtained by multiplying conversion by selectivity. We defined the product ranges by the result of GC analysis. Hydrocarbon ($C_5$ and above) with peaks before that of *n*-$C_9$ (inclusive) are reported as gasoline, products with peaks aF-Ter *n*-$C_9$, up to and including *n*-$C_{20}$ as jet and diesel fuel, and products with peaks from *n*-$C_{21}$ to *n*-$C_{32}$ as lube-base oil. Small amounts (< 5 wt %) of products smaller than $C_5$ were found and are not reported.

Results and Discussion

We have found that the $H_2$ pressure affects the reactivities and selectivities of tungstated zirconia and sulfated zirconia differently in the conversion of long-chain paraffins. As shown in Figure 1, Pt-promoted tungstated zirconia achieved the highest reactivity and selectivity of middle distillates at about 100 psi. With increase of $H_2$ pressure, both parameters dropped. On the other hand, as shown in Figure 2, the reactivity of sulfated zirconia (Pt-promoted) in converting n-$C_{36}$ increased with higher $H_2$ pressure. However, with $H_2$ pressure above 300 psi, selectivity to middle distillates declined.

**Figure 1.  Effect of hydrogen pressure on hydrocracking of n-$C_{36}$ using PtWZr**
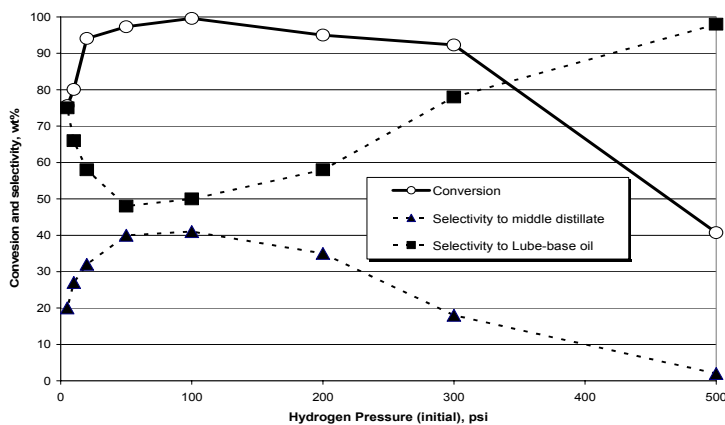


Reaction conditions: 0.25 g PtWZr, 1.0 g n-$C_{36,}$ 200°C, 25 min.

**Figure 2.  Effect of hydrogen pressure on hydrocracking of n-$C_{36}$ using PtSZr**
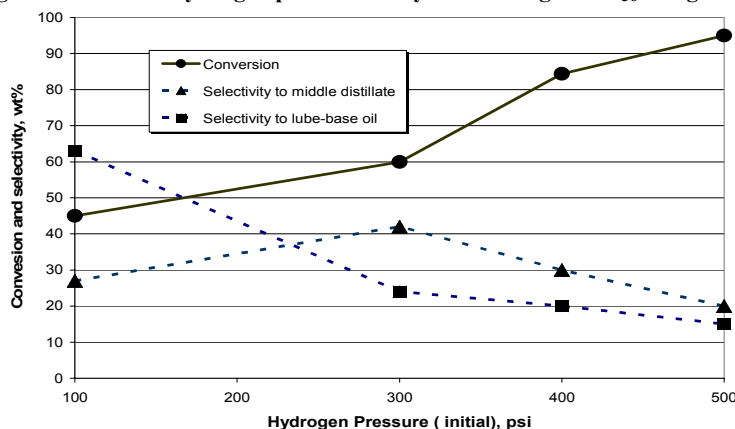


Reaction conditions: 0.2 g PtSZr,  0.8 g n-$C_{36}$ , 200°C, 20 min.

Because of the important effect of $H_2$ pressure, we carried out tests of hybrid catalysts consisting of Pt-promoted tungstated zirconia and sulfated zirconia, termed as PtWZr/SZr, at different $H_2$ pressures. A series of PtWZr/SZr catalysts with various component ratios were tested with n-$C_{36}$ at 200°C and for 25 minutes.  The reactivity of sulfated zirconia alone is less than 5% under these conditions. The results of PWZr/SZr catalysts in converting n-$C_{36}$ with 100 psi $H_2$ are presented in Figure 3.

17

**Figure 3.  Effect of component ratios on the conversion of n-C$_{36}$ using PtWZr/SZr catalysts**
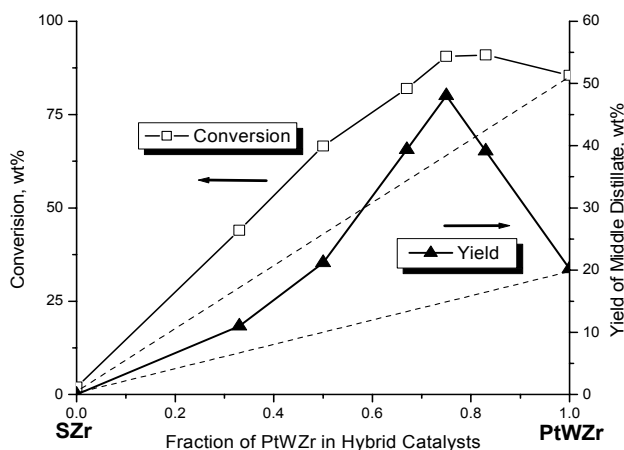


Catalyst:  0.2 g; Reactant:  0.8 g n-C$_{36}$   Reaction conditions:  200°C, 25 min.

     If there is no active interaction between the two components of hybrid catalysts, their performances should be a linear addition of the components following a straight line connecting the two ends. In Figure 3, the curves of both conversion and yield of middle distillates demonstrate an interaction within the hybrid catalyst system. The H$_2$ pressure of 100 psi allows PtWZr to have a good reactivity (85 wt%) by itself. Its yield of middle distillates was low (20 wt%), probably due to lack of cracking. For the PtWZr/SZr (3:1) hybrid catalyst, 25% of the PtWZr was replaced by SZr. Although the reactivity, indicated by its conversion, did not change much (but is well above the linear addition value), the selectivity of middle distillates with the hybrid catalyst increased from 23wt% to 56wt%, as shown in Table 1. The yield of middle distillates products increased from 20wt% to 51wt%. This increase in yield can be attributed to the increase in the cracking functions of the hybrid catalyst. An optimum ration of 3:1 was observed for the highest yield under the given conditions. The CO chemisorption data of some catalysts are also listed in Table 1.

**Table 1.  Platinum conditions over hybrid catalysts containing sulfated zirconia**

| Catalyst | Platinum Dispersion , % | Pt Surface Area, m$^2$/g.Sample | n-C$_{36}$ Conversion, wt% | Middle Distillates | |
|---|---|---|---|---|---|
| | | | | Selectivity, wt% | Yield, wt% |
| PtWZr | 58.8 | 0.73 | 85 | 23 | 20 |
| PtWZr/PtSZr (1:1) | 0.8 | 0.01 | 30 | 35 | 10 |
| PtWZr/SZr (1:1) | 43 | 0.16 | 67 | 50 | 35 |
| PtWZr/SZr (3:1) | 12.4 | 0.11 | 91 | 56 | 51 |

Reaction conditions: 200°C, 25 min, catalyst/n-C$_{36}$ = 1:4 wt, P$_{H2}$=100 psig

     Compared to PtWZr catalyst, PtWZr/SZr hybrid catalysts have lower Pt dispersion and surface area but higher yields of middle distillate products. It also showed that Pt dispersions can

be affected by the component ratio of the hybrid catalyst. Results of PWZr/SZr catalysts in converting n-$C_{36}$ at 300 psi $H_2$ also showed the active interactions within the hybrid catalysts more clearly. With elevated $H_2$ pressure, reactivity of PtWZr is lowered and the activity of sulfated zirconia is increased. When part of the PtWZr was replaced by SZr, the hybrid catalysts converted n-$C_{36}$ with both higher reactivity and selectivity to middle distillate. Under a hydrogen pressure of 300 psi, the hybrid catalysts sustained reactivity over a wider range of component ratios.

## Conclusions

There are active interactions between the components with the hybrid catalysts consisting of Pt-promoted tungstated zirconia and sulfated zirconia (PtWZr/SZr) in converting a long-chain paraffin. Using PtWZr/SZr hybrid catalysts, an appropriate balance of hydroisomerization and hydrocracking functions can be achieved to increase yields of middle distillates, including jet and diesel fuels. The component ratio of hybrid catalysts affects the Pt dispersions and surface areas, which may relate to catalytic performance. $H_2$ pressure is an important factor in affecting the reactivities and selectivities of the hybrid catalyst systems.

## Papers Presented or Published

1.  Z. Zhou, Y. Zhang, J. W. Tierney, I. Wender, "Producing fuels from Fischer-Tropsch Process", Petroleum Technology Quarterly, Vol. 9 (1), P. 137-144, 2004
2.  Z. Zhou, Y. Zhang, J.W. Tierney, I. Wender, "Hybrid Zirconia Catalysts for Conversion of Fischer-Tropsch Waxy Products to Transportation Fuels", Fuel Processing Technology, Vol. 83, p.67-80, 2003
3.  Z. Zhou, Y. Zhang, J.W. Tierney, I. Wender, "Novel Catalysts for Hydroisomerization and Hydrocracking of Fischer-Tropsch Wax", 2003 *AIChE* Spring National Meeting, New Orleans, Louisiana

## Future Work

To investigate the effects of Pt and its interactions with hybrid catalysts, we plan to carry out CO chemisorption and $NH_3$ temperature-programmed desorption (TPD) analysis for our prepared catalysts. SEM and EDX analysis will also be used to identify the Pt components. Other materials, such as Y-zeolite[17] and especially amorphous silica-alumina[18] have been reported to produce transportation fuels from long-chain paraffins. Combining these materials with PtWZr catalysts may result in a hybrid catalyst with enhanced yields of middle distillates.

## References

1.  Sie, S. T.; Senden, M. M. G.; Van Wechem, H. M. H. *Catal Today* **1991**, *8*, 371.
2.  Jager, B.; Espinoza, R. *Catal Today* **1995**, *23*, 17.
3.  Dry, M. E. *Catal Today* **1990**, *6*, 183.
4.  Calemma, V.; Peratello, S.; Perego, C. *Appl. Catal. A-Gen* **2000**, *190*, 207.
5.  Grau, J. M.; Parera, J. M. *Appl. Catal. A-Gen* **1993**, *106*, 27.
6.  Lugstein, A.; Jentys, A.; Vinek, H. *Appl. Catal. A-Gen* **1999**, *176*, 119.

7.  Wu, H. C.; Leu, L. J.; Naccache, C.; Chao, K. J. *J. Mol. Catal. A.-Chem.* **1997**, *127*, 143.

8.  Martens, J. A.; Jacobs, P. A.; Weitkamp, J. *Applied Catalysis* **1986**, *20*, 283.

9.  Chen, N. Y.; Garwood, W. E. *Advances in Chemistry Series* **1973**, *121*, 575.

10.  Arata, K. *Applied Catalysis A: General* **1996**, *146*, 3.

(11) Iglesia, E.; Barton, D. G.; Soled, S. L.; Miseo, S.; Baumgartner, J. E.; Gates, W. E.; Fuentes, G. A.; Meitzner, G. D. *11th International Congress on Catalysis - 40th Anniversary, Pts a and B* **1996**, *101*, 533.

(12) Song, X. M.; Sayari, A. *Catal Rev* **1996**, *38*, 329.

(13) Davis, B. H.; Keogh, R. A.; Alerasool, S.; Zalewski, D. J.; Day, D. E.; Doolin, P. K. *J Catal* **1999**, *183*, 45.

(14) Keogh, R. A.; Sparks, D.; Hu, J. L.; Wender, I.; Tierney, J. W.; Wang, W.; Davis, B. H. *Energy & Fuels* **1994**, *8*, 755.

(15) Cheung, T. K.; Gates, B. C. *Chemtech* **1997**, *27*, 28.

(16) Zhou, Z.; Zhang, Y.; Tierney, J. W.; Wender, I. *Fuel Process Technol* **2003**, *83*, 67.

(17) Martens, G. G.; Marin, G. B.; Martens, J. A.; Jacobs, P. A.; Baroni, G. V. *J Catal* **2000**, *195*, 253.

(18) Calemma, V.; Peratello, S.; Pavoni, S.; Clerici, G.; Perego, C. *Studies in Surface Science and Catalysis* **2001**, *136*, 307.

# Fischer-Tropsch synthesis using Co and Ru supported on silica aerogels as catalysts

Brian C. Dunn, Paul Cole, Daniel Covington, Matthew C. Webster, Zhiru Ma, Ronald J. Pugmire, Greg Turpin, Richard D. Ernst, and Edward M. Eyring

Department of Chemistry, University of Utah, Salt Lake City, UT 84112

## I.  Introduction

Cobalt and ruthenium have long been recognized as highly active catalytic metals for Fischer-Tropsch synthesis.  Due to their cost, both metals are typically dispersed on an oxide support to maximize surface area while minimizing total metal content.  Traditionally, catalytic metals are loaded onto the support via coprecipitation or incipient wetness techniques, but both loading methods have significant disadvantages.  Coprecipitation can occlude metal particles within the oxide matrix which makes the metal unavailable for catalysis and incipient wetness can deposit a significant portion of the metal in micropores which leads to mass transport restrictions near the active metal surface.  The unique properties of silica aerogel may provide a method of overcoming these limitations.

Silica aerogel is a high surface area (800-1600 $m^2$ / g), low density (<0.20 g / $cm^3$) form of silica prepared via a sol-gel route.[1]  The major advantage of silica aerogel is its pore volume and pore structure.  Silica aerogels can be synthesized with >99.5% porosity, but values between 85% and 95% are typical.[1]  The pores exist as an interconnected, 3D network with sizes in the mesoporous (2-50 nm) regime.  The large pores and connectivity lead to mass transport within an aerogel particle which is similar to free diffusion in the gas phase.[2]  The large mass transport, high surface area, porosity, and mesoporous nature make silica aerogel an attractive support for Fischer-Tropsch catalysts.

## II.  Experimental

**Catalyst Preparation**.  Cobalt-containing silica aerogel catalysts were prepared using a four step procedure.[3]  **1)**  A solvent filled gel was prepared by hydrolyzing tetramethoxysilane (TMOS).  A solution of methanol and TMOS was prepared by combining 15 mL of each. Another solution containing 7.5 mL water, 6 mL methanol, and 0.75 mL of 2.8% $NH_4OH$ was added to the first solution and mixed until an optically clear sol was obtained.  Aliquots (10 mL) of the final solution were transferred into cylindrical, polypropylene molds (13 mm i.d. x 60 mm) and sealed with Seal-View™ film.  A semi-solid gel formed within approximately 5 minutes. The gel was aged in the sealed mold for 14 days.  **2)**  The pore-filling solvent was exchanged for ethanol by unmolding the gel into 50 mL of pure ethanol.  The ethanol was replaced every four hours until four exchanges were accomplished.  Cobalt was loaded into the gel by exchanging the pure ethanol with cobalt nitrate dissolved in ethanol.  **3)**  The cobalt-containing aerogel was formed by removing the solvent as a supercritical fluid.  The gel and cobalt nitrate solution were sealed into a 40 mL autoclave and the system was purged with $N_2$ to remove any trapped oxygen. The autoclave was pressurized to 200 psi with $N_2$ and heated to 250 $^o$C at 5 $^o$C / min.  The temperature was increased to 300 $^o$C at 1 $^o$C / min and the internal pressure was maintained at 1800 psi by controlled venting.  Since both the critical temperature, 243 $^o$C, and critical pressure, 926 psi, are exceeded, the ethanol exists as a supercritical fluid inside the autoclave.  The pressure was released while maintaining 300 $^o$C to transition the supercritical fluid into a gas. The temperature was reduced to 25 $^o$C and the cobalt-containing aerogel was removed from the autoclave.  **4)**  The aerogel was calcined in static air at 500 $^o$C for 12 hours and the cobalt was

reduced to the metal with flowing $H_2$ at 500 °C for four hours. The catalyst was crushed and sieved for size.

Ruthenium supported on silica aerogel catalysts were prepared by using the above procedure to synthesize pure silica aerogel followed by vapor-phase deposition of an organometallic ruthenium compound into the aerogel support.[4]

**Catalyst Testing**. All aerogel-supported catalysts were tested for Fischer-Tropsch activity in a laboratory-scale, packed-bed reactor. A 240 mg sample of the powdered catalyst was loaded into a 6.35 mm OD stainless steel tube and held in place with QMA quartz filter material. A thermocouple was placed inside the catalyst bed for accurate temperature control and the reactor assembly was wrapped with heating rope. $H_2$, CO, and Ar (internal standard) were delivered to the heated reactor with mass-flow controllers. Heavy reaction products were analyzed with online GC/MS and light products and permanent gases were analyzed by online GC/TCD/FID.

## III. Results and Discussion

**Catalyst Characterization**. The silica aerogel catalysts were characterized by transmission electron microscopy, $N_2$ adsorption, and CO chemisorption. Figure 1 shows the micrographs of the 2% Co, 6% Co, and 10% Co aerogel supported catalysts. The metallic cobalt particles are



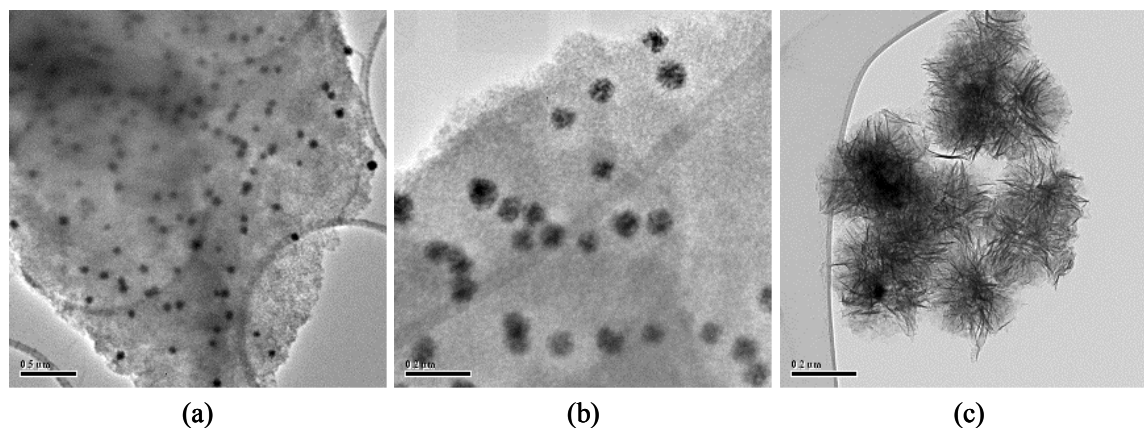(a)                                    (b)                                    (c)

Fig. 1. TEM images of cobalt supported on silica aerogel catalysts: (a) 2% Co, (b) 6% Co,
and (c) 10% Co. Note the differences in magnification as indicated by the scaling
marks [0.5 μm in Fig. 1(a); 0.2 μm in Fig. 1(b); and 0.2 μm in Fig. 1(c)].

seen as the dark features while the surrounding silica aerogel appears as the lighter background. Both the 2% Co and 6% Co show well-dispersed cobalt particles with remarkable uniformity in particle diameter. No measures were taken to direct the size of the cobalt particles. The 2% Co catalyst shows 50 nm diameter particles and the 6% Co catalyst has a particle diameter of 70 nm. The 10% Co catalyst appears substantially different than the lower loaded catalysts with the cobalt appearing as needles rather than spherical particles. This needle formation may have occurred during the supercritical drying step of the preparation. With the higher concentration of cobalt nitrate, exceeding saturation of the supercritical ethanol solvent is more probable and may lead to crystal growth that manifests itself as needles of metallic cobalt when the processing is complete.

Adsorption of $N_2$ was used to measured the surface area, pore volume, and mean pore diameter of the silica aerogel supported catalysts. The dispersion of the cobalt within the aerogel support was measured with CO chemisorption and all of the results appear in Table 1.

**Table 1**. Surface Area, Porosity Properties, and Dispersion of Cobalt on Silica Aerogel Catalysts

| Catalyst | Surface Area[a] $m^2 / g$ | Pore Volume[b] $cm^3 / g$ | Mean Pore Diameter[b] nm | Dispersion[c] % |
|---|---|---|---|---|
| 2% Co | 766 | 3.79 | 21.6 | 0.15 |
| 6% Co | 798 | 4.69 | 27.1 | 0.75 |
| 10% Co | 574 | 4.65 | 36.9 | 0.90 |

[a] Brunauer-Emmett-Teller determination by Micromeritics (Norcross, GA).
[b] Barrett-Joyner-Halenda method determination by Micromeritics (Norcross, GA).
[c] CO chemisorption method determination by Micromeritics (Norcross, GA).

The surface area measured for the silica aerogel supported catalysts are typical of supercritical fluid dried aerogels.[1]  The pore volume measured by $N_2$ adsorption can be compared with the pore volume calculated from measurements of bulk density.  The aerogel supported catalysts have a bulk density of 0.15 g / $cm^3$ and assuming the density[5] of the silica backbone is 2.0 g / $cm^3$, the pore volume is calculated to be 6.2 $cm^3$ / g.  The difference between the measured and calculated pore volumes can be attributed to failure of $N_2$ to condense in the mesopores of the aerogel support[5] or large pores (>300 nm) not included in the pore volume determination.

Since the particles of cobalt are spherical and uniform in the 2% Co and 6% Co samples, the percentage of surface atoms present (dispersion) can be calculated and compared with the measured values in Table 1.  The needle structure of the cobalt in the 10% Co sample does not permit a similar calculation.  Cobalt appears as 50 nm particles in the 2% Co catalyst, therefore the dispersion is calculated to be approximately 2%, and the 70 nm particles in the 6% Co catalyst have 1.5% surface atoms.  The difference between the measured and calculated dispersions may be the result of incomplete reduction.  A previous report[6] indicated that the extent of reduction is related to metal particle size with larger particles showing enhanced reduction.  The present data show the same trend.

**Catalyst Activity**.  All three aerogel supported cobalt catalysts produced hydrocarbons in the laboratory reactor.  The conversion of carbon monoxide was 5.3%, 19.8%, and 22.3% for the 2% Co, 6% Co, and 10% Co catalysts, respectively.  These conversions are low compared with other silica supported cobalt catalysts,[7] but the low density of the present catalysts allows for only a small amount of catalyst to be loaded into the reactor.  The product distribution of hydrocarbons is shown in Figure 2.  With the exception of methane, the hydrocarbons have been grouped in pairs for the sake of clarity.  Maximum hydrocarbon selectivity is in the $C_9$-$C_{10}$ range with products up to $C_{15}$ detected.  It is likely that larger hydrocarbons were produced during the reaction, but remained in the wax trap and are not included in the product distribution.  The fraction of hydrocarbons that were produced as olefinic species appears in Figure 3.  With the 2% Co catalyst, more than 40% of $C_{10}$, $C_{11}$, and $C_{12}$ were produced as the olefin rather than as the paraffin at 265 °C.  This unusual behavior may be the result of the enhanced mass transfer within an aerogel catalyst particle.  When the olefinic chain desorbs from the surface of the cobalt metal, the large pores of the aerogel support allow it to quickly move away from the
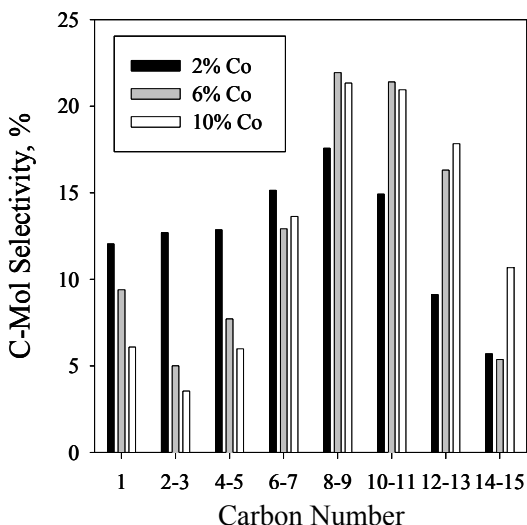
Fig. 2. Product distribution for hydrocarbons produced from Fischer-Tropsch synthesis using 2% Co, 6% Co, and 10% Co on silica aerogel catalysts.
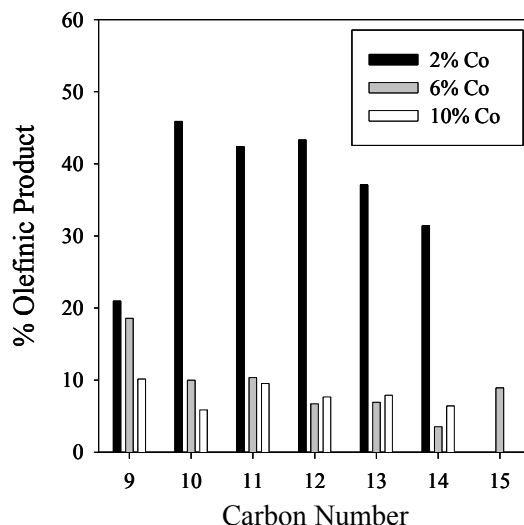
Fig. 3. Fraction of each hydrocarbon that was detected as the 1-olefin product using 2% Co, 6% Co, and 10% Co on silica aerogel catalysts.

surface thus diminishing the probability of readsorption[8] and subsequent hydrogenation. The increased amount of cobalt in the 6% Co and 10% Co catalysts provide more surface area which increases the probability of readsorption and the fraction of olefinic products is lower compared to the 2% Co sample.

Silica aerogel supported ruthenium catalysts were evaluated in a manner identical to the cobalt catalysts. Figure 4 shows the product distribution using a 2% Ru catalyst at 265 $^\circ$C and a 10% Ru catalyst at 225 $^\circ$C and 265 $^\circ$C. The CO conversion of the ruthenium catalysts was 4.6% and 53% for the 2% Ru and 10% Ru at 265 $^\circ$C, respectively, and the conversion dropped to 30% with the 10% Ru catalyst at 225 $^\circ$C. Temperature impacts product selectivity by shifting the distribution towards larger hydrocarbons as the temperature is lowered. The highest selectivity is in the $C_{12}$-$C_{13}$ range at 225 $^\circ$C and the $C_{10}$-$C_{11}$ range at 265 $^\circ$C. The olefin / paraffin ratio is also influenced by temperature and the results with the 10% Ru catalyst are shown in Figure 5. A larger percentage of olefins was produced at 225 $^\circ$C than at 265 $^\circ$C. Since both the cobalt and ruthenium catalysts supported on silica aerogel yielded significant amounts of olefinic products, the aerogel support appears to have some influence on the overall activity on these Fischer-Tropsch catalysts.

## IV. Conclusions

Cobalt and ruthenium catalysts supported on silica aerogel are active towards the production of hydrocarbons via Fischer-Tropsch synthesis. The silica aerogel support has high surface area and is mesoporous. In loadings less than 10%, cobalt exists as discrete metal particles suspended within the silica aerogel support and the interconnected, 3D network of mesopores allows for very fast mass transport. Hydrocarbons as large as $C_{15}$ were produced and the product distribution was centered around $C_9$ with the cobalt catalysts and $C_{10}$ with the ruthenium catalysts at 265 $^\circ$C. A large fraction of the hydrocarbons were detected as the olefinic species which may directly result from the increased mass transport within the aerogel support.
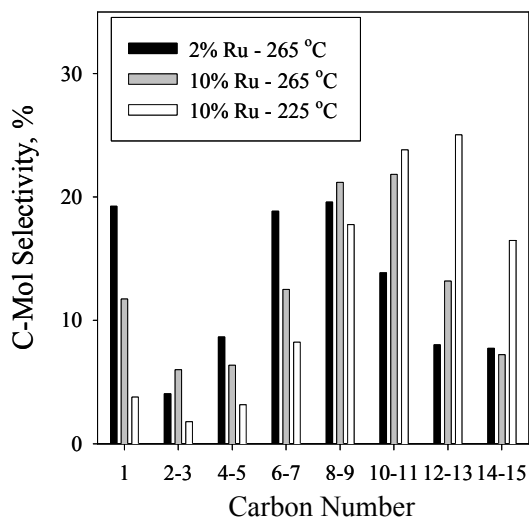
Fig. 4. Product distribution for hydrocarbons produced from Fischer-Tropsch synthesis using ruthenium catalysts.
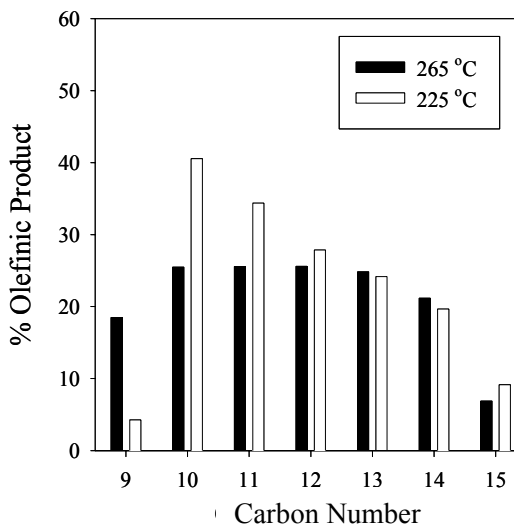
Fig. 5. Fraction of each hydrocarbon that was detected as the 1-olefin product using 10% Ru catalyst.

## V. Papers presented or published

1. Dunn, B. C.; Covington, D. J.; Cole, P.; Pugmire, R. J.; Meuzelaar, H. L. C.; Ernst, R. D.; Heider, E. C.; Eyring, E. M., "Silica Xerogel Supported Cobalt Metal Fischer-Tropsch Catalysts for Syngas to Diesel Range Fuel Conversion," *Energy & Fuels*, submitted for publication.

2. Dunn, B. C.; Cole, P.; Covington, D. J.; Webster, M. C.; Pugmire, R. J.; Ernst, R. D.; Eyring, E. M.; Shah, N.; Huffman, G. P., "Silica Aerogel Supported Catalysts for Fischer-Tropsch Synthesis," *Applied Catalysis A*, submitted for publication.

3. Dunn, B. C.; Cole, P.; Turpin, G. C.; Ma, Z.; Pugmire, R. J.; Ernst, R. D.; Eyring, E. M.; Shah, N.; Huffman, G. P., "Silica Aerogel Supported Catalysts for Fischer-Tropsch Synthesis," 227th ACS National Meeting, March 28 - April 1, 2004, Anaheim, CA.

4. Ma, Z.; Dunn, B. C.; Turpin, G. C.; Cole, P.; Eyring, E. M.; Ernst, R. D.; Pugmire, R. J. "Solid State NMR Investigation of Fischer-Tropsch Catalysts," 45th Experimental Nuclear Magnetic Resonance Conference (ENC), April 18 - 23, 2004, Pacific Grove, CA.

## VI. Future Work

The technique of incorporating $Co(NO_3)_2$ into the semi-solid gel before supercritical drying leads to uniform particles in the 50 – 70 nm range. The size of the particles is comparatively large for efficient heterogeneous catalysis. A decrease in size would allow for more available metal surface area and increased catalysis. Forming cobalt nanoparticles prior to incorporation into the wet gel may be a method for obtaining increased CO conversion. Cobalt nanoparticles with diameters <10 nm can be formed in reverse micelles[9] and isolated. These nanoparticles can then be incorporated into the silica aerogel preparation and should lead to an efficient catalyst for Fischer-Tropsch synthesis.

Hydrogen production from steam-reforming of coal-derived ethanol may be a useful method of generating $H_2$ for use in fuel cells.  Cobalt oxide on dense oxide supports[10] has been shown to be an effective catalyst for steam-reforming of ethanol.  It should be possible to increase the activity of the catalyst by using an aerogel support rather than the dense oxide.  While silica aerogel would not be suitable,[10] aerogels composed of titania, alumina, or ceria can be prepared and used as a catalytic support.  Future research will be conducted to synthesize and test the activity of aerogel-supported catalysts intended for steam-reforming of ethanol.

**VII.References**

(1)     Husing, N.; Schubert, U. *Angew. Chem. Int. Ed.* **1998**, *37*, 22-45.

(2)     Leventis, N.; Elder, I. A.; Rolison, D. R.; Anderson, M. L.; Merzbacher, C. I. *Chem. Mater.* **1999**, *11*, 2837-2845.

(3)     Casula, M. F.; Corrias, A.; Pashina, G. *J. Mater. Chem.* **2002**, *12*, 1505-1510.

(4)     Ernst, R. D. *CFFS Six Month Report* **2004**.

(5)     Scherer, G. W. *Advances in Colloid and Interface Science* **1998**, *76-77*, 321-339.

(6)     Jacobs, G.; Das, T. K.; Zhang, Y.; Li, J.; Racoillet, G.; Davis, B. H. *Appl. Catal. A* **2002**, *233*, 263-281.

(7)     Ohtsuka, Y.; Arai, T.; Takasaki, S.; Tsubouchi, N. *Energy & Fuels* **2003**, *17*, 804-809.

(8)     Huang, X.; Roberts, C. B. *Fuel Proc. Tech.* **2003**, *83*, 81-99.

(9)     Lisiecki, I.; Pileni, M. P. *Langmuir* **2003**, *19*, 9486-9489.

(10)     Llorca, J.; Dalmon, J. A.; Piscina, P. R.; Homs, N. *Appl. Catal. A* **2003**, *243*, 261-269.

**Metal impregnation of silica aerogels using metal pentadienyl complexes**

October 1, 2003 – March 31, 2004

Richard D. Ernst


## I.   Introduction

The Fischer-Tropsch synthesis of hydrocarbons from syn gas ($CO$, $H_2$) mixtures is a process of great economic importance, particularly overseas.  Given the uncertainties in future oil supplies, the F-T process may well assume greater global importance.  From the vast amount of work in this area, it is well recognized that the most active catalysts incorporate iron, cobalt, and ruthenium on oxide supports.[1]  What seem to have attracted little attention, however, are approaches involving silica aerogels, whose high surface areas and large pore sizes could lead to substantial advantages.[2]  Our efforts focus on the gas phase introduction of iron, cobalt, and ruthenium into these aerogels, generally through the use of their reactive complexes with pentadienyl ligands,[3] which offer the following advantages over traditional catalysts:

1. A wide variety of metals may be incorporated.  In addition to Fe, Co, and Ru, analogous volatile sources are available for Ti, V, Cr, Fe, Zr, Os, and others.
2. Strong and immediate catalyst/support interactions allow for effective incorporation of catalyst, with the potential for more efficient catalyst dispersal over the surface.  Greater exposure of catalyst should lead to higher reactivities.
3. High loadings ($\geq$10% metal content by weight) are possible.
4. Single site metal catalysts should be achievable, which are becoming of great interest for other processes.[4,5]
5. Use of a "redox-targeting" approach should allow for additional metal incorporation, especially the selective delivery of one metal center to another (e.g., Co to Ru, etc.).

Our early results reveal some promise for these approaches.


## II.  Experimental

The metallocenes,[6] open metallocenes,[7] and $Fe(C_5H_5)(2,4\text{-}C_7H_{11})$[8] were prepared by published procedures.  The aerogels were kindly prepared and supplied by Dr. Brian Dunn in the Eyring group.  Prior to the incorporation of metal complexes, the aerogels were heated to 150º and maintained under vacuum at that temperature for 2 hours.  They were then stored in a glovebox until needed.  F-T reactions were carried out by the Eyring group.

Deposition into monolithic aerogels was carried out under static vacuum.  The appropriate organometallic compound and the aerogel were prevented from physical contact using wire screen.  For deposition into powdered samples for spectroscopic studies, a finely powdered aerogel was placed together with the appropriate compound into a Schlenk tube, which was then evacuated and rotated continuously for several hours to ensure uniform incorporation.

Solid state NMR spectroscopic studies were carried out by Dr. Zhiru Ma and Prof. Ron Pugmire.  XAFS/XANES, TEM, and Mössbauer studies have been carried out by Prof. Frank E. Huggins, Prof. Naresh Shah, and Prof. Gerald P. Huffman, while ESR and magnetic measurements were carried out by Dr. Prasanta Dutta and Prof. Mohindar Seehra.  Samples for F-T reaction studies under supercritical conditions have been sent to Prof. Chris Roberts.

## III. Results and Discussion

A simplified depiction of the incorporation process is provided below:
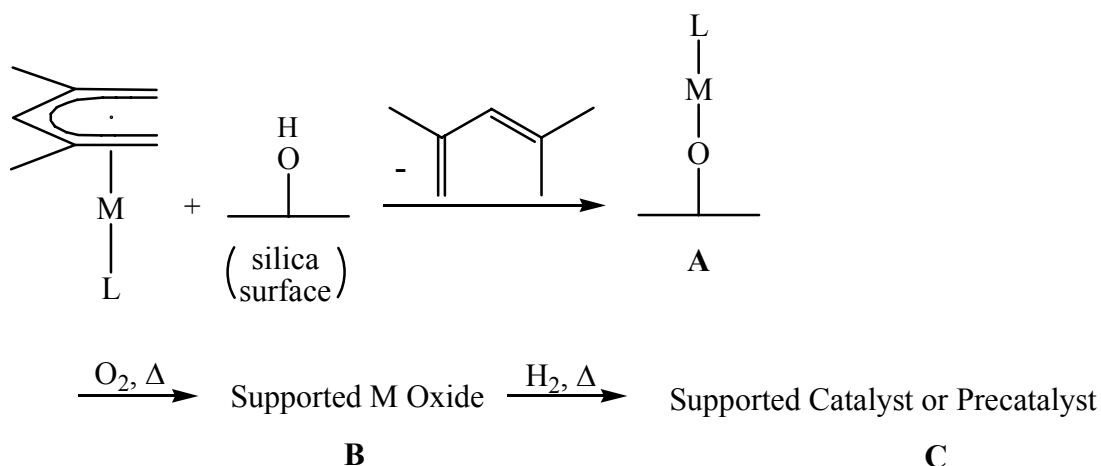


In these reactions, M may be Fe or Ru and L may be either a second 2,4-dimethylpentadienyl ligand (2,4-$C_7H_{11}$) or a less reactive, aromatic cyclopentadienyl ligand ($C_5H_5$). To date we do not have an appropriate Co analogue to the above, although we have found an alternative that will be described later in the report. In all cases, the expected diene has been detected with **A**.

Before we examine the activities of these species, it is important to have some understanding of how and in what form the metal centers are attached to the aerogel surface. Particular questions of interest here relate to the extent of association, if any, for the species **A-C** (as well as the catalyst after actual use), and whether the metal centers in any of these species are present in a single environment or in a variety of environments.

Our initial assumption is that species **A** would be diamagnetic, and almost certainly situated randomly. The surprising air-sensitivity of these (pyrophoric) species, however, is unlike any related molecular complex, reflecting the uniqueness of the metal-support interaction. The sensitivity has so far prevented us from obtaining good NMR and XAFS data which would provide answers to the questions above. Recent maintenance on our glovebox and the addition of an anti-static device will solve problems in manipulating the samples. Additionally, the Pugmire group has obtained new NMR sample cells that are designed to hold air-sensitive materials. This should allow us to obtain the data needed to characterize the various **A** species. Alternatively, we have found that the use of L = the bulky $C_5Me_5$ ligand leads to a much less sensitive product which ought to be more amenable to study.

For the subsequent species – **B**, **C**, and perhaps the used catalyst – ESR, magnetic susceptibility, XAFS, and TEM data will be most helpful in assessing their natures. In the case of ruthenium, species **C** has proven to yield an active catalyst whose TEM images reveal the presence of agglomerated particles, which at ca. 2% loadings appear as small, uniform clusters, but at ca. 10% loadings appear as mixtures of these small clusters and much larger needles. The results also indicate a nearly uniform distribution of the metal particles throughout the aerogel (i.e., there is no surface segregation as may be observed with traditional supports).

Since aggregation of ruthenium has taken place in the catalyst, TEM studies of species **B** and **C** will be carried out. Should either or both of these not show significant evidence of agglomeration, they would be considered for additional physical studies, particularly XAFS.

As noted above, a viable (pentadienyl)cobalt complex for vapor phase depositions has not yet been obtained, although efforts are in progress. Some success has been obtained using

28

cobaltocene, the 19 electron analogue of ferrocene.  We had earlier found that both the 18 electron ferrocene and ruthenocene can incorporate into aerogels, to an extent of ca. 6%.  As no chemical reaction occurs initially, the incorporation is reversible; however, after several days the ferrocene samples begin taking on a greenish color, apparently due to the formation of the blue, 17 electron $Fe(C_5H_5)_2$ cation.[9]  This demonstrates a remarkable enhancement of the reactivity of ferrocene, which also could lead to some opportunities for preparing mixed metal domains.  In any event, due to its unfavorable 19 electron count, cobaltocene is a strong reducing agent,[10] which suggested that it could be incorporated irreversibly.  Indeed, it is.  While ferrocene and ruthenocene incorporate randomly throughout an aerogel, and the pentadienyl compounds incorporate selectively on the monolith surface (in essence, as soon as a surface hydroxyl is encountered), an intermediate level of reactivity and surface selectivity is observed for cobaltocene.  Quite unexpectedly, however, incorporation is accompanied by expulsion of $C_5H_8$ (cyclopentene), revealing the pickup of three hydrogen atoms by one of the $C_5H_5$ ligands.  We do not know what to make of this result.  Additional study of the nature of these adsorbed cobalt species is required; solid state NMR spectra will first be pursued, and based on these results it may be desirable to pursue magnetic, ESR, and/or XAFS studies to further characterize the nature of this phase.  Subsequent oxidation of this phase leads to a bluish aerogel.  Magnetic measurements reveal it is paramagnetic, but the lack of any significant ESR signal suggests the presence of Co/Co interactions.  XAFS (and XANES) data have been obtained for this phase, and together with TEM studies should reveal the extent of any Co/Co interactions.  Based on these results, various studies of a reduced phase (**C**) and/or actual catalyst phase may be undertaken.

As cobaltocene only gave rise to relatively low cobalt contents, efforts are underway to develop more effective pentadienyl-based sources.  Concurrently, however, we have found that the known complex **1** (below)[11] functions quite well as a cobalt source, readily giving at least up to 10% incorporation, with the expected expulsion of cyclooctene.  Studies of these cobalt-loaded aerogels will be undertaken shortly for all possible phases (**A**, **B**, **C**, and actual catalyst).



**1**
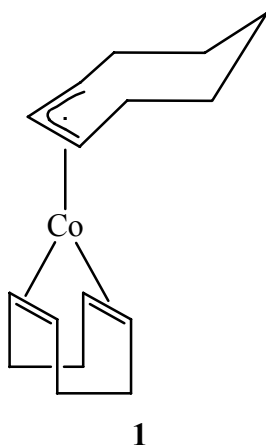
A Redox Targeting Approach to Polymetallic Domains

As the reactivities of Co F-T catalysts can be substantially enhanced by addition of relatively small Ru contents,[12] it would be desirable to develop gas phase approaches to such mixed metal catalysts.  The fact that the 19 electron cobaltocene can reduce oxides of Fe, Co, and Ru to the metals provides a potential route to these species, with the possibility of

unprecedented degrees of intimacy.  An illustration of this approach is provided below.
Subsequent oxidation
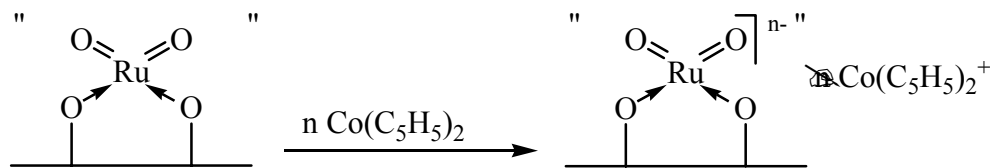


could than lead to small mixed metal oxide domains, which would be studied through the
methods applied above for species **B** and **C**.  These oxides could then be either reduced to
catalysts for study, or exposed to additional cobaltocene which would then target both the
ruthenium and cobalt oxides.  With additional cobalt incorporation cycles, progressively greater
amounts could be added each time.  An interesting variation of this approach involves the use of
the $Co(C_8H_{12})(C_8H_{13})$ complex (**1**).  While we do not know whether there would be any driving
force for its targeting metal oxide sites, the fact that it incorporates into the aerogels much more
readily than does cobaltocene might still result in catalysts with higher reactivities.  Further, the
19 electron ruthenium complex, $Ru(C_5H_5)(C_6Me_6)$,[10] is an even more powerful reducing agent
than cobaltocene.  Hence, one should be able to selectively deliver ruthenium to cobalt (or other
metal) oxide sites, giving what could be an ideal combination.  As will be described in the
following subsection, we already have preliminary results that support these propositions.
    At some future time iron could also be utilized to make mixed metal domains.


F-T Reactivity of Gas Phase Impregnated Aerogels
    Given that volatile pentadienyl complexes of Fe and Ru (but not Co) were available for
study, we initially had to decide which to investigate first.  While Fe would be an obvious choice
relative to cost and commercial considerations, the requirement of promoters would introduce
extra complicating variables, so that we began by looking at Ru.  Indeed, the first sample studied
by the Eyring group (10% Ru) was so active that they had to dilute the flow stream for study.
For the most part, only qualitative results will be included here.  More detail for these studies
will be provided in the accompanying Eyring report.  However, a significantly higher conversion
was observed relative to their Co catalysts prepared by aqueous impregnation.  Generally Ru
catalysts would be expected to show higher activities than Co,[12] so it would be especially
interesting to compare the activity of the Ru catalyst formed from gas phase deposition with one
formed via solution methods.  At the very least, however, these results provide a proof of
concept for the gas phase methodology.  In any event, samples with 2 and 6% Ru incorporation
were also examined, and as expected showed lower activities.  A substantial fraction of the
resulting hydrocarbons did involve diesel range species.  Although pure ruthenium catalysts
would be too expensive for commercial applications, for possible emergency (e.g., military)
applications, in which time is a priority, it seems likely that Ru would actually be most cost
effective, and the catalyst of choice.
    As we could achieve modest incorporation (ca. 2%) of cobalt using cobaltocene, we did
study the gas phase-derived cobalt aerogel catalyst for F-T activity.  However, the Eyring group
found very little activity.  Obviously, however, now that we have found a source that can lead to
10% incorporation, this will be of great interest to study, and these experiments are underway.

There is also our cobaltocene-based redox approach to mixed metal catalysts.  We have already taken an oxidized 2% Ru aerogel and incorporated 2% cobalt (not quite a 2:1 atom ratio).  The Eyring group has found that this catalyst is far more reactive than either 2% Co or Ru; in fact, it is approximately 80% as active as the 10% ruthenium catalyst.  This seems to provide a nice demonstration of the promise of our approach, and a variety of experiments with differing metal compositions are of interest, as well as TEM studies of the catalyst phases.

## IV. Conclusions

Our work has demonstrated that metal pentadienyl complexes are very effective for the incorporation of Fe and Ru into aerogels; furthermore, high catalytic activities have been obtained in some cases.  A suitable Co source has also been identified.  In contrast, metallocene sources are less effective for simple incorporation.  However, the strong reducing nature of cobaltocene has opened up the possibility of a redox-targeting approach for directing the incorporation of a second metal to existing metal oxide in the support.  Early results indicate significantly enhanced reactivities in accord with expectations.

## V.  Papers Presented or Published

1.     "Silica aerogel supported catalysts for Fischer-Tropsch synthesis," B.C. Dunn, P. Cole, D.J. Covington, M.C. Webster, R.J. Pugmire, R.D. Ernst, E.M. Eyring, N. Shah, and G.P. Huffman, *Appl. Catal. A*, submitted for publication.
2.     "Silica xerogel supported cobalt metal Fischer-Tropsch catalysts for syngas to diesel range fuel conversion," B.C. Dunn, D.J. Covington, P. Cole, R.J. Pugmire, H.L.C. Muezelaar, R.D. Ernst, E.C. Heider, and E.M. Eyring, *Energy & Fuels*, submitted for publication.
3.     "Silica aerogel supported catalysts for Fischer-Tropsch synthesis," B.C. Dunn, P. Cole, G.C. Turpin, Z. Ma, R.J. Pugmire, R.D. Ernst, E.M. Eyring, N. Shah, and G.P. Huffman, 227th ACS National Meeting, March 28-April 1, 2004, Anaheim, CA.
4.     "Solid state NMR investigation of Fischer-Tropsch catalysts," Z. Ma. B.C. Dunn, G.C. Turpin, P. Cole, E.M. Eyring, R.D. Ernst, and R.J. Pugmire, 45th Experimental Nuclear Magnetic Resonance Conference (ENC), April 18-23, 2004, Pacific Grove, CA.

## VI. Future Work

Many important questions remain concerning the natures of the metal centers in **A-C**.  Species of type **A** will be examined by solid state NMR, and depending on the results, possibly also XAFS.  Species of types **B** and **C** will first be examined by TEM, after which XAFS, ESR, and magnetic studies will be carried out should there be no evidence of agglomeration.

A wealth of reactivity studies will be of interest.  First, there is the $Co(C_8H_{12})(C_8H_{13})$ complex (**1**), for which we can study the F-T reactivities for gas phase incorporated Co as a comparison to reactivities displayed by solution phase incorporated Co.  Given the enhanced reactivity of our 2% Ru/2% Co catalyst, derived from a ruthenium pentadienyl complex and cobaltocene, a much broader investigation of mixed metal species is in order.  Just allowing for 2, 6, and 10% content for each type of metal leads to nine potential samples to study.  However, it would also be of interest to see how mixed metal catalysts derived from the other cobalt source (**1**) (not believed to be active in a redox-targeting mode) would compare to those from cobaltocene.  Additionally, it will be of interest to examine how catalyst reactivities would differ in the absence of the oxidation step after the first metal has been incorporated.  Further, it will be

of interest to examine what affect the order of metal addition (i.e., Co then Ru vs. Ru then Co) would have on the activities.  Finally, in addition to these studies under relatively traditional F-T conditions, other studies using supercritical media will be undertaken in order to see if the combination of our tailored catalysts and the retention of the aerogel structure that is possible under supercritical conditions may lead to some particularly beneficial results.

One other opportunity has arisen for making aerogels conductive by the incorporation of $RuO_2$.[13]  Our method of incorporation could be substantially better, particularly in selectively delivering the metal to the aerogel surface.  Hence we hope to investigate this opportunity also.

## VII. References

1.  a.  M.E. Dry *Appl. Catal. A: General*, **1996**, 138, 319.
    b.  H. Schulz *Appl. Catal. A: General*, **1999**, 186, 3.
    c.  B.H. Davis *Fuel Proc. Tech.* **2001**, 71, 157.
2.  N. Hüsing and U. Schubert *Angew. Chem. Int. Ed.* **1998**, 37, 22.
3.  R.D. Ernst *Comments Inorg. Chem.* **1999**, 21, 285.
4.  a.  C. Nozaki, C.G. Lugmair, A.T. Bell, and T.D. Tilley *J. Am. Chem. Soc.* **2002**, 124, 13194.
    b.  A.T. Bell *Science* **2003**, 299, 1690.
5.  K. Mori, Y. Hara, T. Mizugaki, K. Ebitani, and K. Kaneda *J. Am. Chem. Soc.* **2003**, 125, 11460.
6.  "Organometallic Synthesis," Vol 1, p. 64, R.B. King, Ed., Academic Press (1965).
7.  D.R. Wilson, L. Stahl, and R.D. Ernst *Organomet. Synth.* **1986**, 3, 136.
8.  Ch. Elschenbroich, E. Bilger, R.D. Ernst, D.R. Wilson, and M.S. Kralik *Organometallics* **1985**, 4, 2068.
9.  D.N. Hendrickson, Y.S. Sohn, and H.B. Gray *Inorg. Chem.* **1971**, 10, 1559.
10.  D. Astruc, "Electron Transfer and Radical Processes in Transition Metal Chemistry," VCH, New York (1995).
11.  a.  S. Otsuka and M. Rossi *J. Chem. Soc. A.* **1968**, 2630.
    b.  L.W. Gosser and M.A. Cushing, Jr. *Inorg. Syn.* **1977**, 17, 112.
12.  G. Jacobs. T.K. Das, Y. Zhang, J. Li, G. Racoillet, and B.H. Davis *Appl. Catal. A : General* **2002**, 233, 263.
13.  J.V. Ryan, A.D. Berry, M.L. Anderson, J.W. Long, R.M. Stroud, V.M. Cepak, V.M. Browning, D.R. Rolison, and C.I. Merzbacher *Nature* **2000**, 406, 169.

# Hydrocarbon Product Distributions in Supercritical Hexane Fischer-Tropsch Synthesis over an Alumina Supported Cobalt Catalyst: Effect of the Reaction Mixture Phase Behavior

Nimir O. Elbashir, Deborah B. Boroughs, Ram B. Gupta, Christopher B. Roberts
Department of Chemical Engineering, 230 Ross Hall, Auburn University, AL 36849

## 1. Introduction

The main objective behind conducting Fischer-Tropsch synthesis (FTS) in near-critical or supercritical phase media involves employing their unique pressure/temperature tunable fluid properties to overcome certain limitations in the conventional FTS processes. Supercritical fluids (SCFs) possess gas-like transport properties (diffusivities) and therefore offer high reaction rates similar to that of the gas-phase FTS (fixed-bed-reactors). In addition, they provide liquid-like solubilities and heat capacities which results in excellent temperature distribution inside the reactor along with in-situ extraction of heavy hydrocarbons similar to that of liquid-phase FTS (slurry reactors). In our previous studies of FTS under supercritical phase conditions, we have demonstrated the advantages of operating the FTS reaction in supercritical fluid (SCF) media compared to conventional reaction media [1-5]. Those advantages include significant improvements in heat transfer inside the reactor coupled with considerable enhancement in α-olefins selectivity and chain growth probability compared to conventional gas-phase FTS [2, 5]. As such, $CH_4$ and $CO_2$ selectivities were significantly decreased under SCF operation [6]. We also demonstrated that changing either pressure or temperature has a dramatic effect on the selectivity and conversion of an alumina supported cobalt catalyst when conducting the reaction under supercritical solvent (pentane and hexane) [2]. As a matter of fact, this tuning process will not only affect the bulk physical properties of the reaction mixture (e.g. density, diffusivity, thermal conductivity, viscosity, etc.) but also the rates at which different reactions take place on the catalyst surface. As a result, optimization and control of the performance of supercritical phase FTS requires a quantitative evaluation of the influence of tuning parameters (i.e. temperature and pressure) not only on the phase behavior of the reaction mixture, but also on the rates of the different reactions taking place on the catalyst surface, including the chain growth mechanism.

In this report, the phase behavior and the critical properties of a reaction mixture collected from the effluent of the reactor and (composed of solvent (hexane)-reactant (syngas)-products (hydrocarbons and water)) were measured in a high pressure variable volume view cell (VVVC) apparatus. The performance of an alumina supported cobalt catalyst was then studied in single phase (with regards to the reaction mixture) FTS operation. The reaction environment was then tuned from liquid-like properties to vapor-like properties and vice versa by either changing the reaction temperature or pressure. An interesting phenomenon observed in these SCF-FTS studies involves deviations in hydrocarbon product distributions from the standard Anderson-Shultz-Flory (ASF) model. This phenomenon is also accompanied by a high chain growth probability within the middle distillate hydrocarbon region. The objective of this study is to explore the possibility of maximizing the production of gasoline and diesel fractions within the FTS product spectrum by proper conduction of the reaction within the various phase regimes in the near-critical and supercritical medium.

## 2. Experimental

A variable volume view cell (VVVC) unit (Fig. 1) was used to measure the critical properties of hexane and SCH-FTS mixture. The VVVC unit consists of high-pressure variable volume view cell, manual pressure generator, temperature controller, heating tape, pressure gauge, syringe pump, stirring bar, and stirring plate. The volume of the cell can be adjusted by displacement of an internal movable piston controlled by a manual pressure generator (High Pressure Equipment Model 87-6-5) filled with isopropanol and used to manipulate the pressure in the view cell. The dynamic seal between the piston and the walls of the vessel is achieved by using four Viton O-rings. A video camera (QuickCam Pro 4000) system with a fluorescent ring light was mounted close to the ½`` thick quartz window on the front of the cell. Images of the phase transition from vapor-liquid equilibrium (VLE) to supercritical phase and vice versa were digitally recorded on the PC. The temperature in the cell was measured and controlled with a type PR-11 1/16" RTD (Omega Engineering) and a self tuning PID controller (Omega CN76030) wired to a magnetic contactor (Omega MC-2-2-40-120), respectively. The cell was heated by using a heavy insulated tape 1/2"×2' (Omega; FGH051) and the accuracy of the measured temperatures was ±0.2 °C. The pressure was measured with a Dynisco flush mount transducer (model TPT-432A) with an accuracy of ±0.5 bar.

Fig. 2 shows our high pressure FTS unit that used to measure the FTS performance of a 15% $Co/Al_2O_3$ catalyst purchased from Union Carbide Co. Detailed information about this unit, and the gas-chromatograph analysis of the reactants and products in addition to the experimental procedure is given elsewhere [2, 5, 7].


## 3. Results and Discussion
### 3.1 Phase behavior and critical properties of the reaction mixture

To test the performance of our VVVC apparatus we initially measured the phase behavior (vapor-liquid equilibrium (VLE) and critical properties) of pure hexane. Fig. 3 shows the P-T diagram of pure hexane that includes the VLE coexistence line and location of the supercritical phase region as defined by the location of measured critical temperature and pressure. The experimentally measured VLE was found to be in a very good agreement with the calculated P-T behavior from both the Peng-Robinson equation of state and the Antoine equation. Similarly, the measured critical temperature (233.2 °C) and critical pressure (30.03 bar) are within the range of reported critical properties of pure hexane. Fig.3 also shows images of the phase transition taken within our VVVC apparatus from the VLE to the near-critical and supercritical phase regions. The bottom image shown in Fig. 3 depicts a typical VLE of pure hexane, whereby the meniscus is positioned exactly at the center of the VVVC. The middle image shows VLE at conditions closer to the critical point (subcritical), whereby the liquid phase looks less dense and the vapor-liquid interface become less distinct. Exactly at the critical point the meniscus (located in the center of the VVVC) disappears indicating the formation of single supercritical phase as seen in the top image. Further increase of the pressure (up to 60 bar) beyond the critical point would result in no change in the single phase (supercritical) as seen in the top image.

The focus of this study involves the phase behavior and critical point location of the FTS reaction mixture represented by the solvent, reactant gases (CO, $H_2$), and products. The location of the critical point (temperature and pressure) of the FTS mixture (75 mole% hexane, 5 mole% syngas, and 20 mole% hydrocarbons and water) was measured by collecting sample from the reactor effluent. The sample from the reactor effluent was trapped into a collection container and

then transferred into the evacuated VVVC through the high pressure valve shown in Fig. 1. The sample was allowed to condense inside the VVVC and form two phases (liquid and vapor) prior to the determination of the critical temperature and pressure. The measured critical pressure of the FTS sample mixture, as seen in Fig. 4, was found to be 37.2 bar (7 bar higher than that of pure hexane), however, the critical temperature (238.2 °C) of the mixture was found to be slightly higher than that of pure hexane.

## 3.2. Fischer-Tropsch synthesis: Reaction performance over the alumina supported cobalt catalyst.

The 15% Co/ $Al_2O_3$ catalyst performance in the FTS reaction was measured under near-critical and supercritical hexane conditions. The scenario of the tuning process of temperature and pressure in the near-critical and supercritical regime is seen in Fig. 4. Pressure was varied from 35 bar (gas-like density) to 80 bar (liquid-like density), while temperature was varied from 230 °C to 260 °C. 250 °C and 65 bar were selected at the base conditions as shown in Fig. 4. This selection is based on our investigation of the catalyst activity and selectivity at near-critical and supercritical hexane conditions at constant $H_2/CO$ ratio of 2 and hexane/syngas molar ratio of 3 (Figs. 5 & 6) where these conditions illustrate optimal performance (CO conversion% and chain growth probability) within the supercritical phase.

Non ASF distributions, represented by nonlinear plots of the logarithm of the normalized weight percentage versus carbon number (Eqn. 1), were observed under typical SCH-FTS (Fig. 8) experiments ($P_{syngas}$ = 20 bar, $P_{hexane}$ = 45 bar, and temperature 250 °C).

$$\ln\left(\frac{W_n}{n}\right) = n \ln \alpha + \ln\left(\frac{(1-\alpha)^2}{\alpha}\right) \tag{1}$$

The samples analyzed in determining the product distributions in SCF-FTS were collected after more than eighty hours time-on-stream, after which both the activity and the selectivity of the cobalt catalyst showed steady performance with time. As seen in Fig. 8, the $\alpha_{overall}$ of 0.875 is higher from that from the gas-phase FTS ($\alpha_{overall}$ of 0.795; Fig. 7); however, the data is poorly fit by single straight line (solid line) and significant deviations from the ASF model are seen in the overall hydrocarbon product distributions. The product distributions in the case of SCH-FTS can be better divided into three stages (dotted lines). The first stage involves the light hydrocarbons product distributions that show steep declines with carbon number up to $C_3$ to yield a very low chain growth probability of $\alpha_{lh}$ = 0.363. It is noteworthy to mention here that $\alpha_{lh}$ has no physical significance and it only represents the slope of the line connecting the experimentally measured $W_n$ of light hydrocarbons. The second stage involves the middle-distillate growth probability indicating very high chain growth probability of $\alpha_{md}$ = 0.951 with the least dependence of chain growth on carbon number in this region. The last stage involves the heavy hydrocarbons distributions that showed a decline in chain growth with the carbon number to give $\alpha_{hp}$ = 0.781, which is slightly lower than the overall chain growth in the gas phase reaction.

### 3.2.1 Effect of Temperature on Hydrocarbon Distribution.

Fig. 9$a$ shows the product distributions at reaction temperature $T_1$ (230 °C), which is below the critical temperature of the mixture (compressed liquid phase) according to the

measured critical properties of the collected reaction mixture illustrated in Fig. 4. The overall hydrocarbon distribution followed closely the ASF model with $\alpha_{overall}$ of 0.809 where slight deviations are observed in the light hydrocarbons ($C_2$-$C_4$) range. Increasing the temperature to $T_2$ (240 °C), whereby the reaction mixture is maintained near the critical point, the overall chain growth probability dropped to 0.776 as seen in Fig. 9$b$. The product distributions in Fig. 9$b$ follow closely the ASF model in middle distillate and heavy hydrocarbons range whereas marked deviations are observed in the light hydrocarbon range. As shown in Fig 9$b$ the deviations extend to $C_8$ (i.e. deviations are in the range of $C_2$-$C_8$). Surprisingly, upon increasing the temperature to $T_3$ (250 °C) (well within the supercritical region) no drop in the chain growth probability of heavy hydrocarbons ($\alpha_{hp}$ = 0.781) was observed despite the increase in the reaction temperature (Fig. 9$c$). In addition, the region of deviation from the ASF model extended up to $C_{14}$ (i.e. deviation range from $C_2$-$C_{14}$) as seen in Fig. 9$c$. The distribution in both the light hydrocarbons (excluding $C_1$) and middle distillates range yield very high $\alpha$-values. A further increase in temperature, resulting in a gas-like density ($T_4$ of 260 °C), resulted in a drastic drop in the chain growth probability ($\alpha_{overall}$ = 0.663) as seen in Fig. 9$d$. The overall product distribution of hydrocarbons up to $C_{20}$ followed closely the ASF model, while only very slight deviation in $C_2$ selectivity is seen in the product distribution at this elevated temperature.

  The influence of temperature on the performance of FTS reaction is extremely complex. It has a direct influence on both the kinetics (including all reaction rates) and the chain growth mechanism. Primary reactions, secondary reactions (hydrogenations and isomerizations), and chain termination rates are strongly influenced by the reaction temperature. Furthermore, physical properties that control the rate of reaction, such as diffusion, are dependent on the temperature [8]. The positive effect on increasing the reaction temperature on FTS operation involves the enhancement of the reactant consumption rates and primary reactions that result in higher activity and better selectivity towards certain products (light hydrocarbons and gasoline fractions). On the other hand, high temperature operation can enhance secondary reaction rates and other side reactions (methanation and $CO_2$ formation), which negatively affect the overall performance of the FTS process. The major challenge in designing an operation scheme is to finely balance those influences. In this study, the influence of the reaction temperature on the chain-growth mechanism of SCH-FTS (Fig. 9$a$-$d$) was evaluated at constant pressure, space velocity, and gas feed composition ($H_2$/CO ratio of 2/1). The dramatic changes in hydrocarbon product distributions with variations in temperature can be largely attributed to the impact of density-dependent properties of the solvent rather than to the direct influence of temperature on kinetics and reaction rates [2]. Our findings show that lower reaction temperatures favor the production of heavy hydrocarbons with linear dependence of the hydrocarbon selectivities on carbon number. Despite the fact that increasing the temperature results in higher termination rates and secondary reaction rates [9], our findings show that in SCH-FTS the overall chain growth probability ($\alpha_{overall}$) shows an optimum value at 250 °C (see Fig. 5). Furthermore, deviations from the ASF model in the light hydrocarbon and middle distillate hydrocarbon ranges are found to be affected by changes in the reaction medium (solvent medium) environment ranging from compressed liquid to near-critical to supercritical conditions. Nevertheless, at the highest temperature of 260 °C, where the density is closest to gas-like medium, the influence of density-dependent properties are likely outweighed by the impact of temperature on the kinetics of undesired reaction rates (methanation, hydrogenation, and water gas shift reactions).

### 3.2.2 Effect of Pressure on Hydrocarbon Distribution.

The influence of reaction pressure on the hydrocarbon distribution was also studied according to the scenario illustrated in Fig. 4. At a pressure lower than the critical pressure of the reaction mixture ($P_1$ =35 bar), and in the region of gas-like density, the overall distribution favors the productions of heavy hydrocarbons with high chain growth probability ($\alpha_{hp}$ = 0.849) as illustrated in Fig. 10$a$. Significant deviations from the ASF model are observed in the middle hydrocarbons range ($C_2$-$C_{10}$), illustrating a very high chain growth probability. Increasing the pressure to $P_2$ (50 bar), within the supercritical phase region, resulted in a significant drop in heavy hydrocarbon production ($\alpha_{hp}$ = 0.785), with deviations from the standard ASF model also extending to $C_{10}$ as seen in Fig. 10$b$. In the same figure, we can also see that there is a high chain growth probability in both the light and middle distillate hydrocarbon range. As discussed earlier (Fig. 9$c$), under the baseline conditions of 65 and 250 °C the deviations from ASF extended to $C_{14}$, while the heavy hydrocarbons chain growth probability slightly decreases to 0.781. Upon increasing the pressure to 80 bar (liquid-like density), no significant change in heavy hydrocarbons chain growth probability was observed ($\alpha_{hp}$ = 0.801), however the deviations from ASF in the product distributions are extended to $C_{16}$ as seen in Fig. 10$c$. This illustrates extremely high chain growth probability in the $C_5$-$C_{16}$ range at this high density.

At constant temperature (250 °C), space velocity (93.75 hr$^{-1}$), and syngas ($H_2$/CO) feed ratio of 2/1, we have studied the product distribution in SCH-FTS over broad range of pressures (35-80 bar). It is important to mention here that the partial pressure of syngas was kept constant at 20 bar, while the hexane partial pressure was varied to achieve the desired total pressure. The bed residence time (defined as the volume of feed at the applied pressure passing through the volume of the catalyst bed per second) was changed as a result of varying the total pressure. Predictions of the bed residence times at the conditions studied were performed based on density calculations at the specified temperature and pressure for a mixture composed of 75 mol% hexane, 16.7 mol% $H_2$, and 8.3 mol% CO. The density of this mixture was determined by using the Peng-Robinson equation of state (with kij = 0) in a flash calculation in ICAS Version V software. The volumetric flow rate of the mixture was then obtained from the multiplication of the density with the total molar flowrate (hexane and syngas). Finally, the contact time was estimated by dividing the volume of the catalyst bed by the volumetric flowrate. The contact times were found to vary from 5.3s at 35 bar, 12.1s at 65, to 15.7s at 80 bar. The overall product distribution ($\alpha_{overall}$) and heavy product distribution ($\alpha_{hp}$) was found to be less affected by contact time in the range of 50 bar to 80 bar. However significant changes with regards to the deviation from the ASF model within the middle distillate hydrocarbons are observed as the pressure increases from the gas-like density range (35 bar) to the liquid-like density range (80 bar). The bed-residence time (affected by the total pressure) is believed to influence the dynamic adsorption/desorption equilibrium of the FTS primary products (mainly $\alpha$-olefins) allowing higher probability towards the readsorption process.

### 4. Conclusions

The analytical results of this study demonstrates significant deviations of the hydrocarbon distributions from the ASF model when the FTS reaction is conducted in a near-critical and supercritical hexane medium over an alumina supported cobalt catalyst. The degree of these

37

deviations from the standard ASF model was found to be related to the physical properties of the reaction mixture as the medium is shifted from near-critical conditions to supercritical conditions by simply tuning the reaction temperature and pressure.

Rather than a single chain growth probability ($\alpha$-value) for the product distribution as in the standard ASF model, three distinct chain growth probabilities ($\alpha_{lh}$, $\alpha_{md}$, and $\alpha_{hp}$) are required to accurately represent the product distributions obtained in the SCH environment. Multiple chain-growth probabilities of the FTS product distributions are not the innovation of this study, since numerous studies have reported the existence of more than one $\alpha$-value in certain FTS product distributions. Nonetheless, this study reports an interesting phenomenon within the middle hydrocarbon product range of the distributions indicating a unique deviation from ASF behavior with a relatively very high $\alpha$-value ($\alpha_{md}$ .0.95) owing to enhanced incorporation of olefins in the SCH medium. The extent to which the middle distillate compounds incorporate in the chain growth and hence deviate from standard ASF is strongly related to the physical properties of the reaction mixture (gas-like properties vs. liquid-like properties) under the specified reaction temperature and pressure. This phenomenon is attributed to the enhanced solubility of heavy products in the dense medium yielding vacant sites made available by supercritical solvent phase. Such an environment has a significant impact on the dynamic adsorption/desorption equilibrium of active species inside the catalyst pores.

## 5. Publications and Presentations (October 2003-April 2004)

1.  Huang X. , N. O. Elbashir and  C. B. Roberts "Supercritical fluid Fischer
-Tropsch synthesis; Influence of Solvent and Reaction conditions." *Ind. Eng. Chem. Res*. **In press** (2004).
2.  Elbashir, N. O. and C. B. Roberts (2004). "Reaction pathway and kinetic modeling of Fischer-Tropsch synthesis over an alumina supported cobalt catalysts in supercritical-hexane." *Preprints of Symposia, Fischer-Tropsch: Materials, Theories, and Practice. American Chemical Society, Division of Petroleum Chemistry* **49**(2): 157-160.
3.  Elbashir, N. O. and C. B. Roberts (2004). "Enhanced Incorporation of alpha-olefins in the Fischer-Tropsch Synthesis Chain-growth Process over an Alumina Supported Cobalt Catalyst in Near-critical and Supercritical Hexane Medium." *Ind.  Eng. Chem. Res*. **Submitted.**
4.  Elbashir, N. O. and C. B. Roberts (2004). "Non-ideal behavior in kinetics modeling of supercritical-phase Fischer-Tropsch synthesis." **to be submitted** to *Fuel Processing Technology* May 2004.
5.  Elbashir, N. O. and C. B. Roberts (2004). Kinetics model of Fischer-Tropsch synthesis over an alumina supported cobalt catalyst in supercritical hexane medium. Fischer-Tropsch: Material, Theories, and Practice; **2004 National Meeting of the American Chemical Society, Anaheim, CA, Division of Petroleum Chemistry, American Chemical Society**, Anaheim CA, March 28-April 1.
6.  Elbashir N. O. **,** Huang X.,   Boroughs D., and Roberts C. B. (2003) Enhanced hydrocarbon chain-growth in SCF Fischer-Tropsch synthesis:  Experiments & Modeling **AIChE 2003-Annual Meeting**, [546f] - Reactions in Near Critical and Supercritical Fluids I , San Francisco Hilton, CA,  November 16-21.

## 6. Future work

(1) Establish a reaction pathway and chain growth mechanism that explains the consistent non-ASF phenomena observed under the supercritical phase FTS operation and identify the parameters influence this behavior. The purpose of this step is to identify the parameters that can be used to control the FTS product distributions in the supercritical phase.

(2) Cobalt catalysts were known to be more sensitive towards the pressure than iron catalysts. The performance of cobalt catalysts in FTS is highly influenced by the cobalt dispersion on the support, pore volume, surface area, and the reduction methods. We have synthesized a number of cobalt catalyst systems by varying properties, such as surface area, pore volume, and cobalt dispersion.  These catalysts will be tested under supercritical phase conditions.

(3) A kinetic model describing the reaction behavior in the supercritical phase FTS process will be developed.  The model will be verified against the experimental results of the cobalt systems under different $H_2$/CO feed ratios and reaction conditions (volumetric space velocity, residence time, temperature, etc.). The purpose of this model is to simultaneously quantify the influence of parameters such as pressure and temperature on the reaction kinetics and on the phase behavior of the reaction mixture.

References

1.      Huang, X., C.W. Curtis, and C.B. Roberts, *Reaction behavior of Fischer-Tropsch synthesis in near critical and supercritical hexane media.* Preprints of Symposia - American Chemical Society, Division of Fuel Chemistry, 2002. **47**(1): p. 150-153.

2.      Huang, X., N.O. Elbashir, and C.B. Roberts, *Supercritical Solvent Effects on Hydrocarbon Product Distributions in Fischer-Tropsch Synthesis over an Alumina Supported Cobalt Catalyst.* Ind. Eng. Chem. Res., 2004. **In press**.

3.      Elbashir, N.O. and C.B. Roberts, *Reaction pathway and kinetic modeling of Fischer-Tropsch synthesis over an alumina supported cobalt catalysts in supercritical-hexane.* Preprints of Symposia, Fischer-Tropsch: Materials, Theories, and Practice. American Chemical Society, Division of Petroleum Chemistry, 2004. **49**(2): p. 157-160.

4.      Elbashir, N.O. and C.B. Roberts, *Enhanced Incorporation of  alpha-olefins in the Fischer-Tropsch Synthesis Chain-growth Process over an Alumina Supported Cobalt Catalyst in Near-critical and Supercritical Hexane Medium.* Industrial & Engineering Chemistry Research, 2004. **submitted**.

5.      Huang, X. and C.B. Roberts, *Selective Fischer–Tropsch synthesis over an Al2O3 supported cobalt catalyst in supercritical hexane.* Fuel Processing Technology, 2003. **83**: p. 81-99.

6.      Elbashir, N.O., X. Huang, and C.B. Roberts. *Utilization of Supercritical Phase in Fischer Tropsch over Alumina supported Cobalt Catalysts*. in *Gordon Research Conference 'Hydrocarbon Resources'*. 2003. Ventura, Los Angeles, CA Jan 12-17.

7.      Elbashir, N.O., X. Huang, and C.B. Roberts, *Optimization of Fischer-Tropsch Synthesis Under Supercritical Fluids Conditions:Solvent Effects on Reaction Performance*. 2003,

Consortium of Fossil Fuel Science, US Department of Energy, Contract No. DE-FC26-02NT41594. p. 31-52.

8.      Hurlbut, R.S., I. Puskas, and D.J. Schumacher, *Fine details on selectivity and kinetics of the Fischer-Tropsch synthesis over cobalt catalysts by combination of quantitative gas chromatography and modeling.* Energy & Fuels, 1996. **10**: p. 537-545.

9.      Kellner, C.S. and A.T. Bell, *The kinetics and mechanisms of carbon monoxide hydrogenation over alumina-supported ruthenium.* Journal of Catalysis, 1981. **70**(2): p. 418-32.

| 1 | Variable volume cell | 6 | Injection port | PG | Pressure generator |
|---|---|---|---|---|---|
| 2 | Movable piston | TC | Temperature controller | SP | Syringe pump |
| 3 | Viton O-Rings | P | Pressure indicator | MS | Magnetic stirrer |
| 4 | Stir bar | PC | Computer | FRL | Fluorescent ring light |
| 5 | Quartz window | VC | Video camera | | |
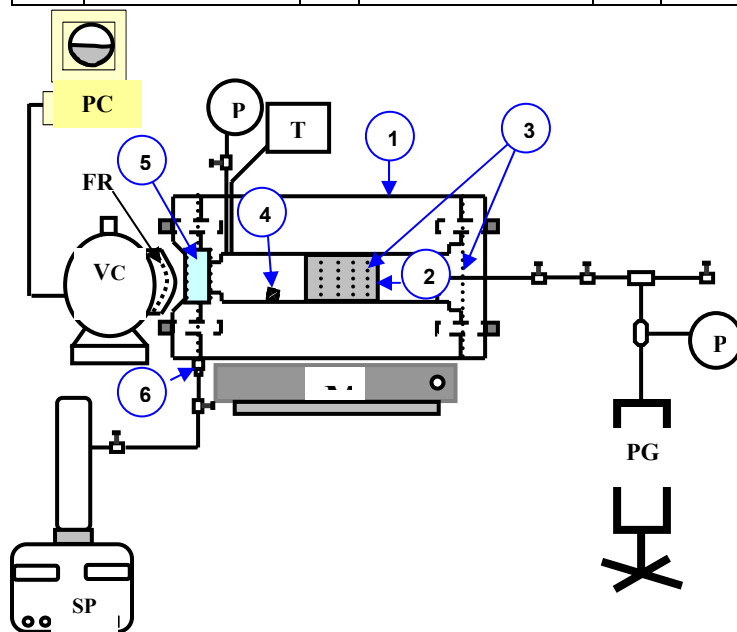


**Figure 1** Variable volume view cell (VCCC) apparatus for phase behavior and critical property measurements.
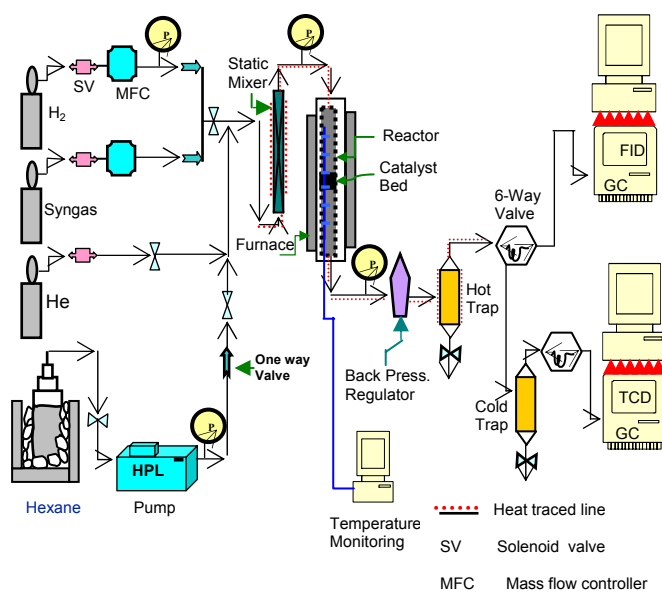


**Figure 2 H**igh pressure Fischer-Tropsch synthesis reactor and analysis system.
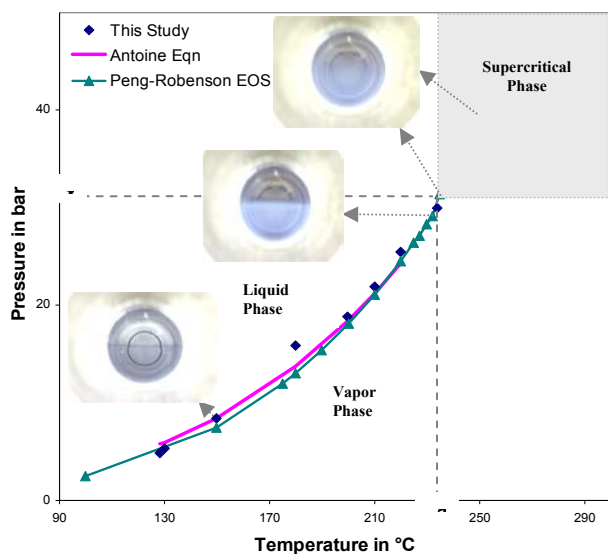
**Fig. 3** Vapor-liquid coexistence curve and critical point loci of the pure solvent hexane as measured using the VVVC (symbols) compared to phase behavior estimated from Peng-Robinson EQS, and Antoine equation (lines). Images show the phase transition from vapor-liquid-equilibrium to the supercritical phase.
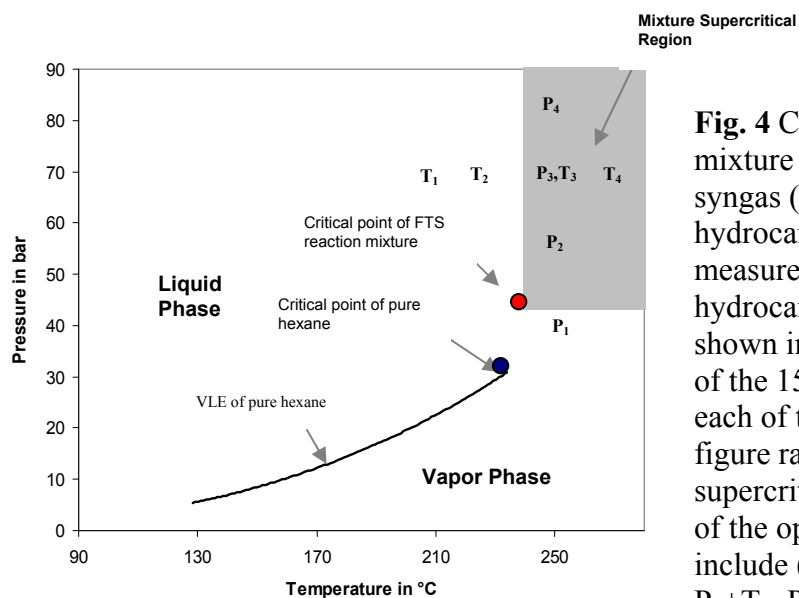


**Fig. 4** Critical point loci of a FTS reaction mixture composed of hexane 75 mole%, syngas (CO and $H_2$) 5 mole%, hydrocarbons and water (20%) as measured using the VVVC. The hydrocarbon products distribution is shown in Table 1. The FTS performance of the 15% $Co/Al_2O_3$ was measured at each of the operating points shown in the figure ranging from near-critical to the supercritical conditions. The combination of the operating temperature and pressure include ($P_1+T_3$, $P_2+T_3$, $P_3+T_3$, $P_4+T_3$, $P_3+T_1$, $P_3+T_2$, $P_3+T_3$, $P_3+T_4$).
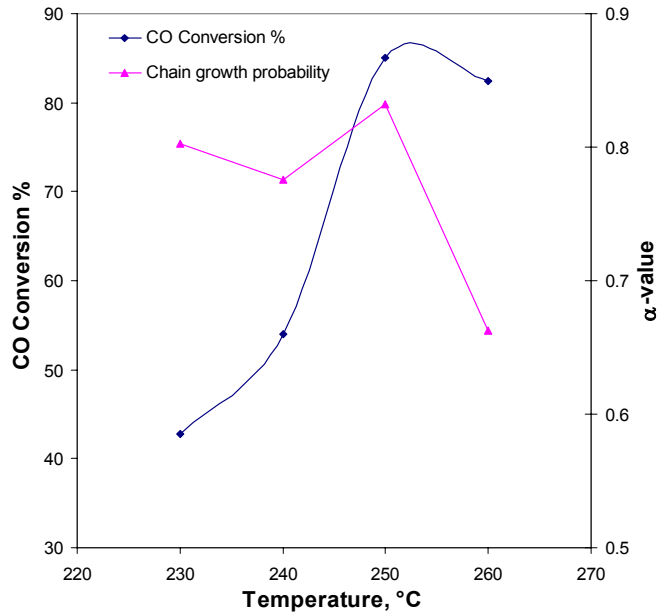
**Fig. 5** Effect of reaction temperature on CO conversion and chain-growth probability ($\alpha$-value) at a total pressure of 65 bar and syngas/hexane molar ratio of 1/3.
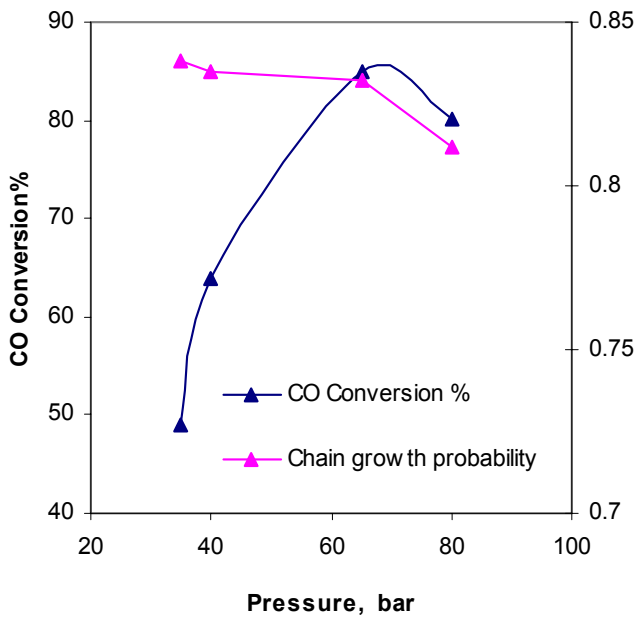


**Fig. 6** Effect of reaction pressure on CO conversion and chain-growth probability ($\alpha$-value) at a total pressure of 65 bar and syngas/hexane molar ratio of 1/3.
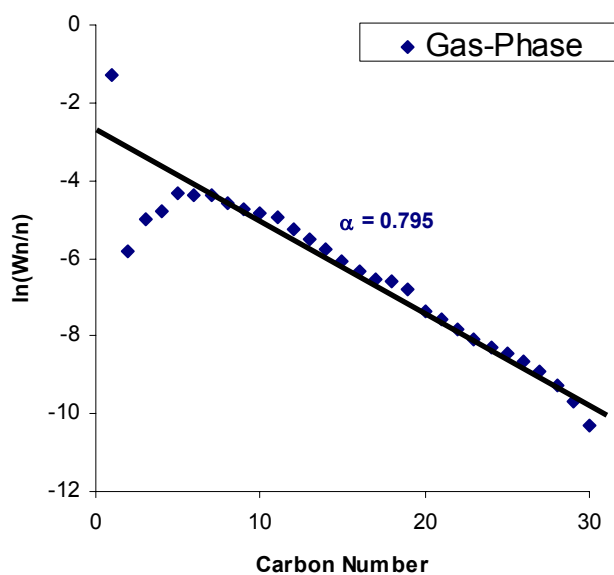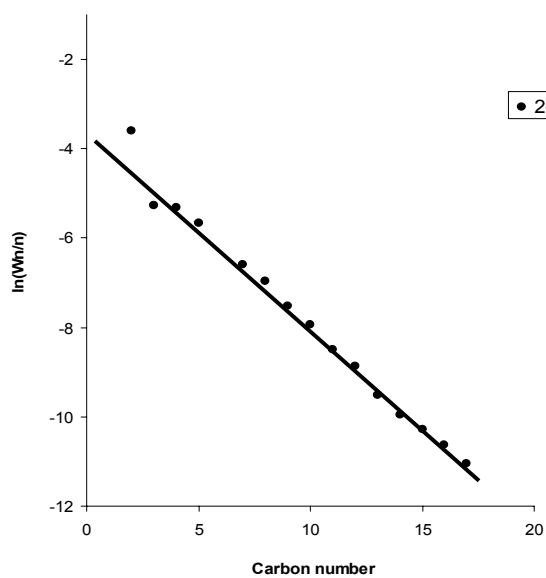
**Fig. 7** Hydrocarbon product distribution from gas-phase FTS at 50sccm/$g_{cat}$ syngas flowrate, T= 250 °C , $P_{total}$ = 20 bar, and $H_2$/CO feed ratio = 2.
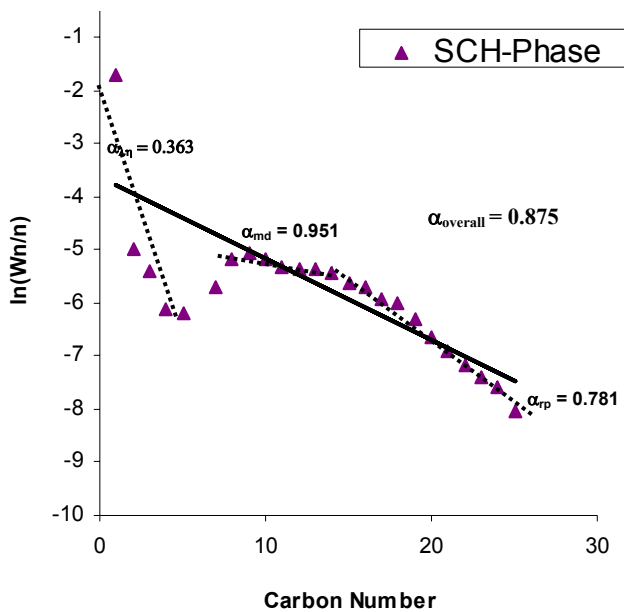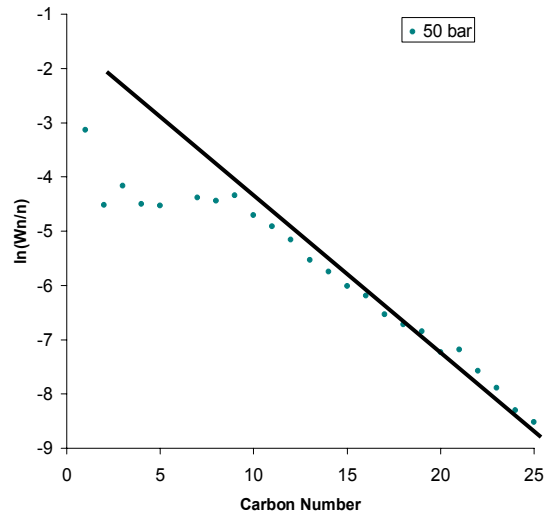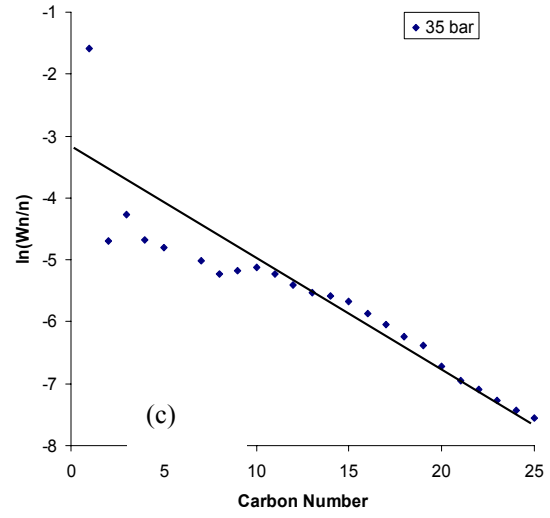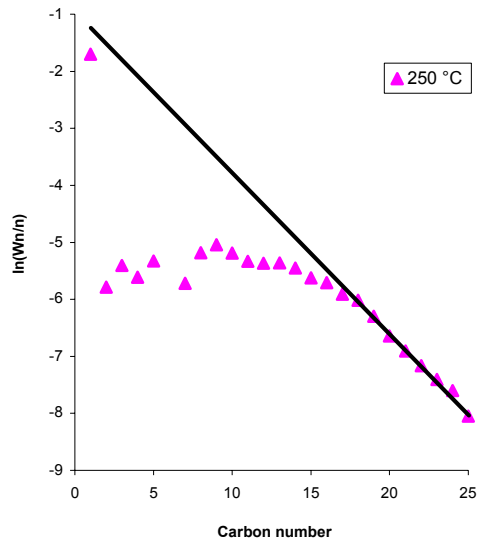


**Fig .8** Hydrocarbon product distribution from SCH-FTS at 65 bar T= 250 °C, syngas flowrate = 50 sccm/ $g_{cat}$, hexane flowrate =1.0 ml/min, and $H_2$/CO feed ratio = 2.

(a)



(b)
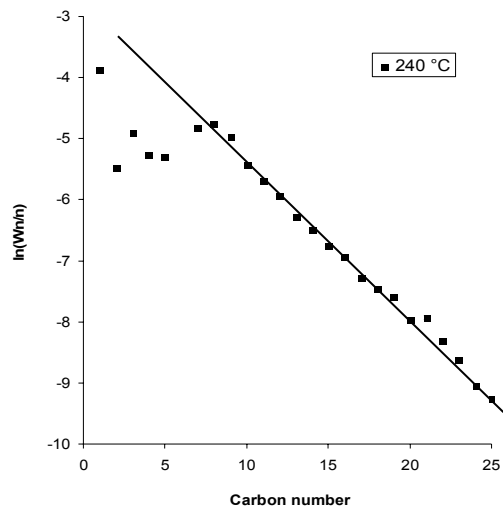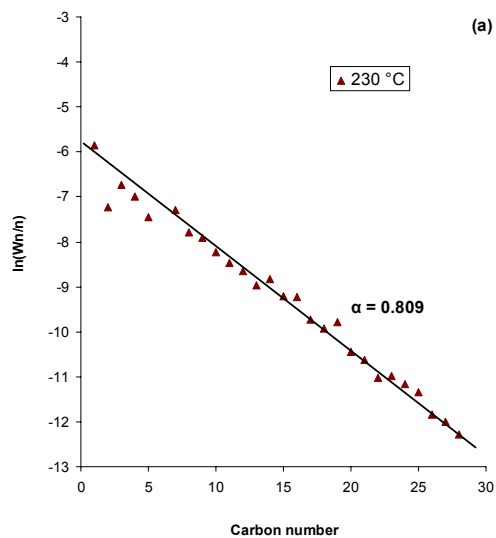
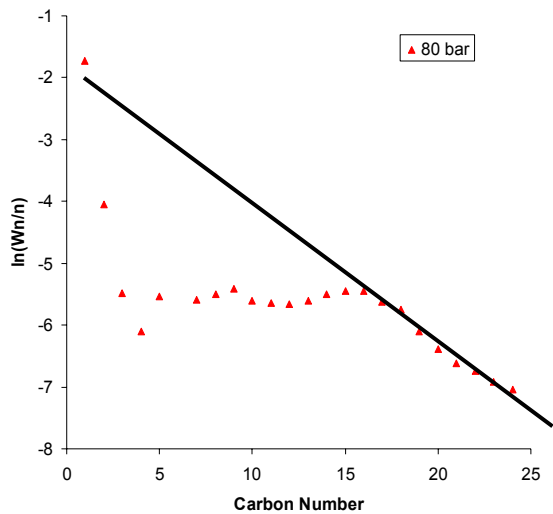**Fig. 9** Hydrocarbon product distribution from SCH-FTS at 65 bar and (a) $T_1$= 230 °C, (b) $T_2$=240 °C, (c) $T_3$=250 °C, and (d) $T_4$=260 °C. Reaction conditions; 50 sccm/ $g_{cat}$ syngas flowrate, 1.0 ml/min hexane flow rate, and $H_2$/CO feed ratio = 2.



(d)

(a)



(b)

(c)

**Fig. 10** Hydrocarbon product distributions in SCH-FTS reaction at 250 °C and (a) $P_1$= 35 bar, (b) $P_2$=50 bar, (c) $P_3$=80 bar. Reaction conditions; 50 sccm/$g_{cat}$ syngas flowrate, 1.0 ml/min hexane flow rate, and $H_2$/CO feed ratio = 2.

(c)

# Development of Activated Carbon Supported Molybdenum Promoted Catalysts for Diesel Fuel Synthesis

Wenping Ma, Edwin L. Kugler, Huifang Shao, James Wright and Dady B. Dadyburjor

Department of Chemical Engineering
West Virginia University
Morgantown, WV 26505

## I.  Introduction

It is well known that the Fischer-Tropsch Synthesis (FTS) provides an alternative way to convert coal indirectly to transportation fuels. The traditional industrial catalysts used for this reaction are precipitated iron or cobalt supported on silica, which initially appeared in the FTS plant in Sasol, South Africa and Malaysia [1-2]. These two types of FTS catalysts have been famous for optimal production of high-molecular-weight hydrocarbons, which need to be further treated (by isomerization and hydrocracking) to yield liquid diesel fuels. In order to simplify the conventional FTS technology and to lower the capital cost of the diesel fuels,  selective FTS catalysts have been suggested, on which medium-molecular weight hydrocarbons (mainly diesel fuels) expect to be directly formed from syngas [3-4]. Hydrocarbon chain growth can be limited over iron and cobalt catalysts supported on cheap activated carbon (AC) and on carbon nanotube supports, indicating that carbon material may be a good choice for limiting hydrocarbon chain length to a certain range.

We have been working on AC-supported Mo catalysts since 1991. Mo-Ni/AC catalysts have been successfully used for synthesis of high-molecular-weight alcohols  [5, 6]. These studies also demonstrated that AC-supported catalysts are able to produce hydrocarbons with limited carbon numbers, e.g. less than $C_6$. In the current work, we focus on molybdenum-promoted AC-supported iron catalysts for the synthesis of liquid hydrocarbons. The effects of molybdenum on catalyst activity, selectivity and stability as well as on oxygenate product distribution have been determined.

## II. Experimental

Catalyst Synthesis. Table 1 lists the catalysts synthesized during this reporting period. Mo-promoted metal catalysts (Fe, Co, Ni) were prepared using sequential incipient-wetness impregnation over activated carbon (AC) purchased from Aldrich. Three distinct steps are consisted in the preparation. After the received AC was washed by hot distilled water and calcined at $500^o$C for 2 h by flowing $N_2$, ammonium molybdenum solution was impregnated on the carbon. This was followed by drying in air at 90-$100^o$C overnight. Iron nitrate, copper nitrate, nickel nitrate or cobalt nitrate solutions were then impregnated on the prepared Mo/C samples, and this was followed by drying in air at 90-$100^o$C overnight. Potassium nitrate solution was the last one to be impregnated on the samples, and this was again followed by drying in air at 90-$100^o$C overnight. The synthesized catalysts contained 0-12% Mo, 15.7 % metals (Fe, Ni or Co) and 0.4-1.0 % K.

Catalyst Testing Catalysts were tested in a computer-controlled fixed-bed reactor system. Detailed description of the reactor system has been published previously [5-6]. In brief, flow rates of syngas (containing an internal gas standard of 5%He), $H_2$ and He are adjusted by three mass flow controllers separately. The feed gas (syngas, $H_2$ or He) is then directed to a 304 SS reactor with an inner diameter of 8 mm and length of 63 cm. After leaving the reactor, gases (including unreacted syngas, $CO_2$, hydrocarbons, water vapor and alcohols) pass through a product trap to condense liquid products, with incondensable gases going to a bubble flow meter or to a GC for on-line analysis. Gas and liquid products are analyzed by two GCs (HP-5890 and Varian 3400) using packed and capillary columns.

The catalyst amount used in each test is 1.0 g (20-40 mesh). To minimize axial temperature gradients, the catalyst is diluted with the same-sized quartz chips before loading the reactor (dilution ratio was 1:4). The catalyst reduction conditions were 400$^o$C, 76 psig, and 3 Nl/g-cat/h for 12-16 h by $H_2$, and reaction conditions were 310-350$^o$C, 300 psig, 3 Nl/g-cat/h, and $H_2$/CO = 0.9.

### III. Results and Discussion

Major results on the Mo-Fe/AC catalysts are discussed below. For convenient discussion, we focus on Catalysts A, B and C of Table 1. Note that all three contain 15.7 Fe/0.8 Cu/0.9 K/AC, but Catalyst A contains no Mo, Catalyst B contains 6 Mo and Catalyst C contains 12 Mo.

Figure 1 shows the CO conversion with time on stream (TOS) for the three catalysts. The conversion over Catalyst A decreased significantly (97 –51%) during 72 h of testing at 320$^o$C.

Over Catalyst B, CO conversion increased with TOS, reaching 90.9% at 73 h, and then remained nearly stable for the next 71 h, up to a TOS of 144h. At that time, the temperature was decreased to 310$^o$C and maintained at that value up to a TOS of 312h. With the decrease in temperature, there was a sudden drop in conversion, followed by a slower decrease up to a TOS of 240h. Thereafter, up to 312h, the CO conversion was stable at ~76%. When the temperature was increased to return to 320$^o$C (between 313-360 h TOS), there was a corresponding jump and then a slow increase, and the final value was not too different from the conversion obtained at that temperature at a much lower TOS. When the temperature was again decreased to 310$^o$C (after TOS = 360h) again the steady-state conversion was not too different from that at that temperature at the lower TOS.

In the case of Catalyst C, the CO conversion quickly reached 64% at 5 h (320$^o$C), and then it decreased slowly but steadily with TOS. At TOS = 144h, the temperature was decreased to 310$^o$C. AS in the previous case, there was a sharp drop, but now the conversion continued steadily downward until the run was stopped at 215 h.

Figure 1 indicates that small amounts of Mo significantly improve catalyst activity and stability but loading excess Mo results in lower (and decreasing) conversion rates.

Representative overall hydrocarbon productions of the Mo-Fe/AC catalysts are shown in Fig. 2. The hydrocarbon distribution up to $C_{34}$ can be nearly described by the Anderson-Schulz-Flory (ASF) distribution ($Wn/n = \alpha^{n-1}[1-\alpha]^2$) with a single value of $\alpha$ . This information reflects that the chain-growth mechanism on the Mo-Fe/AC catalysts may be not the same as that on precipitated iron catalysts [7], which may have so-called double-$\alpha$ hydrocarbon distributions.

Changes in the selectivities of $CH_4$ and light hydrocarbons ($C_2$-$C_4$) with TOS are shown in Figures 3 a-b. The Mo loading affects $CH_4$ and light hydrocarbon selectivities, but in a nonlinear fashion. After addition of Mo (6 wt.%), $CH_4$ selectivity for Catalyst B is higher that that (6-8%) for Catalyst A (0% Mo). However, the selectivity for Catalyst B is almost similar to that for Catalyst C (12 wt% Mo), 11.4 compared with 12.6%. For $C_2$-$C_4$ selectivities, again Catalysts B and C behave similarly, but now these values (40-43 %) are lower than those for Catalyst A (40-48%).

The compositions of liquid aqueous product were quantified using internal standards. Table 2 lists the oxygenate productivity and their compositions in the aqueous product over the three catalysts. The internal chemical was tert-amyl alcohol. The water content in the aqueous phase was determined to be 74-83% under all conditions. The oxygenates consist of $C_1$-$C_5$ alcohols, acetone, acetaldehyde and $C_3$-$C_5$ branch alcohols. Ethanol is the dominant alcohol (57–64%) followed by propanol (16-17.5%), methanol (5.5-12%), and butanol (4-5.4%). The addition of Mo increases oxygenate productivity. Mo also changes alcohol distribution. It enhances methanol and $C_3$-$C_5$ alcohols selectivity, whereas it has an opposite effect on ethanol selectivity.


### IV. Conclusions

In summary, AC supported iron catalyst shows high initial activity, but its deactivation rate is also high. Catalyst stability is improved significantly after addition of molybdenum into the Fe/AC catalysts, but activity is suppressed dramatically, especially when Mo loading is over 6%; Also $CH_4$ selectivities on the molybdenum-iron catalysts are increased compared with the Fe/AC catalyst. Hydrocarbons up to $C_{34}$ can be detected on the Fe/AC and Mo-Fe/AC catalysts. Mo also affects oxygenate formation rate and alcohol selectivity. Addition of Mo (6-12 wt.%) increases oxygenate productivity. It decreases ethanol selectivity, whereas it improves $C_1$-, $C_3$-$C_5$-alcohol selectivities.


### V. Paper Presented or Published

None


### VI. Future Work

We will focus on optimizing catalyst composition so that $CH_4$ and gaseous selectivities can be decreased further, while improving $C_5^+$ selectivity. Catalyst activity and stability need to be improved. BET, TPR/TPD, XRD, and SEM will be used to characterize the fresh and used catalysts (texture properties, metal phases, metal size and morphology) so that we may explain catalyst performance (including chain growth mechanism) from characterization information. Also we will do more tests with different Mo-Ni/AC catalysts and catalysts prepared from different types of AC.


### VII.   References

[1]  Dry M. E. *Catal. Lett.* 1991, 7: 241.

[2]  Eilers J., Posthuma S. A., Sie S. T. *Catal. Lett.* 1991, 7: 253.

[3]  Venter J. J., Kaminsky M., Geoffroy G. L., Vannice M. A. *J. Catal.* 1987, 103: 450.

[4]  Steen E. van, Prinsloo F. F. *Catal. Today* 2002, 71: 327.

[5]  Kugler, E.L., Feng, L., Li, X., Dadyburjor, D.B. *Studies in Surface Science and Catalysis.* 2000, 130A: 299-304.

[6]  Li, X.G., Feng, L.J., Liu, Z.Y., Zhong, B., Dadyburjor, D.B., Kugler, E.L. *Ind. Eng. Chem. Res.* 1998, 37, 3853.

[7]  Donnell T.J., Satterfield C.N., *Appl. Catal. A* 1989, 52: 93.

## Table 1 List of Activated Carbon Supported Diesel Catalysts

| No. | Composition: atom weight % (atom ratio) | Size/mesh | Dried | Tested | Comment |
|---|---|---|---|---|---|
| 1 | 5%Mo/20%Ni/0.25%K (1:6.54:0.12)/AC1 | 20-40 | 100-105, 8h | No | |
| 2 | 5%Mo/20%Ni/0.25%K (1:6.54:0.12)/Al$_2$O$_3$ | 20-40 | 100-105, 8h | No | |
| 3 | 12.3%Mo/4.45%Ni/5.97%K (1:0.6:1.2)/AC1 | 20-40 | 100-105, 8h | No | |
| 4 | 15%Mo/5%Co/0.4%K (1:0.54:0.07)/AC1 | 20-40 | 100-105, 8h | No | |
| 5 | 15%Mo/5%Co/0.4%K (1:0.54:0.07)/AC2 | 20-40 | 100-105, 8h | No | |
| 6 | 4%Mo/20%Co/0.4%K (1:8.14:0.25)/AC1 | 20-40 | 100-105, 8h | No | |
| 7 | 4%Mo/20%Co/0.4%K (1:8.14:0.25)/AC2 | 20-40 | 100-105, 8h | No | |
| 8 | 12%Mo/20%Co/0.42%K (1:2.71:0.09)/AC2 | 20-40 | 100-105, 8h | No | |
| 9 | 15.7%Mo/0.41%K (1:0.06)/AC2 | 20-40 | 100-105, 8h | Yes | |
| 10 | 1.33%Mo15.7%Ni/0.41%K (1:19.2:0.75)/AC2 | 20-40 | 100-105, 8h | Yes | |
| 11 | 15.7%Fe/0.79%Cu/0.94%K (1:0.04:0.09)/AC2 | 20-40 | 100-105, 8h | Yes | Catalyst A |
| 12 | 6%Mo/15.7%Fe/0.79%Cu/0.94%K (0.22:1:0.04:0.09)/AC2 | 20-40 | 100-105, 8h | Yes | Catalyst B |
| 13 | 12%Mo/15.7%Fe/0.79%Cu/0.94%K (0.44:1:0.04:0.09)/AC2 | 20-40 | 100-105, 8h | Yes | Catalyst C |
| 14 | 12%Mo/15.7%Ni/0.94%K (0.46:1:0.09)/AC2 | 20-40 | 100-105, 8h | No | |
| 15 | 6%Mo/15.7%Ni/0.94%K (0.24:1:0.09)/AC2 | 20-40 | 100-105, 8h | No | |
| 16 | 15.7%Ni/0.94%K (1:0.09)/AC2 | 20-40 | 100-105, 8h | No | |

## Table 2 Oxygenate Selectivity Comparison

| Catalyst [a] | A | B | | C | |
|---|---|---|---|---|---|
| | | | | AC Supported | |
| Temperature (°C) [b] | 320 | 320 | 310 | 320 | 310 |
| TOS (h) | 25 - 72 | 49 - 144 | 145 - 288 | 48 - 143 | 144 - 215 |
| CO Conv. (%) | 88 - 51 | 82-93 | 84 - 74 | 58 - 53 | 43 - 39 |
| H$_2$ Conv. (%) | 68 - 41 | 65-77 | 67 - 59 | 46 - 44 | 36 - 34 |
| Productivity g OXY/kg-cat/h | 3.8 -2.2 | 9.9 - 12.7 | 9.5 - 10.3 | 9.5 - 10.3 | 7.3 - 9.1 |
| Ave. oxygenate Select. (wt. % basis) | | | | | |
| CH$_3$OH | 5.5 | 6.7 | 8.5 | 12.3 | 12.1 |
| 1-C$_2$H$_5$OH | 64.4 | 61.7 | 59.1 | 57.1 | 58.6 |
| 1-C$_3$H$_7$OH | 17.0 | 16.9 | 16.1 | 17.5 | 17.1 |
| 1-C$_4$H$_9$OH | 4.0 | 4.4 | 4.1 | 5.4 | 5.3 |
| 1-C$_5$H$_{11}$OH | 1.1 | 1.0 | 0.8 | 1.6 | 1.5 |
| Other oxygenates[c] | 8.0 | 9.3 | 11.4 | 6.0 | 5.5 |

(a) Catalyst compositions in Table 1
(b) Other reaction conditions: 3 Nl/g-cat/h, 300 psig, H$_2$/CO=0.9
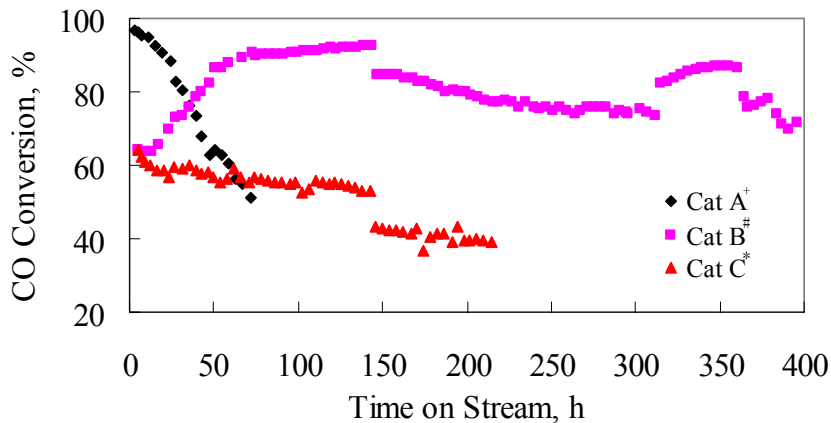(c) Including acetone, acetaldehyde and C$_3$-C$_5$ branch alcohols.

Figure. 1. Change of CO conversion with time on stream. Catalyst compositions in Table 1. Reaction Conditions: 300 psig, 3Nl/g-cat/h, $H_2/CO = 0.9$. Temperature progression: Cat A - 320 $^o$C; Cat B – 0-144h, 320 $^o$C; 145-312 h, 310 $^o$C; 313-360h, 320$^o$C; 361-396h, 310 $^o$C; Cat. C - : 0-143h, 320 $^o$C; 144-215 h, 310 $^o$C
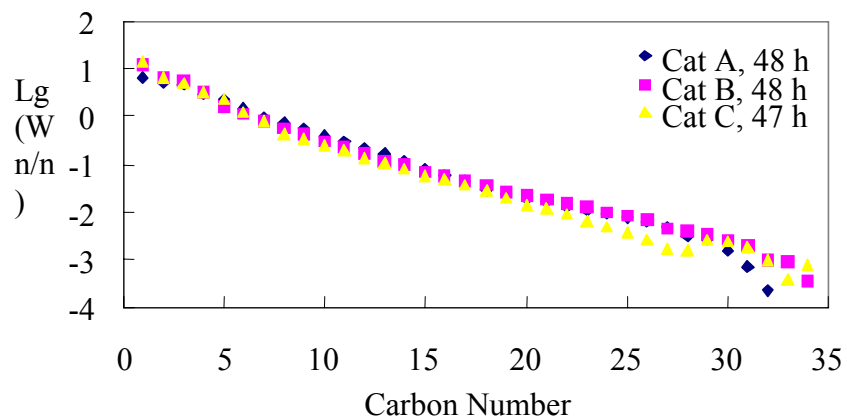


Figure 2. Overall hydrocarbon distribution on Mo-Fe/AC Catalysts. Catalyst compositions in Table 1.
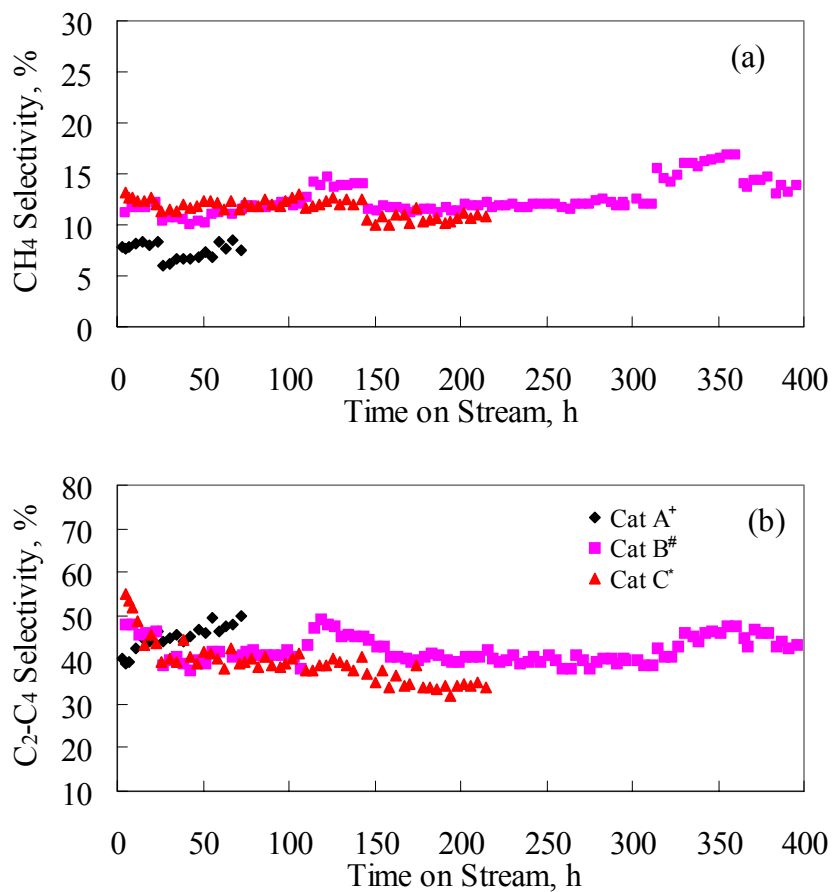
Figure. 3. Change of (a) $CH_4$ selectivity and (b) $C_2$-$C_4$ selectivity with time on stream. Catalyst compositions in Table 1. Reaction Conditions: 300 psig, 3Nl/g-cat/h, $H_2$/CO = 0.9. Temperature progression as in Figure 1

# Production of Light Olefins from Syngas on a Methanol Synthesis – SAPO Hybrid Catalyst System

James A. Guin, Xiwen Huang, Luckner Jean
Auburn University, AL, 36849

## I. Introduction

There are many incentives to promote technology development in the conversion of natural gas and coal to valuable products due to vast worldwide reserves. Production of light C2- C4 olefins via C-1 chemistry is attractive due to its great significance in the production of clean transportation fuels, as well as chemical intermediates for a number of important industrial and consumer products. Methanol conversion to olefins (MTO) is an effective route to produce such value-added products. In previous studies, we have been focusing on the development of various modified SAPO series catalysts for the MTO process, and have found that, many modified SAPO catalysts synthesized in our lab demonstrated excellent reactivity (methanol conversions up to 100%) and selectivities to C2-C4 olefins. The selectivity to C2-C4 olefins was as high as 90% using SAPO-34 and SAPO-18 catalysts with lifetimes of over 30 hrs on stream.

This past 6 months, we focused our research emphasis on the utilization of syngas as the C-1 carbon supply for light olefins production through a Gas-To-Olefins (GTO) concept. The GTO concept is an extension of the MTO process, in which light olefins are produced more directly from syngas in a single step.

There are two synthesis routes for syngas conversion to light olefins, one of which is the conversion of syngas to methanol and then to light olefins via a two-step process. One drawback of this route is the equilibrium limitation caused by the buildup of the product MeOH. Another route is the Fischer-Tropsch synthesis; however this yields a broad spectrum of products, rather than maximizing light olefins. To moderate these problems, we have studied the use of a hybrid catalyst system composed of a commercial methanol synthesis catalyst C-79 (CuO/ZnO/Al2O3) and a SAPO catalyst using both follow-bed and mixed bed systems for syngas conversion. One potential advantage of this system, especially in the mixed bed, is that methanol produced by the C-79 catalyst can be effectively "drained-off" by converting it in-situ to olefins on the SAPO catalyst. This in-situ removal of methanol can minimize the reverse reaction, allowing CO conversion to proceed past the normal methanol equilibrium limit, and the light olefins selectivity may be increased. This route has been proved viable for hydrocarbon synthesis over bi-functional catalysts such as Zr/ZSM-5[1] and Cr-Zn/ZSM-5[2], as well as a physical mixture of Pd/SiO2 and Zeolite[3].

Our research objective is thus focused on the development of an improved reaction pathway to produce light olefins directly from syngas. We have performed a detailed investigation of reaction kinetics by employing various catalysts and varying process parameters to probe the optimal reaction pathway for improved light olefins productivity.

## II. Experimental

*Catalyst preparation and pretreatment*

SAPO-34 catalyst prepared by Dr. P. M. Adekkanattu as reported in our previous publications [4,5] was used in the current study. A commercial MeOH catalyst, C-79, was obtained from SUD-CHEMIE Company with the composition: 55-70% CuO, 20-35% ZnO, 1-15% $Al_2O_3$. A pretreatment of this catalyst was performed as follows: C-79 catalyst was loaded into the reactor, followed by the initiation of 50 sccm $N_2$ flow to dispel air in the reactor, meanwhile increasing the system pressure to 50 psi and temperature to 220 $^o$C at a ramp of 5 $^o$C /min. Once the

temperature and pressure were stabilized, 10 sccm $H_2$ flow was initiated while keeping 50 sccm $N_2$ flowing. The catalyst was reduced by the 15% $H_2/N_2$ mixture at 220 $^o$C, 50 psi for 24 hrs. Following pretreatment, $H_2$ flow was stopped and $N_2$ flow continued to avoid the catalyst being re-oxidized by contacting air.

*Catalyst Loading*

The reactor is an 18" by 0.5" O.D. stainless steel tube with heating elements surrounding it. There are three heating zones along with the length of the reactor at spacings of 3.5". 1 g MeOH catalyst and 0.5 g SAPO catalyst are loaded into heating zones 1 and 3 respectively, which are separated by glass wool. The space between these two catalysts beds is long enough to guarantee a temperature gradient between two catalyst beds. A thermocouple is situated on top of the MeOH catalyst bed to measure catalyst temperature. A reactor diagram is shown in Fig. 1.

*Reaction Procedure*

The CO hydrogenation reaction is performed in a continuous-flow system with a fixed-bed stainless steel reactor. The overall reaction system is shown in Figure 2 and is contained in a fume hood. The flow of $H_2$, $N_2$ and syngas is controlled by two mass-flow controllers (Brooks 5850E). The reactant gases are well mixed and preheated by passing through a static mixer and pre-heater. The reactor is



**Fig 1 Stainless Steel Reactor**

situated in a furnace with three heating zones controlled by three temperature controllers located in an electronics unit. A therm-o-watch has a thermocouple between the reactor and the furnace. If the temperature exceeds an adjustable set point, the power to the electrical box will be shut off. Three types of safety sensors control the flow of power from the box. One sensor detects the pressure drop produced by the fume hood air flow to verify that the hood is operational. Two additional gas sensors detect toxic (CO) and flammable gases. This control system stops the current to the appliances if either of the sensors goes off. This system is designed to allow safe experimentation with carbon monoxide and hydrogen.

     To prevent liquid product condensation, the exit line between the reactor outlet and products collector is wrapped with heating cord to keep the temperature around 200 $^o$C. The effluent heads to a 10" x 9/16" ID Tygon tubing connected to a 50 mL Pyrex gas collection tube with a rubber septum from which samples are taken. The products from the reactor go to a collection tube and bubble flow meter. A back pressure regulator located between the reactor outlet and product collection tube is employed to set and control the reaction system pressure.

     Before the reaction starts, the methanol catalyst C-79 has to be well reduced by 15% $H_2/N_2$ mixture for 24 hrs, and the reaction system pressure and temperature should be stabilized at the designed value for the experiment. Once all the reaction variables are stable, the syngas flow is initiated. The mass flow controller is set to the appropriate value and syngas flow commenced. The reaction is allowed to continue 24-48 hrs depending on the SAPO catalyst deactivation rate, with analysis of products by GC (FID) every 1~2 hrs. When the reaction is halted, the syngas flow is stopped first followed by initiation of $N_2$ flow. The pressure is then reduced to atmospheric pressure slowly, and meanwhile the temperature is reduced to room temperature. The experimental conditions are listed in Table 1.
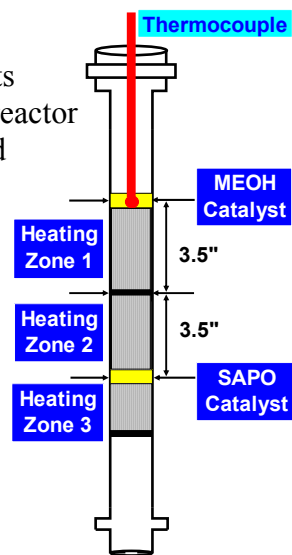
Figure 2.    CO hydrogenation reaction system
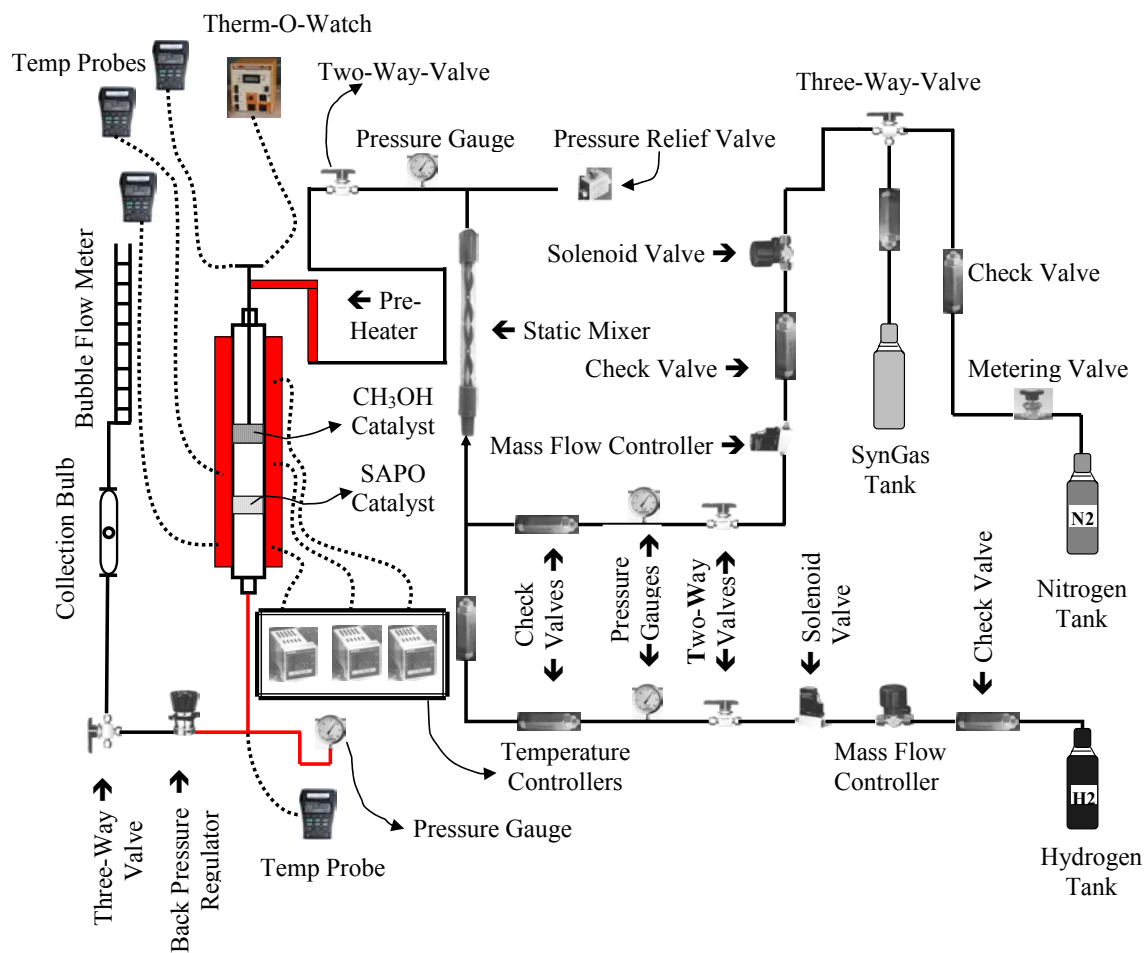
**Table 1  Experimental Conditions**

| Reactor: Stainless steel, D=0.5", L=18" | |
|---|---|
| Catalyst: | CuO/ZnO/Al2O3: 1g;  SAPO-34: 0.5g |
| Syngas flowrate: | 30~75 sccm |
| Syngas Ratio($H_2$/CO): | 0.5~2 |
| Temperature: | Zone 1-2(C-79 catalyst bed): $210 \sim 250^{\circ}C$ |
|  | Zone 3 (SAPO-34 catalyst bed): $350^{\circ}C$ |
| Pressure: | 50 ~300psi |
| Catalyst Pretreatment: | Reducing gas: 15%$H_2$/$N_2$ |
|  | Flowrate: $H_2$: 10sccm, $N_2$: 50sccm |
|  | Pressure: 50psi; Temperature(Zone 1-3 ): $220^{\circ}C$ |
|  | Time: 24hrs |

## III. Results and Discussion

*Comparison of the CO hydrogenation behavior on SAPO-34, C-79 and hybrid C-79/SAPO-34 catalyst systems.*

Figure 3 shows a comparison of catalytic performance over MTO catalyst SAPO-34, methanol synthesis catalyst C-79, and hybrid catalysts C-79/SAPO-34. The CO conversion is obviously higher on the hybrid catalyst than that on C-79 or SAPO-34 catalyst alone. Under steady state, a CO conversion as high as 14% is achieved on hybrid C-79/SAPO34 catalyst; in contrast, SAPO-34 alone does not show much activity in CO hydrogenation, with the total CO conversion only around 2%. C-79, as a commercial methanol synthesis catalyst, demonstrates a relatively high CO conversion, however, as expected most of the product is methanol rather than the desired C2-C4 light olefins, as shown later in Figure 5. In general, Figure 1 shows that high CO conversion results using a hybrid catalyst system in a GTO process with a single reactor.

A high CO conversion alone is not the only goal in the syngas conversion to light olefins process (GTO). The light olefins selectivity must also be taken into account as an important target. A high CO conversion with low C2-C4 light olefins selectivity is not adequate. The C2-C4 olefins selectivity is shown in Figure 4 in the CO hydrogenation process on these three catalysts. Neither SAPO-34 nor C-79 catalyst produces a high C2-C4 olefins selectivity, as only around 2% C2-C4 olefins can be obtained. The maximum C2-C4 olefins gas concentration was only 250 ppm for the C-79 catalyst and only 150 ppm for the SAPO-34 catalyst. This again confirms neither SAPO nor methanol synthesis catalyst alone is adequate as an active catalyst in the light olefins production process from syngas. However, if both catalysts are employed in a hybrid process, the experimental results show that the C2-C4 olefins selectivity can be increased to 20% at a much higher concentration of 6200 ppm. This is a result of the in-situ MTO process. The maximum in olefins production occurs at about 10 hours TOS. The initial increase in production in Fig. 4 is due to the activation period for the MeOH synthesis C-79 catalyst (see Fig. 3) with the decrease in C2-C4 olefins after 10 hrs resulting from the deactivation of SAPO-34, which is typical of SAPO series catalyst.
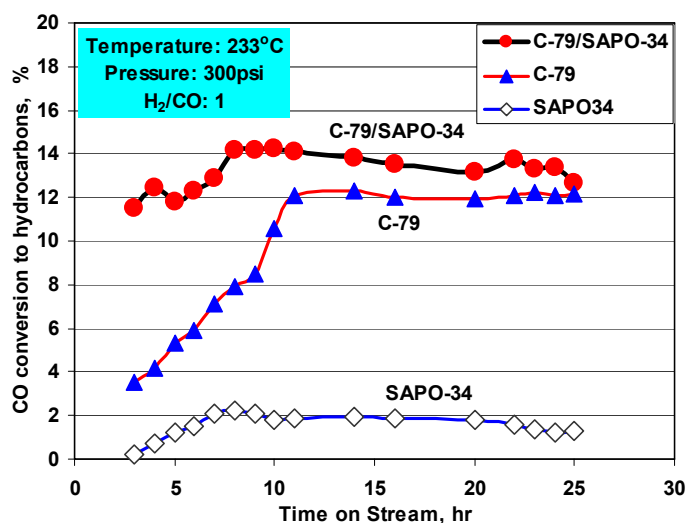


Figure 3. CO conversion to hydrocarbons on SAPO-34; C-79; and C79/SAPO-34
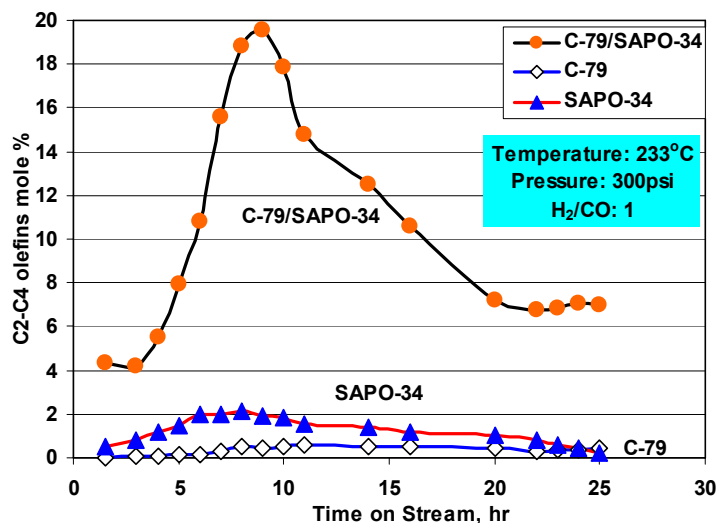
Figure 4.   C2-C4 olefins distribution in CO hydrogenation

58

Figure 5 shows the amount of C in the products per mole CO fed over these three catalysts. One can observe that the SAPO-34 catalyst alone exhibits very little activity in the CO hydrogenation process, as few compounds are produced. For the C-79 catalyst alone, the main product is methanol as expected. In contrast, the hybrid C-79/SAPO34 catalyst system produces larger amounts of valuable products. The C2-C4 olefins productivity accounts for 30% of the total products and the selectivity of undesirable methane also remains relatively low (around 30%). The results from Figures 3, 4, 5, show that C2-C4 light olefins production from syngas can be significantly improved with relatively



Figure 5.   Yields in CO hydrogenation process

high CO conversions by employing a C-79/SAPO-34 hybrid catalyst system. Additional study of process variables such as temperature, pressure, CO/H$_2$ ratio on C-79/SAPO-34 catalyst system performance will be reported in subsequent reports and at the annual meeting.
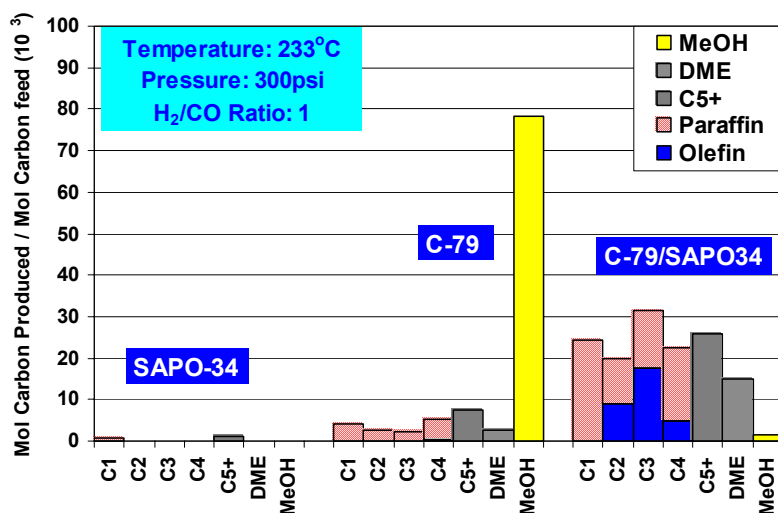
## IV. Conclusions

A hybrid catalyst system consisting of a methanol synthesis catalyst C-79 and MTO catalyst SAPO-34 was employed for syngas conversion to light olefins. The experimental results demonstrate that CO conversions and C2-C4 light olefins selectivity can be significantly increased by employing the hybrid catalyst system as compared to either catalyst alone.

## V. Papers presented or published

1. Xiwen Huang, Luckner Jean, James A. Guin. Selective Synthesis of Light Olefins from Syngas on a Hybrid Catalyst System Composed of a Methanol Synthesis Catalyst and SAPO catalyst ( In preparation).
2. P. Dutta, A. Manivannan, M. S. Seehra, P. M. Adekkanattu, and J. A. Guin, Determination of the Electronic State and Concentration of Nickel in NiSAPO Catalysts by Magnetic Measurements, Catalysis Letters, 94, (3-4), 2004, 181-185.

## VI. Future Work

In our future work we plan to study the effects of several additional process and catalytic variables including crystallite size and metals impregnation on the performance of several SAPO catalysts in methanol conversion. We will also study the development of a novel highly dispersed bimetallic nanoparticle catalyst using mesoporous supports to improve catalytic activity and selectivity in hydrocarbon dehydrogenation processes for hydrogen production.

## VII. References

1. C.D. Chang, W. H. Lang and A. J. Silvestri, J. Catalysis, 56 (1979) 274
2. C.D. Chang, R.F. Socha, J. Catalysis. 90, (1984) 84
3. K. Fujimoto, H. Tominaga, J. Catalysis. 87 (1984), 136
4. Delphine R. Dubois, Daniel L. Obrzut, James A. Guin, Fuel Processing Technology. 83(2003), 203-218
5. Daniel L. Obrzut, Prakash M. Adekkanattu, James A. Guin, React. Kinet. Catal. Lett. 80(1), (2003), 113-121

# Hydrogen production by catalytic dehydrogenation of cyclohexane and methylcyclohexane

Yuguo Wang, Naresh Shah, and Gerald P. Huffman, Consortium for Fossil Fuel Science and
Department of Chemical & Materials Engineering, University of Kentucky

## Introduction

Non-oxidative, catalytic decomposition of hydrocarbons is an alternative, one-step process to produce pure hydrogen. Nanoscale, binary Fe-based catalysts supported on high surface area alumina (0.5 wt.% M-4.5 wt.% Fe/Al$_2$O$_3$, M=Mo, Pd or Ni) have shown high activity for the catalytic decomposition of undiluted methane, ethane, and propane into pure hydrogen and carbon nanotubes[1, 2, 3]. One of the problems with non-oxidative dehydrogenation is coking of the catalyst and reactor due to carbon build up. Under proper reaction conditions, these binary catalysts promote the growth of carbon nanotube (CNT) structures which transports carbon away from the catalyst surfaces, significantly increasing catalyst lifetimes as well as producing a potentially valuable by-product.

It was demonstrated that the structure of the CNT could be controlled by varying the reaction temperature[3], yielding multi-walled CNT above ~650 ºC and stacked cone CNT (SC-CNT) below ~500 ºC. Typical SC-CNT are shown in Figure 1; because of their highly open, corrugated surfaces, we anticipated that these carbon nanostructures might be ideal as catalyst supports.
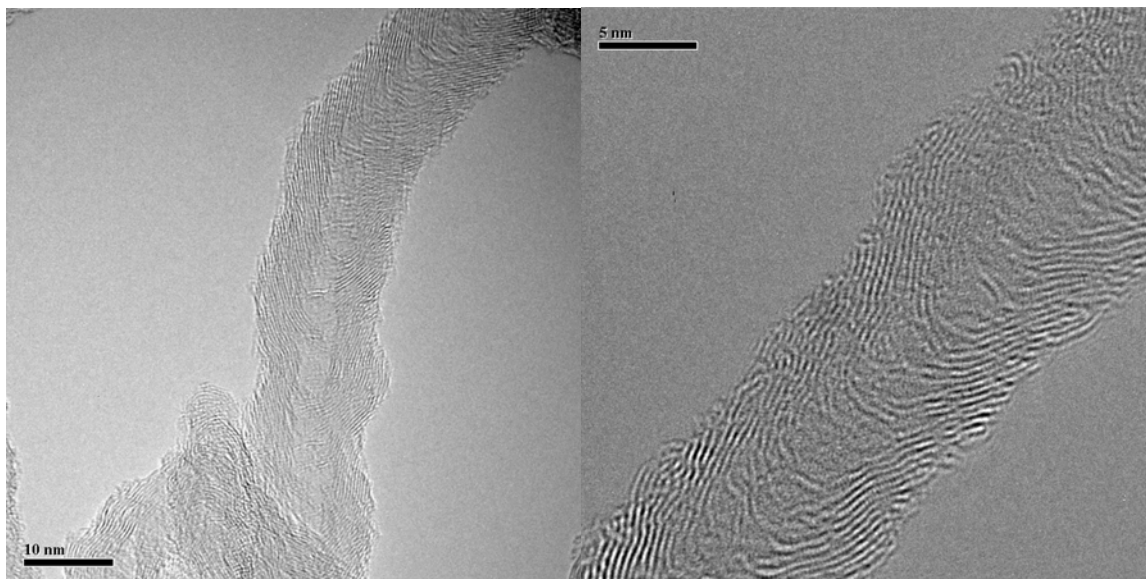


Figure 1. HRTEM images of SC-CNT produced by dehydrogenation of ethane (left) and propane (right) with a Pd-Fe/Al$_2$O$_3$ catalyst at 500 °C and 475 °C, respectively.

To initiate research on the catalytic dehydrogenation of liquid hydrocarbons, we have investigated the partial dehydrogenation of cyclohexane to benzene and methylcyclohexane to

toluene using catalysts consisting of Pt or Pd supported on SC-CNT. Partial dehydrogenation of cyclohexane and methylcyclohexane yields 7.143 and 6.521 weight % hydrogen, respectively, well above the DOE targets of 4.5 weight % by 2005 and 6 weight % by 2010 for hydrogen storage in automotive applications.

**Experimental procedure**

Only SC-CNT produced by ethane decomposition at 500 °C over a (0.5 wt.%Pd-4.5 wt.%Fe)/$Al_2O_3$ catalyst were used as catalyst supports for the work reported in this paper. The SC-CNT were purified by dissolving the high surface area γ-alumina in boiling concentrated NaOH solution for about 2.5 hours. The x-ray diffraction (XRD) patterns in figure 2 show that this purification process is reasonably effective; however, peaks from the $Al_2O_3$ catalyst support are still observed after purification, suggesting that a thin layer of carbon may be protecting some of the alumina from the alkali attack.
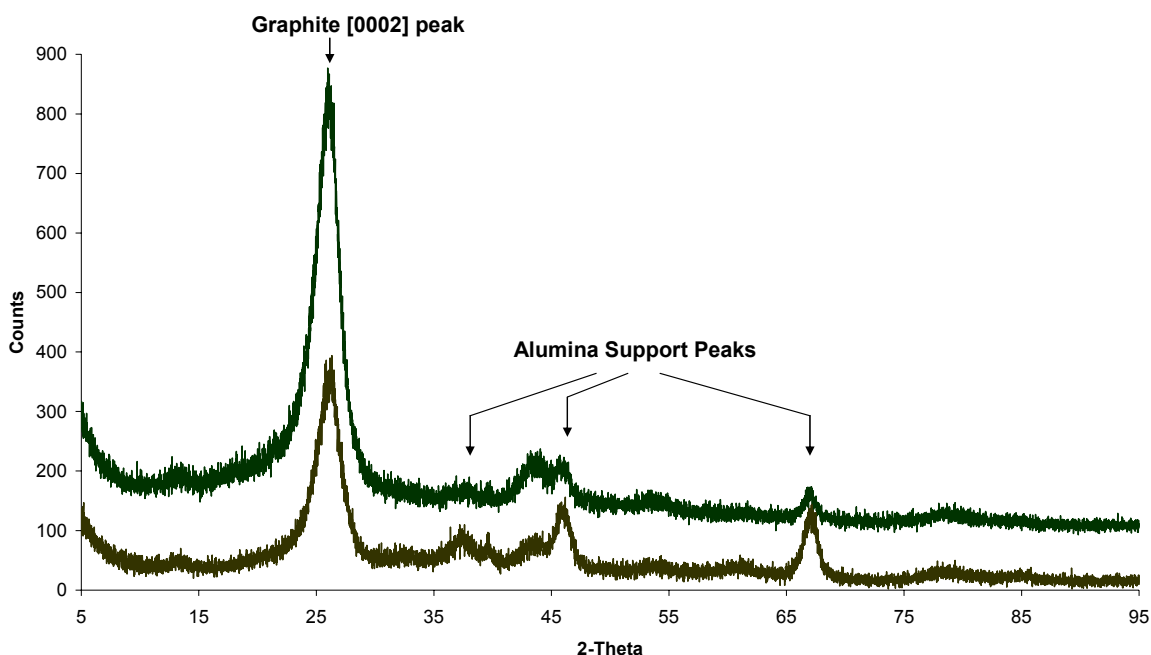


Figure 2. XRD patterns show reduction in the peaks due to the alumina support after purification (top) by boiling the SC-CNT produced by catalytic ethane decomposition in concentrated NaOH.

The purified SC-CNT were impregnated with $Pt(NH_3)_4(NO_3)_2$ solution to prepare the Pt loaded SC-CNT catalysts. Pt/SC-CNT catalysts were prepared with Pt loadings ranging from 0.1 to 1.0 wt%. $Pd(NO_3)_2 \cdot xH_2O$ was used to prepare a 1 wt% Pd/SC-CNT catalyst by the same method. The impregnated catalysts were annealed before use in $N_2$ at a flow rate of 50 mL/min at 500 °C for 12 hours to decompose the metal nitrates. A commercial 1 wt. % Pt/$Al_2O_3$ catalyst was purchased for comparison experiments.

The dehydrogenation experiments for cyclohexane and methylcyclohexane to produce hydrogen were carried out in a fixed bed, plug-flow, stainless steel reactor. Cyclohexane and methylcyclohexane with purities of over 99.5% were purchased from Alfa Aesar. For each run, 0.5 gram of catalyst was used. Prior to reaction, the catalysts were reduced in flowing hydrogen

(50 mL/min) for 2 h at 500 °C.  No methane was produced during this treatment, indicating that the graphitic layers of the SC-CNT do not undergo any gasification under these conditions. After reduction, the reactor was flushed with an inert gas until the GC showed no residual hydrogen peak (~ 15 min.). Liquid cyclohexane or methylcyclohexane were then pumped into the reactor using a syringe pump at a flow rate equivalent to 5 mL/min of gas flow. Since the free energy of the cyclohexane dehydrogenation reaction becomes negative at temperatures over 295 °C, the reactions were carried out at a reactor temperature of 315 °C at atmospheric pressure. The products of the reaction were analyzed online by two GCs with on-line serial sampling valves. The reactor exit stream was carried via a heated transfer line to a GC with a FID detector for the analysis of hydrocarbon products.  Benzene/toluene and cyclohexane /methylcyclohexane were then removed from the gas stream by an online condenser before analysis for the amounts of hydrogen and lower hydrocarbons by a second GC with a TCD detector.

**Results and discussion**

Dehydrogenation of cyclohexane

The results obtained by catalytic dehydrogenation of cyclohexane are shown in figures 3 and 4.  Figure 3 shows the conversion percentage of cyclohexane (molar %) while figure 4 shows the hydrogen production (volume % of product stream), both as a function of time on stream (TOS). Because of the benzene production, hydrogen concentration in the exit stream (even at 100% cyclohexane conversion) cannot exceed 75 volume %.  Results are shown for all of the catalysts prepared in this study, as well as for the commercial 1 wt.% $Pt/Al_2O_3$ catalyst and the SC-CNT with no metal loading.

All of the Pt catalysts exhibit excellent activity, while the Pd/SC-CNT catalyst activity is relatively low.  The activities of the 1wt% $Pt/Al_2O_3$, 1 wt.% Pt/SC-CNT, and 0.25 wt.% Pt/SC-CNT catalysts are nearly identical, producing over 90% conversion of cyclohexane to hydrogen and benzene, with 100% selectivity.  Slight decreases in activity are observed with TOS, with hydrogen production dropping from approximately 74 to 71% over 6.5 hours for the three catalysts.  The 0.1 wt. % Pt/SC-CNT catalyst is only slightly less active, with hydrogen production decreasing from an initial value of 71% to 66% after 6.5 hours TOS.  The order of catalyst activity for conversion of cyclohexane is as follows: 1wt% $Pt/Al_2O_3$ ≈ 1wt% Pt/SC-CNT ≈ 0.25wt% Pt/SC-CNT >0.1wt% Pt/SC-CNT >1wt% Pd/SC-CNT >SC-CNT.

Figure 5 shows transmission electron micrographs of the 1 wt% Pt/SC-CNT catalysts after the cyclohexane dehydrogenation reaction at 315 °C for 6.5 hours.  The Pt particles are ~ 1-2 nm in size and exhibit high dispersion on the SC-CNT support.
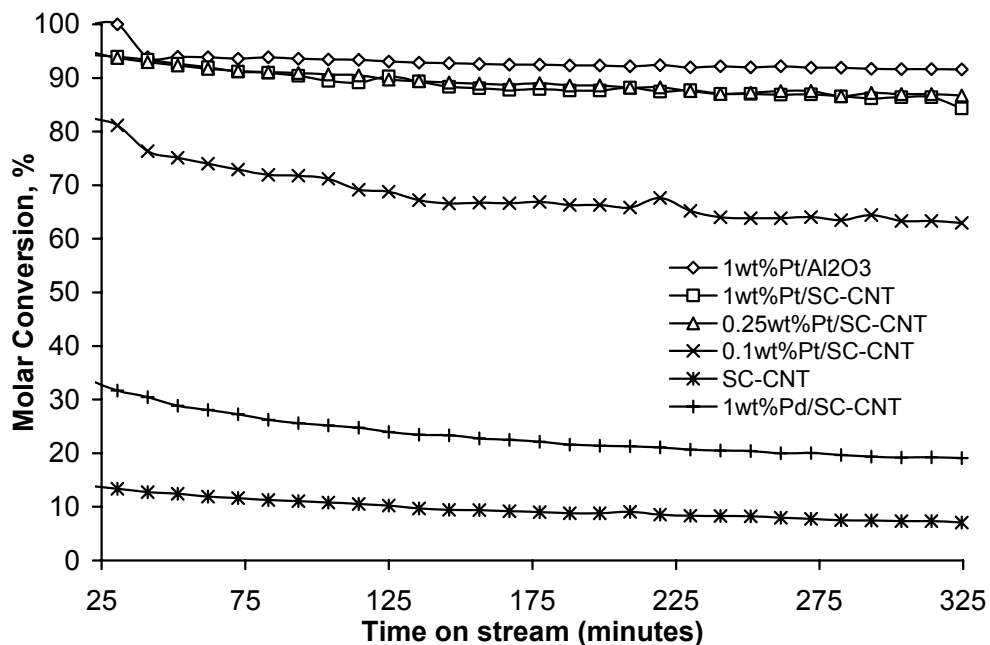
Figure 3. Time on stream molar % conversion of cyclohexane with different catalysts at atmospheric pressure and 315 °C.
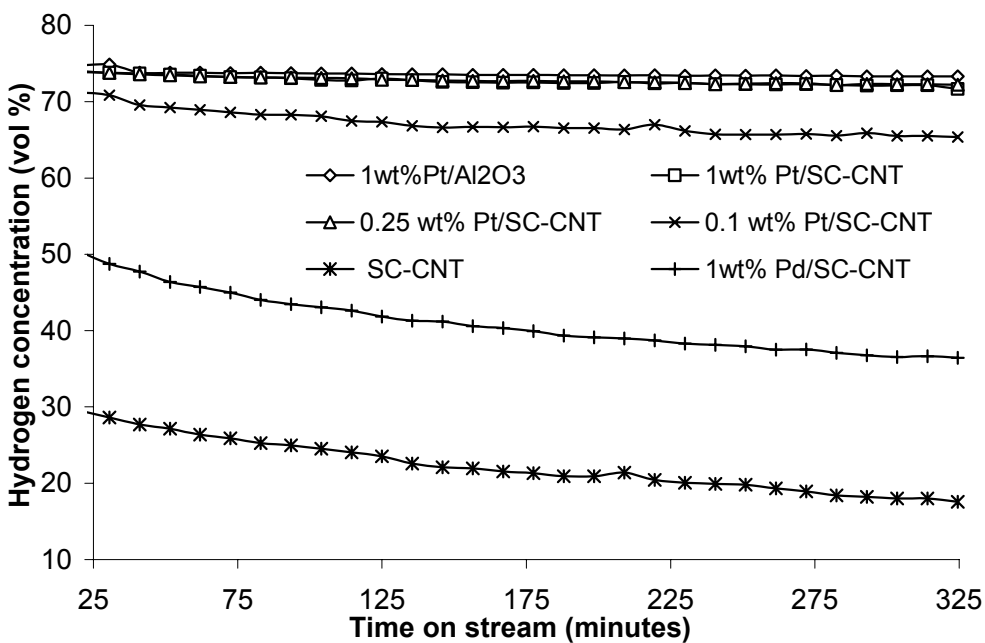


Figure 4. Time on stream hydrogen production for different catalysts from dehydrogenation of cyclohexane at atmospheric pressure and 315 °C.
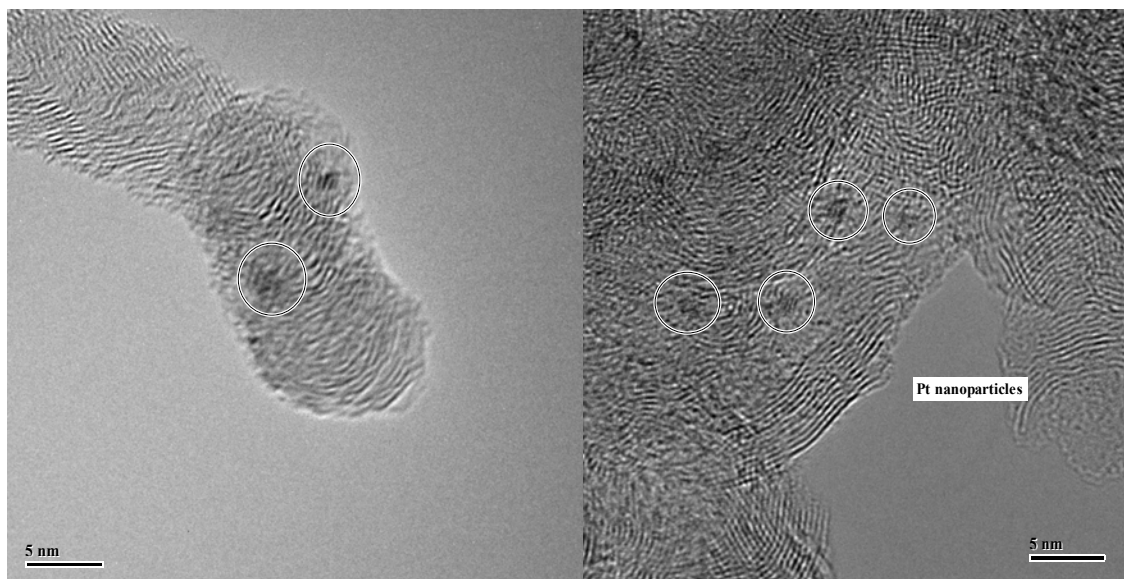
Figure 5. TEM images of the 1 wt. % Pt/SC-CNT catalyst after dehydrogenation of cyclohexane at 315 °C for 6.5 hours.


Dehydrogenation of methylcyclohexane

With 6.1 wt% of removable hydrogen content, methylcyclohexane is another compound that can be partially dehydrogenated to produce pure hydrogen and a liquid aromatic product – toluene. For environmental reasons, toluene is a preferable product of dehydrogenation to benzene.  The catalytic dehydrogenation of methylcyclohexane was carried out with the commercial 1 wt% Pt/Al$_2$O$_3$ catalyst and with catalysts consisting of 1, 0.25, and 0.1 wt% Pt; and 1 wt% Pd on purified SC-CNT.   The results are shown in Figures 6 and 7.  Both the 1 wt% Pt/Al$_2$O$_3$ and the 0.25 wt% Pt/SC-CNT yield high methylcyclohexane conversions to hydrogen and toluene with nearly 100% selectivity over the entire experimental run.  The initial conversion is approximately 95%, which then decreases at a rate of about 1% per hour for 6.5 hours. Hydrogen production is fairly stable at about 74 volume % for both catalysts.  Hydrogen production for the 0.1 wt% Pt/SC-CNT drops from approximately 70 to 58%, while the 1 wt% Pd/SC-CNT catalyst exhibits significantly lower activity, with hydrogen production in the 38 to 5 % range.  The only dehydrogenation products observed are toluene and hydrogen.  Figure 7 shows the time on stream hydrogen volume percentage in the outgoing flow stream from partial dehydrogenation of methylcyclohexane.  The catalyst activity order for partial dehydrogenation of methycyclohexane at 315 °C is: 1 wt% Pt/Al$_2$O$_3$ ≈ 0.25 wt% Pt/SC-CNT > 0.1wt% Pt/SC-CNT > 1wt% Pd/SC-CNT.
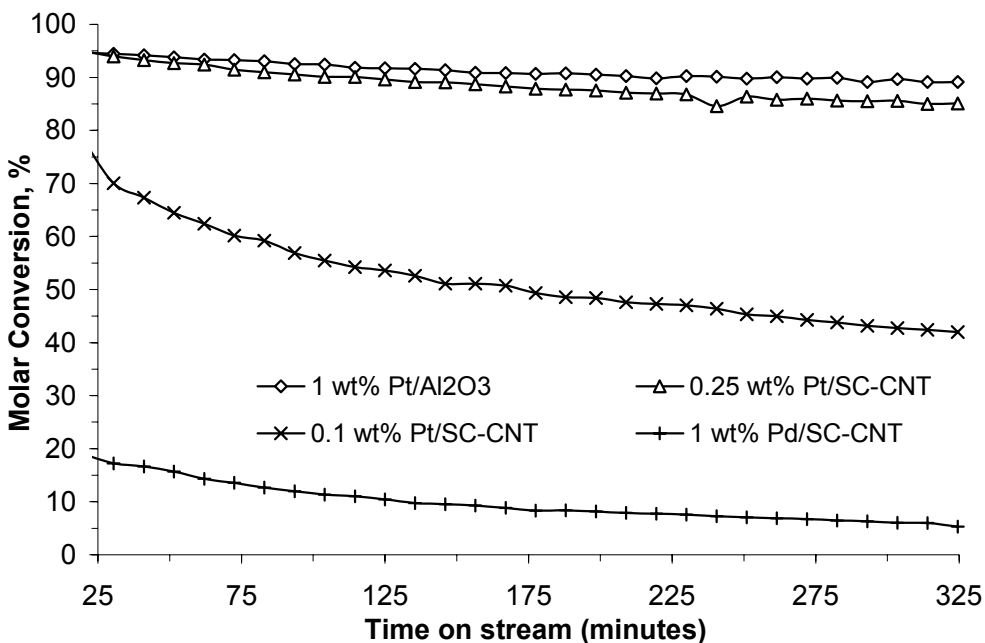
Figure 6. Time on stream conversion of methylcyclohexane with different catalysts at atmospheric pressure and 315 °C.
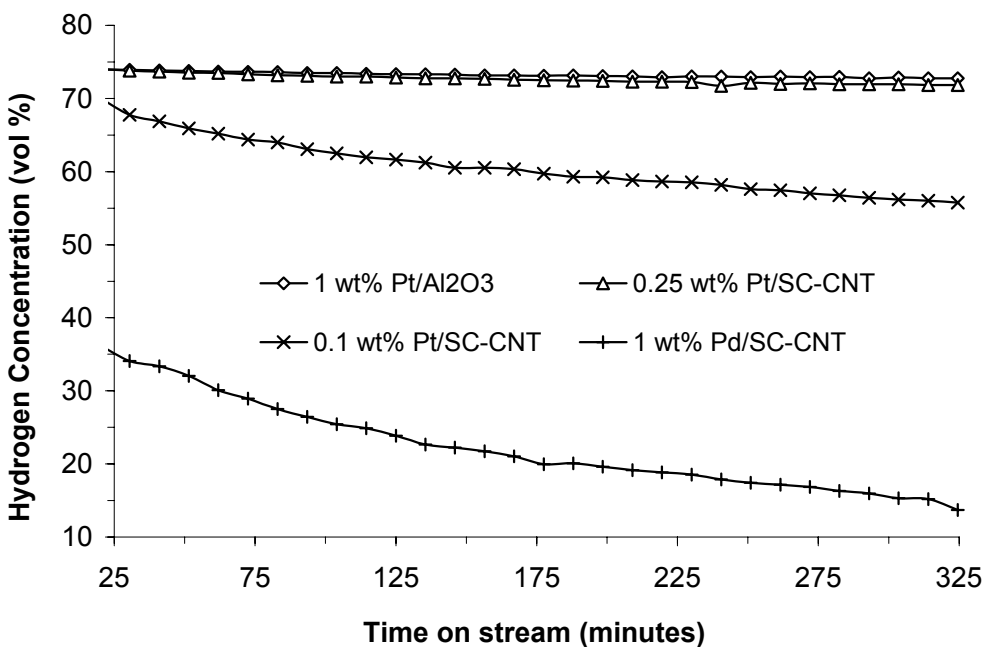


Figure 7. Time on stream hydrogen production for dehydrogenation of methylcyclohexane (atmospheric pressure, 315 °C) using several different catalysts.

To compare the catalytic activity of each metal atom for different catalysts, turnover numbers (TON) are calculated for partial dehydrogenation of cyclohexane and

methylcyclohexane (Table 1). Since there are three molecules of hydrogen released with the production of one molecule of benzene or toluene, the turnover number for hydrogen production was defined as:

TON = 3•[(moles of cyclohexane or methylcyclohexane converted)/(moles of metal present)]/second

The TON for each catalyst is calculated at the start and the end of the TOS period. In Table 1, the 0.1 wt% Pt/SC-CNT catalyst shows the best TON for each loaded Pt atom for both the dehydrogenation of cyclohexane and methylcyclohexane and the TON decreases with increasing Pt loading. The TON for the 1 wt% Pt/SC-CNT and the 1wt% Pt/Al$_2$O$_3$ catalysts are almost identical. The TON for the 1wt% Pd/SC-CNT shows clearly that it is not a good catalyst for dehydrogenation of cyclohexane and methylcyclohexane. These results are in agreement with the results of Kariya and co-workers[4].

Table 1. Turnover number for hydrogen production on each metal atom for different catalysts.

| Catalyst | TON (start) ($s^{-1}$) | TON (end) ($s^{-1}$) |
|---|---|---|
| **Dehydrogenation of cyclohexane** | | |
| 1wt% Pt/Al$_2$O$_3$ | 0.44 | 0.40 |
| 1wt% Pt/SC-CNT | 0.41 | 0.37 |
| 0.25wt% Pt/SC-CNT | 1.83 | 1.67 |
| 0.1wt% Pt/SC-CNT | 3.60 | 2.74 |
| 1wt% Pd/SC-CNT | 0.080 | 0.045 |
| **Dehydrogenation of methylcyclohexane** | | |
| 1wt% Pt/Al$_2$O$_3$ | 0.41 | 0.39 |
| 0.25wt% Pt/SC-CNT | 1.65 | 1.48 |
| 0.1wt% Pt/SC-CNT | 3.40 | 1.83 |
| 1wt% Pd/SC-CNT | 0.045 | 0.013 |

## Conclusions

It has been shown that efficient production of pure hydrogen can be achieved by dehydrogenation of cyclohexane or methylcyclohexane with catalysts consisting of 0.1-1.0 wt.% Pt supported on stacked-cone carbon nanotubes (SC-CNT). The catalysts exhibited 100 % selectivity for conversion of cyclohexane to hydrogen and benzene and methylcyclohexane to hydrogen and toluene. A 0.25 wt.% Pt/ SC-CNT catalyst had approximately the same activity as a commercial 1 wt.% Pt/Al$_2$O$_3$ catalyst. High resolution TEM showed the dispersion of the Pt catalyst particles on the SC-CNT support to be very high after 6.5 hours of reaction, with particle sizes ~ 1 to 2 nm. A 0.1wt% Pt/SC-CNT exhibited the highest efficiency (turnover-number (TON)) for hydrogen production per metal atom. These results will be summarized in more detail in a forthcoming paper to be published in *Energy & Fuels*[5].

## Papers published or presented
1. Shah, N.; Wang, Y.; Panjala, D.; Huffman, G. P. "Production of Hydrogen and Carbon Nanostructures by Non-oxidative Catalytic Dehydrogenation of Ethane and Propane", *Energy & Fuels* , **18** (2004) 727-736.

2. Wang Y.; Shah, N.; Huffman, G. P. "Pure hydrogen production by partial dehydrogenation of cyclohexane and methylcyclohexane over nanotube supported Pt and Pd catalysts", *Energy & Fuels* (2004) in press.

3. Wang Y.; Shah, N.; Huffman, G. P. "Production of pure hydrogen and novel carbon nanotube structures by catalytic decomposition of propane and cyclohexane", Y. Wang, N. Shah, and G.P. Huffman, presented at the American Chemical Society National Meeting, New York, NY, September 7-11, 2003; *ACS Fuel Chemistry Division Preprints*, **48(2)** (2003) 900-901.

4. Wang Y.; Shah, N.; Huffman G. P. "Hydrogen production by decomposition of propane and cyclohexane over alumina supported binary catalysts" submitted to *Catalysis Today*.


## Future work

### Continuous dehydrogenation of lower alkanes

For practical applications of the catalytic dehydrogenation of natural gas, it will be necessary to develop a reaction system in which hydrogen and CNT can be continuously removed. To accomplish this, a closed loop, fluidized bed reactor will be developed. Because of the higher flow rate and shorter residence time, we expect a decrease in methane conversion. However, because the flow stream is recycled, the unconverted methane will continue to decompose into carbon and hydrogen in subsequent passes through the reactor. Based on some preliminary results, it is expected that fluidization of the catalyst bed will provide sufficient agitation to detach the nanotubes from the catalyst surfaces so they can be carried out of the reactor in the gas stream for collection. This process modification will improve the process both by increasing the "time on stream" of the catalyst and by isolating and capturing the valuable CNT by-product.

### Partial dehydrogenation of liquid hydrocarbons

Catalytic dehydrogenation of tetralin, decalin, surrogate JP-8, and F-T liquid products to produce hydrogen will be tested in the future. We will also test more economical liquid dehydrogenation catalysts, such as Ni-Cu alloys.


## References

[1] Shah, N.; Panjala, D.; Huffman G. P. *Energy & Fuels*, **2001**, *15(6)*, 1528.

[2] Makkuni, A.; Panjala D.; Shah N.; Huffman G. P. Preprint Pap. - *Am. Chem. Soc., Fuel Chem. Div. Preprints*, **2002**, 47(2), 782-783.

[3] Shah, N.; Wang, Y.; Panjala, D.; Huffman, G. P. "Production of Hydrogen and Carbon Nanostructures by Non-oxidative Catalytic Dehydrogenation of Ethane and Propane", *Energy & Fuels* , **18** (2004) 727-736.

[4] Kariya N., Fukuoka A., Utagawa T., Sakuramoto M., Goto Y., Ichikawa M.; *Appld. Catal. A*, **2003**, *247*, 247-259.

[5] Wang Y.; Shah, N.; Huffman, G. P. "Pure hydrogen production by partial dehydrogenation of cyclohexane and methylcyclohexane over nanotube supported Pt and Pd catalysts", *Energy & Fuels* (2004) in press.

# Production of Hydrogen in Supercritical Water

J. Gadhe, C.B. Roberts, Ram B. Gupta*

## I.     Introduction

This work focuses on reforming reaction under supercritical water conditions to produce $H_2$. There are various advantages of carrying out reforming under supercritical water conditions which have been mentioned in the literature (references 1-4). The density of supercritical water is higher than that of steam which leads to a higher space-time yield.  Higher thermal conductivity and temperature promotes the endothermic reforming reaction. The hydrogen gas is available at higher pressure which can then be stored directly, thus avoiding compression cost.

Lower alcohols such as methanol and ethanol are a good feedstock for the reforming reaction because of higher energy density. It has been reported in the literature that when a mixture of methanol and water vapor is passed over catalysts such as copper, it is decomposed into gases. The main components of the product gases are hydrogen, carbon dioxide, methane and carbon monoxide, as follows.

| No. | Reaction | | $\Delta H°@298°C$ (kJ/mol) |
|---|---|---|---|
| 1. | Methanol decomposition | $CH_3OH \leftrightarrow CO + 2H_2$ | +91.7 |
| 2. | Water-gas shift reaction | $CO + H_2O \leftrightarrow CO_2 + H_2$ | -41 |
| 3. | Combined reaction of 1 and 2 | $CH_3OH + H_2O \leftrightarrow CO_2 + 3H_2$ | +50.7 |
| 4. | Methanation of CO | $CO + 3H_2 \leftrightarrow CH_4 + H_2O$ | -211 |
| 5. | Methanation of $CO_2$ | $CO_2 + 4H_2 \leftrightarrow CH_4 + 2H_2O$ | -223 |

The main reaction to achieve is the reaction number 3. The reactor used in this study is a tubular reactor made of nickel alloy (Inconel 600). The inner wall of the reactor acts as catalyst for the reforming reaction. The advantage of this reactor configuration is its simplicity and compactness.

## II.     Experimental

An apparatus was designed for carrying out methanol reforming under supercritical water conditions. Various parts and equipment were acquired and assembled. The flow diagram for the process is shown below in Figure 1.

A mixture of methanol and water is fed to the reactor by means of HPLC pump (Waters 590) after passing through a rupture disc. The pump displays the flow rate and pressure on its panel. The reactor consists of a coil of Inconel 600. (Length of the reactor = 1 m, ID = 0.0426") The reactor is heated with the help of a tubular furnace with temperature controller (Barnstead Thermolyne, Model 21100). The ends of the tube furnace are insulated properly in order to minimize the heat loss and for the proper control of the temperature. A K-type thermocouple (Omega) measures the reactor temperature just before the exit of the reactor. The reactor is then cooled to 20 °C using a double coiled heat exchanger with cooling water as coolant. Pressure is read using the pressure gauge P. The pressure is then let down using a back-pressure regulator (Straval) which is set at 4000 psi. The vapor and liquid mixture is then separated in the phase separator packed with glass beads. The liquid flow rate measured and its TOC content is measured using a TOC analyzer (Tekmar-Dohrmann). The gas phase exiting the phase separator passes through a volumetric flow meter (Omega FMA-1600) which displays flow rate, pressure, temperature and the computer attached to it provides the value for totalized flow. The gas

mixture is then sent to a six-port injection valve (Valco) for online injection to the GC. The sample loop has a volume of 100 μL. Helium (BOC gases, 5.0 grade) is used as carrier gas. The gas mixture is fed to a gas chromatograph (Varian 3700) with a TCD detector. The GC contains a carbon molecular sieves packed column. (60/80 Carboxen-1000, Supelco, 15' x 1/8") The Peaksimple chromatography data system (SRI, Model 203) converts the analog signal from GC and feeds it to the computer for peak area analysis. The TCD of the GC was calibrated using a gas mixture of known composition. (BOC gases, $H_2$ 60%, CO 15%, $CO_2$ 20%, $CH_4$ 5%). A carbon monoxide detector (Nighthawk) with alarm is installed for safety purpose.
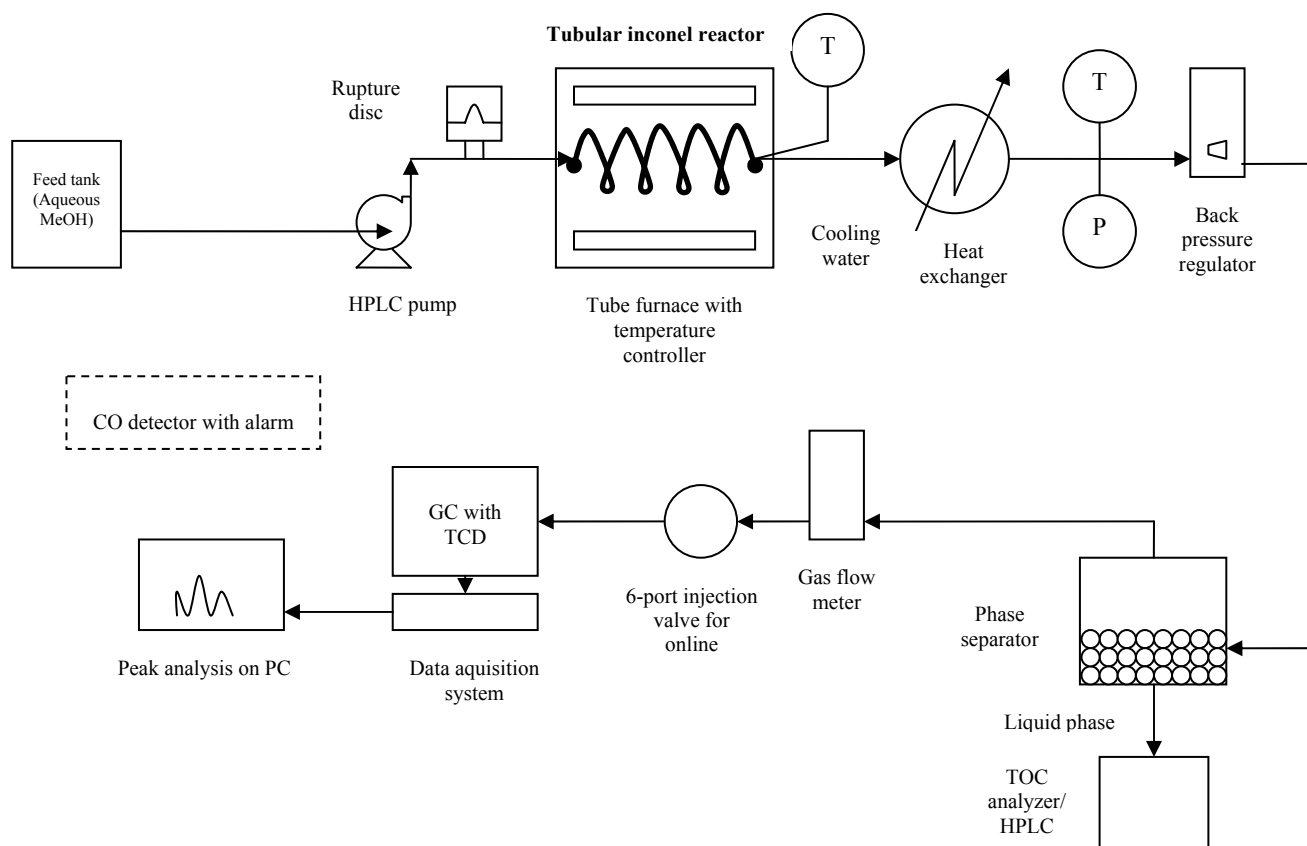


**Figure 1.** Schematic of Apparatus for Hydrogen Production in Supercritical Water

A typical experimental procedure is as follows. Distilled water is pumped through the system and desired pressure is achieved by adjusting the back pressure regulator. After stabilization, the furnace is switched on with a temperature set point. Once it reaches the desired temperature, flow is switched to methanol/water mixture. The steady state is marked by a constant temperature at the reactor outlet and gas flow. The feed flow rate is read from the pump display and confirmed by noting the drop in the level in the feed tank. Gas analysis is repeated at least 3 times. Gas flow is read from the flow meter. Liquid flow rate after the phase separator is measured by noting the mass collected in a specified time. It is later analyzed for TOC. The liquid is diluted so as to have the TOC readings in the range of the instrument (0 to 10000 ppm). The TOC value of the feed is also found out. Molar gas flow rates are calculated based on the total gas flow and confirmed by carbon balance. After the experiment flow is switched back to distilled water and the reactor is well flushed.

70

## III.    Results and Discussion

The results of the screening experiments with methanol and ethanol indicate successful production of hydrogen as shown in Figure 2.
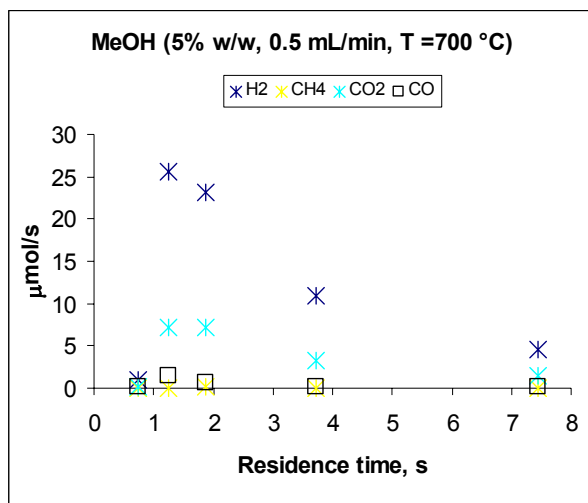


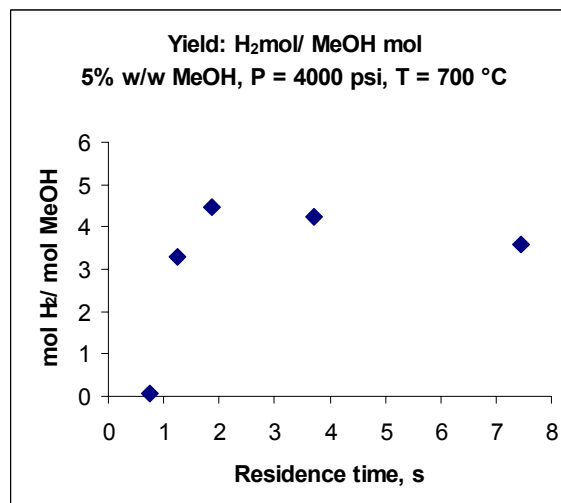**Figure 2a**. Gas products from methanol.



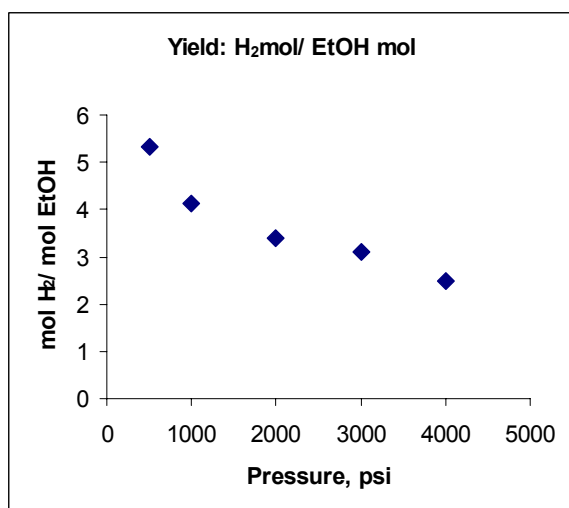**Figure 2b**. $H_2$ yield from methanol



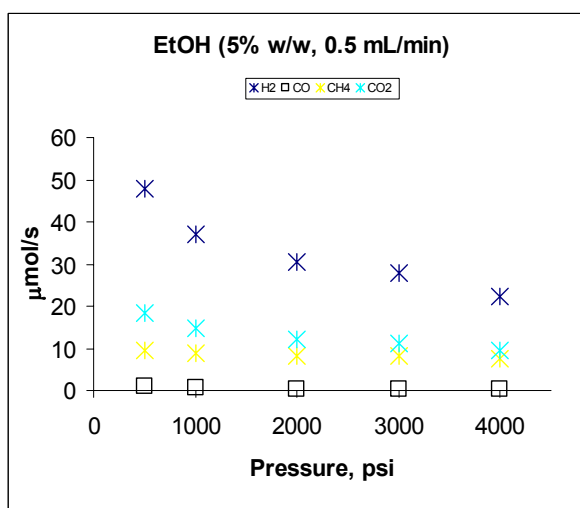**Figure 2c**. Gas products from 5% ethanol at 700°C.



**Figure 2d**. $H_2$ yield from ethanol

## IV.    Conclusions

New apparatus for the production of hydrogen in supercritical water has been assembled and is working correctly.  Depending on operating conditions, 3-4 moles of hydrogen are typically produced per mole of methanol or ethanol.

## V.    Papers presented or published

None

## VI.    Future work

Various experiments will be conducted to study the effect of operating parameters such as temperature, pressure, feed concentration, feed flow rate. A work is being done on the equilibrium calculations and the modeling of the reactor.

It is well known that product removal from the reaction gases will drive the reaction towards hydrogen formation at higher pressures. This breaking of thermodynamic barrier requires the use of hydrogen selective membranes. However, the use of membrane under the harsh supercritical conditions is challenging due to the disability of the membrane to withstand higher pressures. To deal with this a membrane reactor of the following configuration is made in-house.
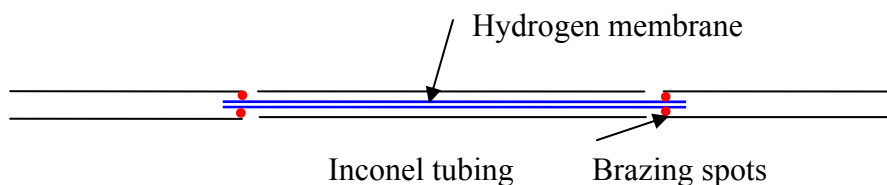


Experiments are also planned with the above membrane reactor.

## VII.    References

1.  Taylor, Joshua D.; Herdman, Christopher M.; Wu, Benjamin C.; Wally, Karl; Rice, Steven F. **Hydrogen production in a compact supercritical water reformer.** *International Journal of Hydrogen Energy* (2003), 28(11), 1171-1178.

2.  Boukis, N.; Diem, V.; Habicht, W.; Dinjus, E. **Methanol Reforming in Supercritical Water.** *Industrial & Engineering Chemistry Research* (2003), 42(4), 728-735.

3.  Kruse, Andrea; Dinjus, Eckhard. **Hydrogen from methane and supercritical water.** *Angewandte Chemie, International Edition* (2003), 42(8), 909-911.

4.  Boukis, N.; Habicht, W.; Franz, G.; Dinjus, E. **Behavior of Ni-base alloy 625 in methanol-supercritical water systems.** *Materials and Corrosion* (2003), 54(5), 326-330.

# Hydrogen Production from Aqueous-phase Reforming of Ethylene Glycol

B Liu, Y Zhang, J.W. Tierney and I. Wender
Department of Chemical Engineering, University of Pittsburgh

## Introduction

The production of hydrogen containing very low levels of CO is critical for the global transition to a hydrogen economy[1]. Production of hydrogen by steam-reforming of hydrocarbons requires a complex combination of multiple processes to achieve the required low CO levels (e.g., 10–100 ppm). An important step toward a simple process for the production of hydrogen containing low levels of CO is made possible by the discovery that hydrogen can be produced by catalytic reforming of ethylene glycol derived from synthesis gas in liquid water at temperatures near $220^{\circ}C$[2-4]. This process has the advantage that the reforming of the oxygenated hydrocarbon and the water–gas shift (WGS) reaction are both thermodynamically favorable at the same low temperatures, thus making it possible to conduct both reactions in one reactor[2-4]. The process eliminates the need to vaporize water and the glycol and leads to low levels of CO, making aqueous-phase reforming of ethylene glycol an attractive process for applications in fuel cells[2-4].

## Experimental

Theoretically, the aqueous-phase reforming of one mole of ethylene glycol would produce five moles of hydrogen.

$$C_2H_6O_2 + 4H_2O = 5H_2 + 2CO_2$$

Alumina-supported platinum catalysts were prepared by incipient wetness impregnation with aqueous solutions of tetraammineplatinum nitrate (Pt $(NH_4)_4(NO_3)_2$), followed by treatment in an oven at $100^{\circ}C$ for 12 h. Then the catalysts with a composition of Pt (1 wt %) and $Al_2O_3$ (99 wt %), were calcinated at $260^{\circ}C$ for 2 h. The calcined catalysts were then sieved to a 120–230-mesh size (particle diameters between 63 and 125 μm) and loaded into a microautoclave.

The aqueous-phase reforming of ethylene glycol was carried out in a horizontal shaking microautoclave system. The microreactor had three parts: a horizontal reactor tube (1 in. o.d. x 4.625 in.), a vertical reactor stem (1/2 in. o.d. x 10 in.) and a multiport valve connected on top of the system. After 0.5 g catalyst was loaded, the reactor was purged with $H_2$ and pressurized to 300 psi at room temperature to test for leakage. The reactor was then purged four times with $H_2$ to remove the air. The reactor was immersed into a fluidized sand bath and heated to the final reduction temperature of $250^{\circ}C$. It was then purged with $H_2$ and pressurized to 400psi at $250^{\circ}C$ for 30 minutes to reduce the catalyst. After reduction, the system was cooled to room temperature. The system was purged with He four times to remove the $H_2$. A 15ml liquid solution of 10 wt% ethylene glycol in deionized water was introduced into the reactor with a pump. The reactor was then immersed into the fluidized sand bath and heated to the final reaction temperature of $220^{\circ}C$, during with it was shaken horizontally at 200 cycles per minute.

After 6 hours the reaction was terminated. The reactor was rapidly removed from the sand bath and cooled with running cold water. Before opening the reactor to collect the liquid product, the gas product was collected by a gas collector and analyzed by GC (HP6890). The liquid product was analyzed by another GC (HP5890).

## Results and Discussion

Aqueous-phase reforming of 10 wt% ethylene glycol feed solutions in the shaking microautoclave system produced primarily hydrogen and carbon dioxide conversions of about 15%, although small amounts of liquid organic byproducts, gaseous alkanes, and carbon monoxide were also detected. Hydrogen and carbon dioxide were the major gas products, (Table 1) with compositions of 80% and 13%, respectively. In addition to $H_2$ and $CO_2$, the catalyst produced smaller amounts of gaseous alkanes (methane and ethane) and liquid-phase products including alcohols (methanol and ethanol), organic acids (acetic and glycolic acids), and aldehydes (acetaldehyde and glycolaldehyde).

Table1 Composition of the gas product and their selectivity of the preliminary experiment

| Gas product | Concentration (%) | Selectivity |
|---|---|---|
| $H_2$ | 80.0 | >99 |
| Ar | 6 | - |
| CO | 0.08 | 0.3 |
| $CO_2$ | 13..0 | >99 |
| $CH_4$ | 0.1 | 0.15 |

[1] 1%Pt/$Al_2O_3$, 220$^o$C, $C_2H_6O_2$/$H_2O$ = 1/10

## Conclusions

A preliminary experiment on the aqueous-phase reforming of ethylene glycol in a batch system has shown that significant amounts of hydrogen are produced.

## Future Work

Future work will include a study of aqueous-phase reforming of ethylene glycol and polyethylene glycols in a continuous system. The effect of operating variables, such as temperature, pressure and various catalysts, will be investigated.
    A critical review of methods of hydrogen storage is underway.

## References
1.  U. Bossel, B. Eliasson, Energy and the Hydrogen Economy, 2003.
2.  R. R. Davda, J. W. Shabaker, G. W. Huber, R. D. Cortright, J.A. Dumesic, Applied Catalysis B: Environmental 43 (2003) 13–26.
3.  J. W. Shabaker, G. W. Huber, R. R. Davda, R. D. Cortright, and J. A. Dumesic, Catalysis Letters 88 1–2 ( 2003).
4.  J. W. Shabaker, R. R. Davda, G. W. Huber, R .D. Cortright, and J. A. Dumesic, Journal of Catalysis 215 (2003) 344–352.
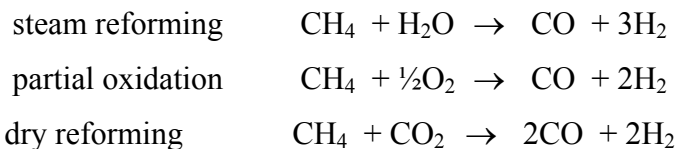
**Dry Reforming of Methane to Synthesis Gas with Cobalt Tungsten Carbide Catalyst**

Huifang Shao, Wenping Ma, Edwin L. Kugler, Dady B. Dadyburjor

Department of Chemical Engineering, West Virginia University, Morgantown, WV

## VIII.   INTRODUCTION

Many industrial processes use methane as a primary feedstock for producing a mixture of carbon monoxide and hydrogen, called synthesis gas (syngas). The methane can arise from natural gas, from coal seams or as an unneeded product during Fischer-Tropsch (FT) synthesis. The syngas serves as the feedstock for a variety of downstream processes, such as methanol synthesis, FT synthesis or ammonia synthesis [1,2]. The use of syngas from FT methane to produce FT products represents a useful way to recycle the unneeded methane from FT. There are three ways to produce syngas from methane:

steam reforming     $CH_4 + H_2O \rightarrow CO + 3H_2$

partial oxidation     $CH_4 + \frac{1}{2}O_2 \rightarrow CO + 2H_2$

dry reforming     $CH_4 + CO_2 \rightarrow 2CO + 2H_2$

Dry reforming is the focus of this research. The second reactant, $CO_2$, is often present in natural gas, in which case dry reforming is potentially of value in converting "stranded" natural gas reserves to liquid products. In any case, $CO_2$ is abundant and is a greenhouse gas, so methods of removing it by reaction (as opposed to temporary storage by sequestration techniques) are of value.

Nickel-based catalysts are traditionally used. But this type of catalyst deactivates rapidly by coke deposition, where coke is formed via methane decomposition and CO disproportionation (Boudouard reaction).[3, 4] Noble metal catalysts (Rh, Ru, Pd, Pt, Ir) exhibit high reactivity and low coke formation in the reforming process, but are expensive.[5] Metal carbides exhibit intermediate activity and intermediate stability. We have shown that bimetallic carbides can improve both activity and stability, and that coke laydown is apparently a requirement for the formation of a stable, active state. We have also shown that carbides with very similar bulk properties do not exhibit the same behavior in the reactor. Hence surface properties are required to be investigated. In this research, we have developed techniques to prepare the bimetallic carbide catalyst in house.[6, 7] Based on these result, additional experiments have been carried out on the activation of the catalyst, and we have also started to characterize the surface properties. These results are briefly described in this report.

## IX.   EXPERIMENTAL

The unsupported cobalt tungsten carbide catalyst is now prepared in our own laboratory. The detailed procedure has been described in an earlier report. The final form of the catalyst is very dependent upon the ratio of $CO_2$ to CO in the reducing gas used in the final step of preparation. Hence, different forms of catalyst were prepared, with $CO_2/CO$

ratios of 0.1, 0.2 and 0.75. The last value results in catalysts similar to the $Co_6W_6C$ obtained  commercially, while the first two values result in improved catalysts.

Typically 300 mg of the catalyst sample is used for each run.  The empty reactor is initially loaded with quartz wool at the center such that the tip of the thermocouple just touches the catalyst bed when loaded.  After this, the downstream end of the reactor is filled with fine quartz chips (approx. 1/16 in), and the bottom is sealed with some quartz wool.  Then the catalyst is poured with a funnel from the top of the reactor, followed by tapping to ensure that all the catalyst is set in the reactorcenter.  Next, the thermocouple is inserted into the reactor, and the top fitting is connected.  Finally, some more quartz chips are added from the side opening of the reactor to fill the upstream of the reactor.  The loaded reactor is then mounted in the furnace enclosure.  The system is then checked for leaks by flowing an inert gas (argon) at a pressure of 60 psig.

The catalyst pretreatment is then started. The catalyst is first reduced by flowing hydrogen at 60 cc/min for one hour, followed by one hour of flushing with argon.  The GC is switched on only after ensuring the flow of the carrier gas through the column and TCD (30 cc/min for each path).  The reaction starts once the pretreatment is finished.  Both the flow rates and temperature could be adjusted by computer.  The computer is preset to take samples at specified time intervals and also to analyze samples for a certain time period.  The calculations of outlet concentrations, activity and selectivity are based on the calibration result as well as GC analysis data report.

Earlier we have reported the results when the catalysts were tested for reactivity and stability at 850°C.  To investigate further the performance of the catalysts during the present period, the reactions were carried out at a range of increasing and decreasing temperatures. The temperature profile was designed as follows:

$$700^oC \rightarrow 600^oC \rightarrow 850^oC \rightarrow 700^oC \rightarrow 600^oC \rightarrow 500^oC \rightarrow 700^oC$$

Thus the performance of the catalysts could be obtained at intermediate temperatures, high temperatures, intermediate temperatures after exposure to high temperatures, low temperatures after exposure to high temperatures, then back to intermediate temperatures to test for catalyst stability. To ensure that the properties of the catalyst had stabilized at each temperature, each temperature stage was maintained for 20 hours.  The other reaction conditions still remained the same as before:

P = 36 psig (3.4 atm),         $P_{CH4} = P_{CO2} = 1$ atm

     $CH_4 : CO_2 : Ar = 1 : 1 : 1.4$,     WHSV = 9000 scc / hr / g-catalyst

Finally, the surface properties of the catalysts were characterized by SEM and XRD to compare the structure and bulk component of the catalyst before and after reaction.


## X.  RESULTS AND DISCUSSION

Variable-temperature tests were carried on for each of the three catalyst samples, which were prepared with different ratios of $CO_2$ to CO.  The conversions, yields, ratios of hydrogen to carbon monoxide and carbon balance were measured and these are shown in Tables 1 through 3.  Qualitatively similar performances were noted for all three.

When the reaction temperature was first raised to $700^{\circ}$C, the conversions and the yields were negligibly low. The values increased dramatically as the reaction temperature went up to $850^{\circ}$C. Afterwards, the reaction temperature was lowered step by step: $700^{\circ}$C→$600^{\circ}$C→$500^{\circ}$C, and the values of conversion and yield decreased correspondingly. However, the values of conversions and yields at $700^{\circ}$C this time were much higher than those obtained in the first step. Later, the reaction temperature was brought back to $700^{\circ}$C, and the values were almost at the same level as those at the second $700^{\circ}$C. Clearly, the catalyst cannot be activated if it is at a temperature of $700^{\circ}$C or lower at the very beginning. In comparison, the reactivity increases greatly once the reaction temperature reachs $850^{\circ}$C. After that, the catalytic activity can be maintained at a relatively high level even if the temperature is lowered again.

Figure 1 through 6 are SEM and XRD results for the fresh and spent catalyst. Only one material was used for these characterizations, that made using the $CO_2$ to CO ratio of 0.75. Before the reaction, the fresh catalyst was shown to be $Co_6W_6C$. The bulk component of the spent catalyst is WC and Co when the reaction temperature is $850^{\circ}$C. But much cobalt tungsten oxide is found as the reaction temperature is $700^{\circ}$C. From the SEM images, the structure of the catalyst is more compact when the reaction is run at the higher temperature ($850^{\circ}$C). Also, carbon deposits, including whisker carbon and carbon tube, can be seen on the surface of the spent catalyst run at $850^{\circ}$C. Further, EDAX confirms that a large amount of oxygen exists in the spent catalyst reacted at the intermediate temperature ($700^{\circ}$C). The existence of the cobalt tungsten oxide probably decreases the amount of the active catalyst and inhibits the desired reaction, which might be the reason that why the reactivity of the catalyst was fairly low in this situation. The specific mechanism of this phenomenon needs to be investigated in the future work.


## XI.    CONCLUSIONS

From the above results, the conclusion could be drawn that this bimetallic carbide catalyst was required to be activated at a higher temperature ($850^{\circ}$C) before exhibiting good reactivity for methane dry reforming. After that, the catalyst maintains high reactivity and good stability over a long period even at lower temperatures. The SEM images and XRD spectra demonstrate the different appearance of the catalyst after it is treated at different temperatures ($700^{\circ}$C and $850^{\circ}$C).


## XII.   PAPERS PRESENTED OR PUBLISHED

"Bimetallic Eta-Carbides and Related Materials as Catalysts for Production of Synthesis Gas from Methane," Seminar presented by D.B. Dadyburjor at Department of Chemical Engineering, University of Akron, April 8, 2004.

M.V. Iyer, L.P. Norcio, E.L. Kugler, M.S. Seehra and D.B. Dadyburjor, "Catalysts for synthesis gas formation from reforming of methane," Topics in Catalysis **29** (3-4) 195-198 (2004).

## XIII.  FUTURE WORK

Based on the previous work and experience, we plan to expand our research to combined methane reforming, including both steam and carbon dioxide in the reactants.  Due to the introduction of steam, the reaction condition may be required to change to optimize the results.  In addition, the reaction kinetics can be impacted by the addition of steam, which is also one point of our future work.

The use of these catalysts for the reforming of methanol and/or ethanol is also being considered.

Finally, carbide catalysts of different compositions are being considered. These materials can be prepared by replacing W with Mo and/or substituting Ni for Co.  The reactivity and stability of the new catalysts will be investigated for methane and/or alcohol reforming.

## XIV.  REFERENCES

[1] J. B. Claridge, A. P. E. York, A. J. Brungs, C. Marquez-Alvarez, J. Sloan, S. C. Tsang and M. L. H. Green, "New Catalysts for the Conversion of Methane to Synthesis Gas: Molybdenum and Tungsten Carbide", Journal of Catalysis, 180: 85-100, 1998

[2] S. Wang and G. Q. Lu, "Effects of Promoters on Catalytic Activity and Carbon Deposition of $Ni/\gamma-Al_2O_3$ Catalysts in $CO_2$ Reforming of $CH_4$", Journal of Chemical Technology and Biotechnology, 75: 589-595, 2000

[3] T. Osaki, T. Mori, "Role of Potassium in Carbon-Free $CO_2$ Reforming of Methane on K-Promoted $Ni/Al_2O_3$ Catalysts", Journal of Catalysis, 204: 89-97, 2001

[4] J. H. Bitter, K. Seshan, and J. A. Lercher, "Deactivation and Coke Accumulation during $CO_2/CH_4$ Reforming over Pt Catalysts", Journal of Catalysis. 183: 336-343, 1999

[5] J. R. Rostrup-Nielsen and J-H. B. Hansen, "$CO_2$-Reforming of Methane over Transition Metals", Journal of Catalysis, 144: 38-49, 1993

[6] E. L, Kugler, L. E. McCandlish, A. J. Jacobson, R. R. Chianelli, "Eta Phase Materials, Methods of Producing the Same, and Use Thereof as Catalysts for Alcohol Synthesis, Hydrocarbon Synthesis, Hydrocarbon Hydrogenation and Hydrocarbon conversion Reactions", US Patent 5,138,111, Aug 11, 1992

[7] R. S. Polizzotti, L. E. McCandlish, E. L, Kugler, "Multiphase Composite Particle Containing a Distribution of Nonmetallic Compound Particles", US Patent 5,338,330, Aug 16, 1994

**Table 1. Conversion, Yield, Product Ratio and Carbon Balance with the catalyst made using CO$_2$/CO=0.75**

| Temperature (°C) | Conversion of CH$_4$ (%) | Conversion of CO$_2$ (%) | Yield of CO (%) | H$_2$/CO Ratio | Carbon Balance (%) |
|---|---|---|---|---|---|
| 700 | 3.63 | 5.37 | 2.03 | 0.223 | 97.52 |
| 600 | 2.84 | 2.88 | 0 | | 97.14 |
| 850 | 78.77 | 73.67 | 63.73 | 1.113 | 87.54 |
| 700 | 29.01 | 35.93 | 27.72 | 0.788 | 95.21 |
| 600 | 9.15 | 13.86 | 8.92 | 0.489 | 97.38 |
| 500 | 4.32 | 5.59 | 2.19 | 0.315 | 97.23 |
| 700 | Not available | | | | |

**Table 2.  Conversion, Yield, Product Ratio and Carbon Balance with the catalyst made using CO$_2$/CO=0.1**

| Temperature (°C) | Conversion of CH$_4$ (%) | Conversion of CO$_2$ (%) | Yield of CO (%) | H$_2$/CO Ratio | Carbon Balance (%) |
|---|---|---|---|---|---|
| 700 | 4.45 | 7.71 | 3.99 | 0.127 | 97.88 |
| 600 | 1.63 | 1.61 | 0 | | 98.38 |
| 850 | 72.09 | 68.45 | 66.75 | 0.989 | 96.50 |
| 700 | 28.43 | 34.13 | 26.42 | 0.795 | 95.10 |
| 600 | 9.15 | 13.29 | 9.01 | 0.467 | 97.76 |
| 500 | 4.12 | 4.55 | 2.24 | 0.307 | 97.86 |
| 700 | 27.66 | 34.50 | 27.05 | 0.759 | 95.92 |

**Table 3.  Conversion, Yield, Product Ratio and Carbon Balance with the catalyst made using CO$_2$/CO=0.2**

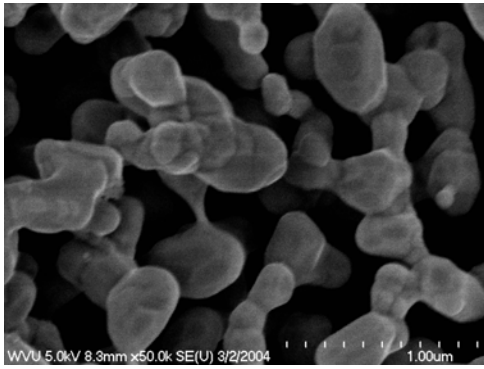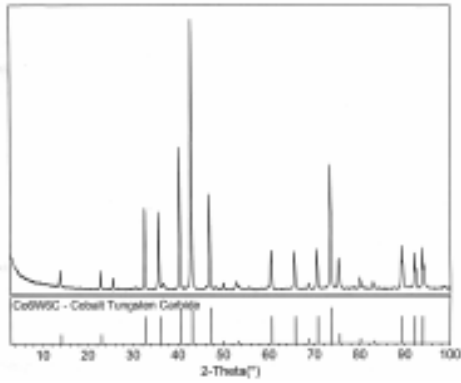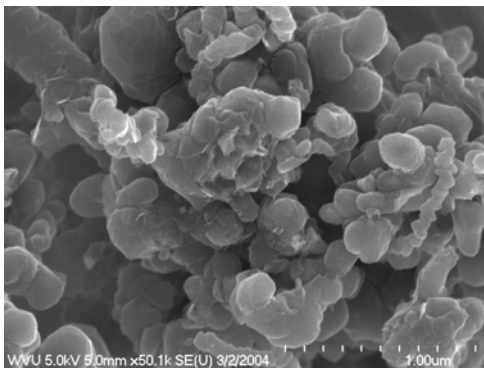| Temperature (°C) | Conversion of CH$_4$ (%) | Conversion of CO$_2$ (%) | Yield of CO (%) | H$_2$/CO Ratio | Carbon Balance (%) |
|---|---|---|---|---|---|
| 700 | 3.84 | 4.14 | 1.88 | 0.233 | 97.89 |
| 600 | 2.46 | 1.43 | 0 | | 98.06 |
| 850 | 80.53 | 76.84 | 67.58 | 1.079 | 88.92 |
| 700 | 29.55 | 35.51 | 28.35 | 0.799 | 95.78 |
| 600 | 8.83 | 12.49 | 8.56 | 0.473 | 97.88 |
| 500 | 4.35 | 4.63 | 2.25 | 0.297 | 97.76 |
| 700 | 27.69 | 33.83 | 26.77 | 0.774 | 95.97 |

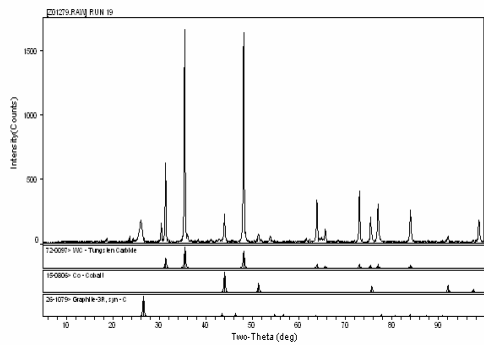Fig 1  SEM image of fresh catalyst


Fig 2  XRD spectrum of fresh catalyst

Fig 4 XRD spectrum of spent catalyst run at 850$^{o}$C

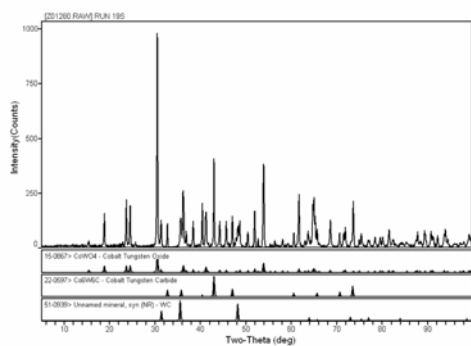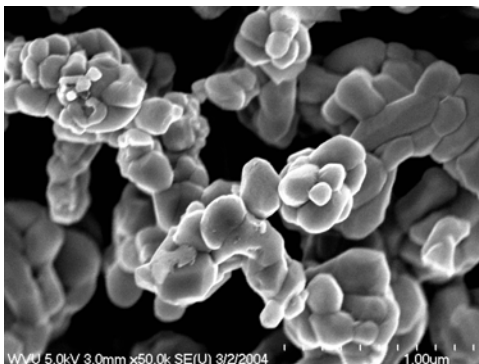Fig 3 SEM image of spent catalyst run at 850$^{o}$C





Fig 5 SEM image of spent catalyst run at 700$^{o}$C

Fig 6 XRD spectrum of spent catalyst run at 700$^{o}$C

# Solid State NMR Study of Fischer-Tropsch Catalysts

Zhiru Ma, Brian C. Dunn, Greg Turpin, Paul Cole, Ronald J. Pugmire, Richard D. Ernst, and Edward M. Eyring

Department of Chemistry, University of Utah, Salt Lake City, UT 84112

## I. Introduction
^{29}Si and ^{13}C solid state NMR methods were applied in the study of different metal based Fischer-Tropsch Catalysts. Total five F-T catalysts (three different weight percent cobalt loaded atalysts, one ferrocene loaded and one ruthenocene loaded) were investigated. The structure of the loaded metal compounds on the silica aerogel support was studied.

## II. Experimental
Materials: 2%, 6% and 10% weight cobalt loaded silica aerogel samples were prepared by Prof. Eyring's lab. Ferrocene and ruthenocene loaded silica aerogel samples were provided by Prof. Ernst's lab. NMR experiments: All the NMR experiments were carried out on a Chemagnetics CMX-200 spectrometer with a 7.5mm PENCIL rotor probe. The samples were ground into powder before packing into the rotor. Most of the samples were packed at ambient condition except the ferrocene and ruthenocene loaded silica aerogel sample which were packed in a glove box filled with nitrogen gas. A single pulse sequence was applied to observe ^{29}Si NMR spectra, while ^{13}C NMR spectra of the ferrocene and ruthenocene loaded aerogel samples were obtained using CP (cross polarization) and CP/MAS (magic angle spinning) techniques. The [29]Si $T_1$ was measured by the saturation recovery method.

## III. Results and Discussion
1) ^{29}Si NMR spectra of metal loaded silica aerogel samples
No major differences were noted in the ^{29}Si NMR spectra among the cobalt loaded, ferrocene and ruthenocene loaded aerogel samples (spectra not shown). However, when compared with the uncalcined silica aerogel, the loading of metal compounds increased the inhomogeneity of the silica structure, resulting in the disappearance of the three distinct $Q_2$, $Q_3$ and $Q_4$ Si tetrahedral sub-units[1,2] observed in the uncalcined silica aerogel sample. Nevertheless, the chemical shift regimes still exist in the metal loaded samples indicating the loading process doesn't significantly disrupt the defined tetrahedral sub-unit structure in the silica aerogel support.
2) [29]Si T1 results of different metal loaded silica aerogel samples
Tables 1 and 2 contain the [29]Si $T_1$ values of three different cobalt loaded silica aerogel samples and ruthenocene loaded aerogel and blank aerogel prepared in a $N_2$ filled glove box. The [29]Si $T_1$ of 2% cobalt loaded sample is much longer than that of 6% and 10% cobalt loaded samples. There is no statistical difference in the [29]Si $T_1$ values of the 6% and 10% cobalt loaded samples. The loading process in a vacuum and inert-atmosphere glove box increases the [29]Si T1 value, while the loading of ruthenocene reduces the [29]Si $T_1$ value compared with the same batch of silica aerogel.

3) ^{13}C NMR spectra of ferrocene and ruthenocene loaded aerogel samples Figures 1 and 2 show the ^{13}C CP spectra of ferrocene and ruthenocene loaded aerogel samples at static and a spinning rate of 4 kHz respectively.  No distinct differences are noted between the static and the MAS spectra except the linewidth of the static spectrum is slightly broader than the MAS spectrum.  The spectra indicate that the ferrocene and ruthenocene molecules are tumbling in the silica aerogel, and this motion averages the anisotropic components of the chemical shift tensor in the same fashion as that observed by Orent et al.[3] for ferrocene.  These data indicate that the ferrocene and ruthenocene molecules in the aerogel are tumbling rapidly in a random fashion as in a gas or liquid state.

## IV.  Conclusions

1.  No distinct differences in the ^{29}Si NMR spectra are observed among the cobalt, ferrocene and ruthenocene loaded silica aerogel samples.  The loading of metal compounds increases the inhomogeneity of the aerogel structure, which results in the disappearance of the three distinct spectral lines from the Q sub-units.  However, the chemical shift regimes of the three Q sub-units are still present, which suggests the silica tetrahedral sub-units do not collapse during these processes.

2.  The loading of metal compounds and the methods to load the metal compounds have significant influence on the [29]Si spin lattice relaxation time.

3.  The ferrocene or ruthenocene molecules exhibit a fast tumbling motion in the silica aerogel support based on the ^{13}C NMR data.  Their behavior indicates that rapid exchange exists within the aerogel structure on a time scale equilibrium to structural observed in liquid and gaseous states.

## V.  Papers presented

Zhiru Ma, Brian C. Dunn, Gregory C. Turpin, Paul Cole, Edward M. Eyring, Richard D. Ernst, and Ronald J. Pugmire, "Solid State NMR Investigation of Fischer-Tropsch Catalysts," The 45th Experimental Nuclear Magnetic Resonance Conference, April 18-23, 2004, Asilomar Conference Center, Pacific Grove, CA.

Brian C. Dunn, Daniel J. Covington, Paul Cole, Ronald J. Pugmire, Henk L. C. Meuzelaar, Richard D. Ernst, Emily C. Heider, Edward M. Eyring, "Silica Xerogel Supported Cobalt Metal Fischer-Tropsch Catalysts for Syngas to Diesel Range Fuel Conversion," *Energy & Fuels*, submitted for publication.

Brian C. Dunn, Paul Cole, Daniel J. Covington, Matthew C. Webster, Ronald J. Pugmire, Richard D. Ernst, Edward M. Eyring, Naresh Shah, Gerald P. Huffman, "Silica Aerogel Supported Catalysts for Fischer-Tropsch Synthesis," *Applied Catalysis A*, submitted for publication.

Brian C. Dunn, Paul Cole, Gregory C. Turpin, Zhiru Ma, Ronald J. Pugmire, Richard D. Ernst, Edward M. Eyring, Naresh Shah, Gerald P. Huffman, "Silica Aerogel Supported Catalysts for Fischer-Tropsch Synthesis," 227th ACS National Meeting, March 28 - April 1, 2004, Anaheim, CA.

## VI.  Future work

1. Continue to study the iron based and ruthenium based or other cobalt compounds based silica aerogel supported aerogel samples using $^{29}$Si and $^{13}$C NMR methods. These samples will be provided by Prof. Ernst's group: $Fe(Cp^*)_2$ ($Cp^*=C_5(CH_3)_5$), $Ru(Cp^*)_2$, etc.

2. Try to measure the $^{59}$Co NMR spectrum of cobalt loaded silica aerogel catalysts and obtain information about the conformation and state of cobalt in the silica aerogel support.

## VII.  References

1.      Young, S. K.; Jarrett, W. L.; and Mauritz, K. A. *Pol. Eng. Science*, **2001**, 41, 1529.

2.      Lippmaa, E.; Magi, M.; Samoson, A.; Engelhardt, G.; and Grimmer, A. R. *J. Am. Chem. Soc*. **1980**, 102, 4889.

3.      Orent, A. M. Facelli, J. C.; Jiang, Y. J.; and Grant, D. M. *J. Phys. Chem. A*, 1998, 102, 7692.

Table 1.  $^{29}$Si $T_1$ values of different CoO loaded $SiO_2$ aerogel samples.

| sample | $T_{1a}$ (s) [a] | $T_{1b}$ (s) [b] |
|---|---|---|
| 2% CoO loaded, SC ethanol, calcined | $298 \pm 100$ | $14 \pm 2$ |
| 6% CoO loaded, SC ethanol, calcined | $53 \pm 7$ | $3 \pm 2$ |
| 10% CoO loaded, SC ethanol, calcined | $56 \pm 6$ | $4 \pm 1$ |

[a] long $T_1$ component
[b] short $T_1$ component


Table 2.  $^{29}$Si $T_1$ values of ruthenocene loaded $SiO_2$ aerogel sample and the blank aerogel sample (prepared in a $N_2$ filled glove box)

| sample | $T_{1a}$ (s) [a] | $T_{1b}$ (s) [b] |
|---|---|---|
| ruthenocene loaded aerogel | $162 \pm 2$ | $0.23 \pm 0.10$ |
| blank aerogel | $505 \pm 279$ | $17 \pm 4$ |

[a] long $T_1$ component
[b] short $T_1$ component
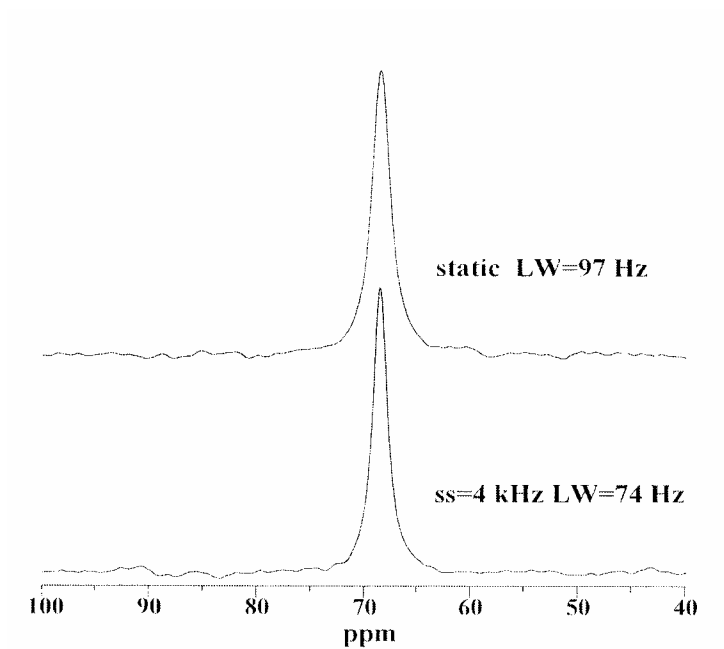
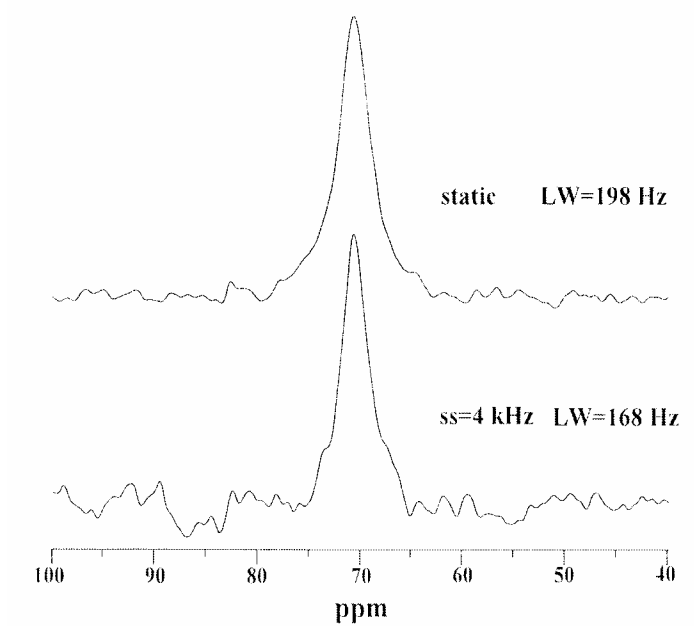Figure 1.   $^{13}$C NMR spectra of ferrocene loaded silica aerogel under static and 4 kHz spinning rate.



Figure 2.   $^{13}$C NMR spectra of ruthenocene loaded silica aerogel under static and 4 kHz spinning rate

# Catalyst Characterization and Determination of Active Species by EMR and magnetometry

M. S. Seehra, P. Dutta and A. Manivannan
Physics Department, West Virginia University.

Semiannual Report for the period October 1, 2003 to March 31, 2004

## I. Introduction

Our objectives under this task are to determine the structural/electronic properties of catalysts used in the C1- program and to correlate these properties with the distribution of product in order to determine the active species in the reactions. In this reporting period, we present the results on the $Co/SiO_2$ and $Co/Al_2O_3$ catalysts received from Roberts et al (Auburn), and Co/aerogel samples received from Eyring et al (Utah), in addition to in-house produced samples of doped ferrihydrites and NiO nanoparticles. The applications of these specific systems to C-1 reactions are given by the appropriate CFFS researchers.

## II. Experimental

The analytical techniques employed in these studies are: (i) X-ray diffraction (XRD) for phase identification and crystallite size determination; (ii) Variable temperature EMR (Electron Magnetic Resonance) studies to determine the electronic states; (iii) Variable temperature magnetometry to determine electronic states, magnetic phases and their concentration; (iv) FTIR/Photoacoustic spectroscopy to determine the structural aspects of surface species.

## III Results and Discussion

### a. Characterization of the Auburn Catalysts:

The six $Co/SiO_2$ and $Co/Al_2O_3$ catalysts received from Dr. Roberts are listed in Table I. These include fresh 15% $Co/SiO_2$ catalysts A1 and B1 and their calcined forms A1/C and B1/C. The remaining two catalysts are: calcined 15% $Co/Al_2O_3$ listed as C1, and C1/U which is C1 used for 12 days in a reactor.

The results of our findings from the XRD, magnetic and EMR investigations are summarized in Table I. For the fresh samples A1 and B1, XRD (Fig. 1) gives only a broad signal due to amorphous $SiO_2$ around $2\theta = 24^o$ and no peaks due to crystalline Co(0), CoO or $Co_3O_4$ are observed even though 15 % Co concentration is high enough for detection by XRD. This implies that Co in these samples is in highly dispersed (noncrystalline) form. Temperature variation of the magnetic susceptibility $\chi$ is found to follow the Curie-Weiss law and magnetic field variation of the magnetization at 2 K shows Co to be in the $Co^{2+}$ state with concentration of 3.7 % for A1 and 3.0% for B1 [1]. These concentrations are a factor of about five smaller than the nominal 15% Co concentration. A possible explanation for this discrepancy is the presence of $Co^{3+}$ in the low spin state with zero magnetic moment. In the EMR studies, a resonance line due to

**Table I.**

| Sample | Description | XRD | Magnetic | EMR |
|--------|-------------|-----|----------|-----|
| A1 | 15% Co/SiO$_2$-Fresh | SiO$_2$ | Curie-Weiss Co$^{2+}$ | Co$^{2+}$-broad line g = 4.3 |
| B1 | 15% Co/SiO$_2$-Fresh | SiO$_2$ | Curie-Weiss Co$^{2+}$ | Co$^{2+}$-broad line g = 4.3 |
| A1/C | Calcined A1 | SiO$_2$, Co$_3$O$_4$ | Co$_3$O$_4$ | No line |
| B1/C | Calcined B1 | SiO$_2$, Co$_3$O$_4$ | Co$_3$O$_4$ | Co$^{2+}$-weak line g = 4.3 |
| C1 | 15%Co/Al$_2$O$_3$-calcined | Co$_3$O$_4$, δ-Al$_2$O$_3$ | Co$_3$O$_4$ | Co$^{2+}$-line,g=4.3 with sharp line |
| C1/U | C1 used for 12 days | CoO, Al$_2$O$_3$(α,δ,χ) | CoO, Co(0) | Co$^{2+}$-line. Co(0)-line |

Co$^{2+}$ is observed. For the calcined samples A1/C and B1/C, we clearly see the presence of Co$_3$O$_4$ (Fig 1) which contains Co$^{2+}$ and Co$^{3+}$ configuration. This is also confirmed in the χ vs T studies where a magnetic transition near 40 K due to Co$_3$O$_4$ is clearly observed [2]. The electronic state of Co$_3$O$_4$ can be written as CoO.Co$_2$O$_3$ so that the concentration of Co$^{3+}$ ions with zero magnetic moment is twice of that of Co$^{2+}$, explaining the above concentration discrepancy. Thus we conclude that in the fresh Co/SiO$_2$, Co is present in highly-dispersed non-crystalline form which is a precursor to Co$_3$O$_4$, and transforms to crystalline Co$_3$O$_4$ upon calcinations.

For the Co/Al$_2$O$_3$ based sample C1, the room temperature XRD pattern shows the presence of Co$_3$O$_4$ and Al$_2$O$_3$. When the sample is used in the reactor for 12 days yielding the sample C1/U, Co$_3$O$_4$ is reduced to CoO and Co(0). The magnetic and EMR studies confirm this transformation. The presence of nanocrystalline Co(0) is particularly significant since it may be the active species in the reaction.

The results of the studies are being prepared for publications in collaboration of Professor Roberts.

**b. Characterization of the Utah Catalysts:**

Following up on our earlier studies of the Co/xerogel catalysts synthesized by prof. Eyring's group at Utah, we received three samples of Co/aerogel samples whose analytical characterization was carried out during this period. A summary of our findings on the three samples using XRD, magnetic and EMR studies is given in Table II. In contrast to Co$_3$O$_4$ present in the Auburn samples, the Utah samples contain CoO and Co(0) and in the FT reaction, transformation of CoO to nanoparticles (NP) of Co(0) is

quite evident. The XRD patterns shown in Fig. 2 are indicated of this, the results of which are confirmed by magnetic and EMR data. The observation of EMR line due to $Co^{2+}$ indicates that the transformation $CoO \rightarrow Co(0)$ is not complete since such a line is not expected either from pure CoO or pure Co(0).

The above results on the Co/aerogel samples will be combined with earlier results on Co/xerogel samples into a single publication in collaboration with Professor Eyring.

**Table II.**

| Sample | XRD | Magnetic | EMR |
|---|---|---|---|
| 2% Co/Aerogel - (Fresh) | $SiO_2$, CoO | CoO, Co(0) - NP | $Co^{2+}$,  Co(0) |
| 2% Co/Aerogel (Used) | $SiO_2$, Co(0) | CoO, Co(0) - NP | Co(0),  $Co^{2+}$, |
| 10% Co/Aerogel (Fresh) | $SiO_2$, CoO, Co(0) | Co(0) - NP | Co(0), $Co^{2+}$, |

### c. Completed Projects:

During this reporting period, a number of projects were brought to completion and the results appeared as published papers. For sake of brevity, we omit details of the results from these papers since they are now available in published form (see section V). These are: (i) Determination of the electronic states and concentration of Ni in Ni-SAPO catalysts in collaboration with Prof. Guin (Auburn) [1]; (ii)Magnetic properties of ferrihydrite nanoparticles doped with Ni, Mo and Ir in collaboration with Prof. Huffman (Kentucky) [2]; (iii) Structural aspects of ferrihydrite nanoparticles doped with Si [3]; Size dependence of electronic and magnetic properties of CuO nanoparticles [4]; (v) Magnetization and EMR investigations of NiO nanoparticles [5]. As discussed in the previous reports, doping of ferrihydrites provides thermal stability to those catalysts in catalytic reactions. The above studies have shown that doping with Mo, Ir amd Si occurs primarily at the surface of the nanoparticles where as Ni substitutes for Fe throughout the nanoparticles. Our studies in NiO and CuO nanaparticles have shown uncompensated surface spins of $Ni^{2+}$ and $Cu^{2+}$ respectively which may play important role in catalytic processes.

### IV. Conclusions

Investigations of Co-based catalysts have clearly shown the need for multitechnique characterization of the catalysts. Since metallic Co(0) is the active catalysts in the FT synthesis, its detection by techniques such as XRD is often difficult if the concentration is less than 1%. However, by magnetic measurements, Co(0) as well as CoO and $Co_3O_4$ are easily detected by their characteristic signatures. Also our studies have shown that reduction follows the sequence $Co_3O_4 \rightarrow CoO \rightarrow Co(0)$ and that the reduction to Co(0) is often not complete. This is clearly important for FT synthesis. For the Ni-SAPO, the electronic state of Ni was found to be Ni(I) for the lightly doped

samples, whereas for higher dopings, both Ni(I) and Ni(0) states were indicated from magnetic measurements. The concentration of Ni determined from these studies varied from 0.2 wt% to 1.75 % for different Ni-SAPO catalysts (for details, see publication 1)

## V. Papers Published

1. Determination of the electronic state and concentration of nickel in Ni-SAPO catalysts by magnetic measurements: P. Dutta, A. Manivannan, M. S. Seehra, P. M. Adekkanattu, and J. A. Guin, Catalysis Letters, Vol. 94 (2004) pp 181-185.

2. Magnetic properties of ferrihydrite nanoparticles doped with Ni, Mo and Ir: A. Punnoose, T. Phanthavady, M. S. Seehra, N. Shah and G. P. Huffman, Physical Review B. Vol 69, (2004) pp 054425-1 to 054425-9.

3. Structural investigations of synthetic ferrihydrite nanoparticles doped with Si: M. S. Seehra, P. Roy, A. Raman and A. Manivannan, Solid State Communications, Vol. 130, (2004) pp. 597-601.

4. Particle size dependence of exchange-bias and coercivity in CuO nanoparticles: M. S. Seehra and A. Punnoose, Solid State Communications, Vol. 128, (2003) pp. 299-302.

5. Temperature dependence of electron magnetic resonance and magnetization in NiO nanorods: M. S. Seehra, P. Dutta, H. Shim and A. Manivannan, Solid State Communications, Vol. 129 (2004) pp. 721-725.

## VI. Future Work

During the next six months, we plan to achieve the following goals: (i) Bring to conclusion the studies of iron-oxide nanoparticle catalyst received from Prof. Huffman; (ii) Complete manuscripts on the analytical characterization of Co/xerogel and Co/aerogel catalysts supplied by Prof. Eyring (Utah); (iii) Complete manuscript on the analytical characterization $Co/SiO_2$ and $Co/Al_2O_3$ catalysts supplied by Prof. Roberts (Auburn); (iv) Continue investigations on the Co catalysts supplied bt Prof. Ernst (Utah); (v) Complete investigation and manuscript on the size dependence of electronic and magnetic properties of NiO nanoparticles prepared in our laboratory; (vi) Initiate new experiments on the synthesis and hydrogen storage capacity of hydrides. Progress on these projects will be reported in future reports.

## VII. References

[1]. See e.g. Introduction to Solid State Physics by C. Kittel (Wiley 1996).

[2]. W. L. Roth, J. Phys. Chem. Solids, 25, 1 (1964).
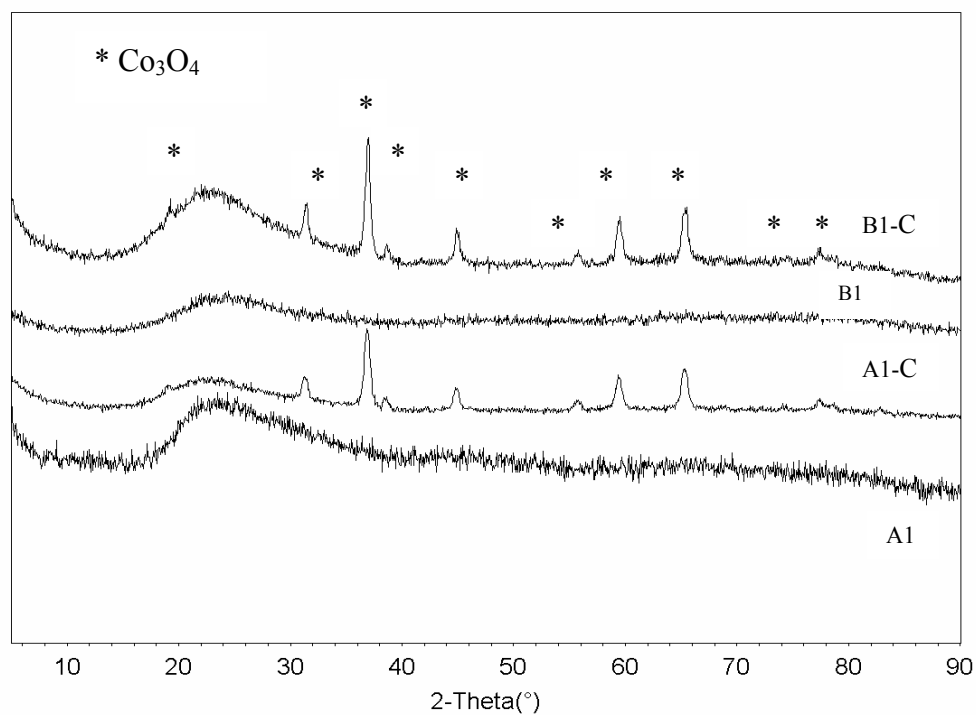
Fig. 1. Room temperature X-ray diffraction patterns of Co/SiO$_2$ samples of Table 1.
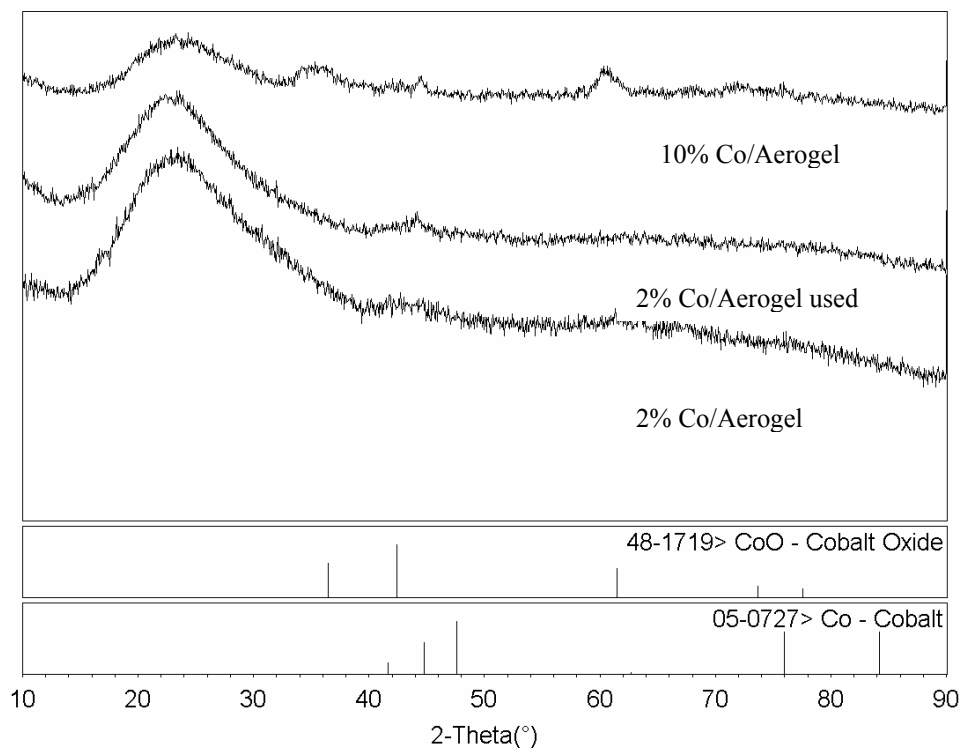


Fig. 2. Room temperature X-ray diffraction patterns of Co/aerogel samples of Table II.

# Mössbauer and XAFS Spectroscopic Characterization of C1 and H₂ Chemistry Catalysts

Frank E. Huggins, Yuguo Wang, Naresh Shah, and Gerald P. Huffman, Consortium for Fossil Fuel Science and Department of Chemical & Materials Engineering, University of Kentucky

## I. Introduction

In this report, we describe results from [57]Fe Mössbauer and X-ray absorption fine-structure (XAFS) investigation of key metal species involved in three different investigations.

   a. Catalytic dehydrogenation of light alkanes (Shah et al., U. KY; references 1 and 2).

   b. Catalytic dehydrogenation of cyclohexane (Wang et al., U. KY; references 3 and 4 and this report).

   c. Investigation of metallocenes and metallocene-doped aerogels for use in FT synthesis (Ernst, Eyring, et al., U. Utah, this report).

More information on these investigations is available elsewhere in this report.

## II. Experimental

[57]Fe Mössbauer spectroscopy is performed at the University of Kentucky using a Halder, GmbH, Mössbauer driving unit and control unit interfaced to a personal computer by means of two Canberra Nuclear MCS/PHA ACCUSPEC data acquisition cards.  One radioactive [57]Co source in a rhodium matrix is used as the source of the 14.4 keV gamma rays used in the Mössbauer experiment, while a second weaker [57]Co source in a palladium matrix is used to collect the calibration spectrum at the opposite end of the driving unit.  The Mössbauer spectra are collected on the ACCUSPEC data cards and then transferred to the hard-drive memory in the PC at the end of the data acquisition.  The spectra are then analyzed using a least-squares minimization FORTRAN fitting program that fits the Mössbauer absorption spectrum as combinations of single peaks, quadrupole doublets, and magnetic hyperfine sextets.  These three situations cover the entire range of different types of Mössbauer absorptions from iron in solids.  A Lorentzian peak-shape is assumed in the least-squares fitting and chi-square is used as the significant statistical parameter in determining the goodness of fit.

XAFS spectroscopy is used to investigate other elements in the catalyst formulations.  The current XAFS measurements were performed at beam-line X-18B at the National Synchrotron Light Source (NSLS), Brookhaven National Laboratory.   The X-ray absorption spectra are collected over an energy range that includes one of the characteristic absorption edges of the element of interest.  The spectrum is collected as a function of energy by means of the rotation of a Si(111) channel-cut crystal from typically about 100 eV below the absorption edge to as much as 1000 eV above the

absorption edge. Spectra are recorded in either absorption or fluorescence geometry, depending on the concentration of the element in the catalyst, using gaseous ionization detectors or solid state detectors such as a PIPS detector or a multi-element germanium detector. The spectral data acquired at NSLS are transferred to the University of Kentucky for detailed analysis. Such procedures are well-described in the literature [5]. Basically, the XAFS spectrum is divided into separate X-ray absorption near-edge structure (XANES) and extended X-ray absorption fine structure (EXAFS) regions, each of which provides complementary information.

### III. Results and Discussion

(a) Characterization of alkane hydrocarbon reforming catalysts

The basic reaction can be represented by:

$$C_nH_{2n+2} \rightarrow nC + (n+1)H_2$$

However, as described elsewhere [1-4], the reaction is not so simple for hydrocarbons other than methane because the reactions appear to be sequential involving hydrocarbon chain breakage and the formation of methane and other intermediary hydrocarbons (both alkane and alkene), prior to ultimately forming hydrogen and carbonaceous products.

In our previous work [1-4], binary Fe-M catalysts supported on alumina (0.5 wt.%M-4.5wt.%Fe/Al$_2$O$_3$, M = Mo, Ni, or Pd) were pre-reduced at 700 ºC in hydrogen prior to reaction with methane, ethane, or propane. The structures of the catalysts in their as-reduced states and after reaction with methane to produce hydrogen and carbon nanotubes for times on stream (TOS) of approximately 6-7 hours were investigated by Mössbauer and XAFS spectroscopy [6]. The resulting metal phases after reduction consisted of a dominant ferrous phase resulting from reaction with the alumina support that appeared to be predominantly hercynite (FeAl$_2$O$_4$). Hercynite contained 60-70% of the iron, a fcc Fe-M alloy contained ~20 % of the iron, and about 10% of the iron was Fe metal. The secondary metal showed variable behavior, with most of the Pd being incorporated into the fcc Fe-Pd alloy, and about half of the Ni and somewhat less of the Mo entering the fcc alloy phase. After 6-7 hours TOS, most of the Fe metal had converted to carbide (Fe$_3$C) and the amount of the austenic Fe-M-C alloy phase had increased, containing about 25-30 % of the total Fe. On the basis of XAFS spectroscopy at the Mo, Ni, and Pd K-edges, it was concluded that most of the Ni and Pd were incorporated into the austenitic alloy phase; however, a substantial fraction of the Mo (~half) formed a Mo carbide phase (Mo$_2$C). The hercynite phase was very stable for the Fe-Ni catalyst, decreased somewhat (25%) for the Fe-Pd catalyst, but decreased markedly (50%) for the Fe-Mo catalyst.

In work completed more recently, in order to simplify the process, the Fe-Mo catalyst was simply heated to 700 ºC in methane with no pre-reduction treatment and run at that temperature for 16 hours TOS. The resulting hydrogen production is shown as a function of TOS in Figure 1; the remainder of the exit gas stream was unconverted methane. It is seen that the hydrogen production rises rapidly to about 68% as the catalyst is reduced, falls to about 60 % in 3 hours, then falls more rapidly to approximately 20% in the next five hours. In a second series of experiments using the

Fe-Mo catalyst under identical conditions, the runs were stopped periodically to obtain catalyst samples for Mössbauer spectroscopy. The resulting Fe phase percentages are shown in Figure 2 and summarized in Table 1 as a function of TOS.

Comparison of the current results to those obtained previously [1, 6] show reasonably good agreement. After two hours TOS in methane, hydrogen production is somewhat above 60% and the Fe phase distribution shows 65% $Fe^{+2}$, 16% Fe-Mo-C, and 19% $Fe_3C$. After 2 hours reduction in hydrogen, the Fe phase distribution was 70% $Fe^{+2}$, 19% Fe-Mo fcc alloy, and 11% Fe metal, and the hydrogen conversion was approximately 60% for the same amount (1g) of catalyst loaded in the reactor. After 6½ hours, hydrogen production had dropped to approximately 25% and the Fe phase distribution was very close to the results shown in Table 1 for 6 hr and 8 hr.

Comparison of Figures 1 and 2 shows that the curve that represents the amount of iron as $Fe^{2+}$/oxide (hercynite) in Figure 2 comes closest to duplicating the hydrogen production curve over time, shown in Figure 1. As the percentage of iron in hercynite and the hydrogen production decrease, it is also seen that the percentage of iron in cementite ($Fe_3C$) increases proportionately. These observations suggest that the decrease in hercynite content and concomitant increase in cementite content may be closely related to the decreasing catalytic production of hydrogen. Possible reaction mechanisms are:

$$FeAl_2O_4 + CH_4 \rightarrow Fe + CO + 2H_2$$

$$3Fe + CH_4 \rightarrow Fe_3C$$
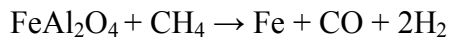
The latter reaction would occur rapidly in a $CH_4 - H_2$ gas mixture at 700 ºC.

Previously, we suggested that the role of hercynite was to keep the metallic austenite (Fe-M-C) catalyst particles bound to the alumina support, permitting carbon to be carried away from the alloy particle surfaces in the form of growing carbon nanotubes. The formation of cementite disrupts the hercynite bonds with the alumina support, permitting the catalyst particles to become detached from the support. Assuming that such detached catalyst particles rapidly become encased in capped multiwalled nanotubes and are therefore inaccessible to the methane, this model could account for the decrease in hydrogen production activity.
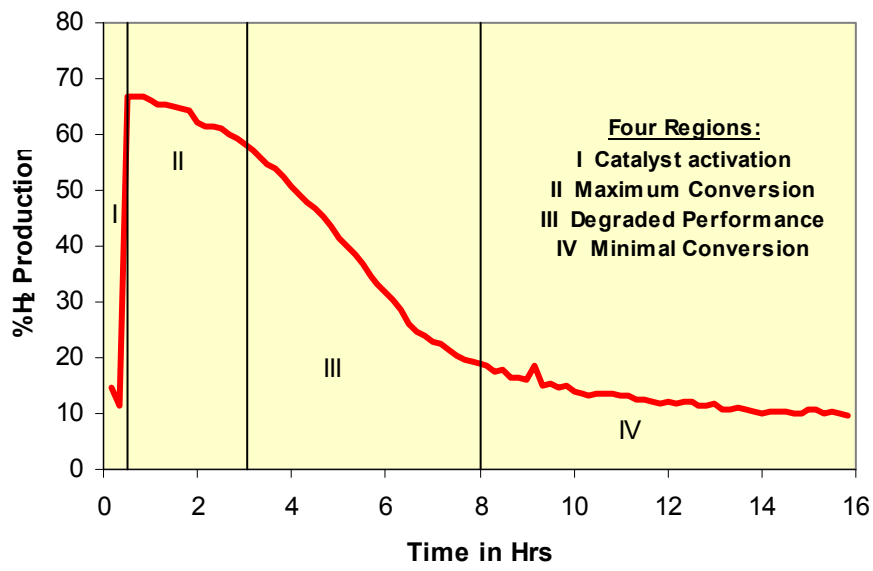
**Figure 1: Typical activity curve for hydrogen production in methane decomposition catalyzed by Fe-Mo binary catalyst on alumina. Temperature = 700°C.**
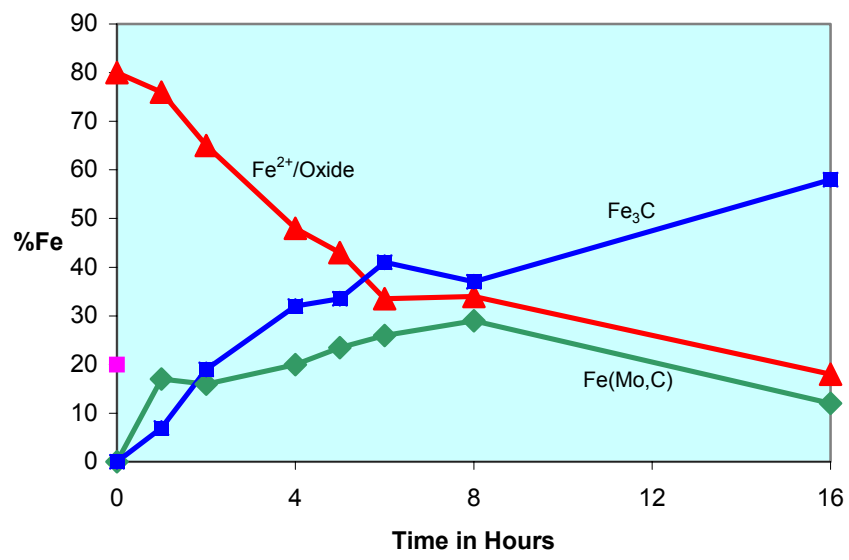


**Figure 2: Variation of concentration of major Fe-bearing catalyst phases with length of time under methane at 700°C**

**Table 1: Data on distribution of iron among different phases derived from analysis of Mössbauer spectra of Mo-Fe-Al$_2$O$_3$ catalysts heated for different times under methane**

| | Time (hrs) | Iron Distribution among Phases, %Fe | | | | | |
|---|---|---|---|---|---|---|---|
| | | Fe$^{3+}$ | Fe$_2$Mo | Fe$^{2+}$ | Fe(Mo,C) | Mo-Fe-C | Fe$_3$C |
| As Prep. | 0 | 100 | | | | | |
| CH$_4$/N$_2$ | 0 | 72 | | 28 | | | |
| CH$_4$/CH$_4$ | 0 | | 20 | 80 | 0 | | 0 |
| 1 hr CH$_4$ | 1 | | | 76 | 17 | | 7 |
| 2 hr CH$_4$ | 2 | | | 65 | 16 | | 19 |
| 4 hr CH$_4$ | 4 | | | 48 | 20 | | 32 |
| 5 hr CH$_4$ | 5 | | | 43 | 23.5 | | 33.5 |
| 6 hr CH$_4$ | 6 | | | 33.5 | 26 | | 41 |
| 8 hr CH$_4$ | 8 | | | 34 | 29 | | 37 |
| 16 hr CH$_4$ | 16 | | | 18 | 12 | 12 | 58 |

(b) Characterization of Pt-based catalysts for dehydrogenation of cyclohexane (in cooperation with Wang and Shah, University of Kentucky)

The partial dehydrogenation of cyclohexane (C$_6$H$_{12}$) to benzene (C$_6$H$_6$) has potential for on-board generation of hydrogen for use in vehicular fuel cells. This reaction can be written as:

$$C_6H_{12} \rightarrow C_6H_6 + 3H_2$$

As described elsewhere in this report and in manuscripts submitted for publication [3, 4], we are exploring the use of Pt and Pd catalysts supported on stacked-cone carbon nanotubes (SC-CNT) for this reaction and for the dehydrogenation of other hydrocarbon liquids. Using a commercial catalyst consisting of 1% Pt supported on alumina, the reaction goes to completion at about 315$^\circ$C.

In this study, we report findings on different formulations of supported Pt catalysts, investigated by means of Pt L$_{III}$-edge XAFS spectroscopy, before and after reaction with cyclohexane. The samples investigated are as follows:

1.  1% Pt/4% Fe/Al$_2$O$_3$ reduced in H$_2$

2.  the same, after reaction for 5 hours

3.  Pt catalyst #1 1.0% Pt/SC-CNT

4.  Pt catalyst #2 0.25% Pt/SC-CNT

5.                Pt catalyst #3 0.1% Pt/SC-CNT

6.                Pt catalyst #5 1.0 wt% Pt/SC-CNT after reaction

7.                Pt catalyst #6 0.25 wt% Pt/SC-CNT after reaction

8.                Pt catalyst #7 0.1 wt% Pt/SC-CNT after reaction

Figure 3 shows the XAFS results for the alumina-supported Pt-Fe catalyst. The top spectrum was obtained from Pt foil, the middle spectrum from the Pt-Fe/$Al_2O_3$ sample after reduction in $H_2$ for two hours at 700 ºC, and the bottom spectrum after a five hour dehydrogenation run in cyclohexane. The results clearly show that the Pt is in a metallic state in all of these samples. There may be some degradation of the metallic particles as the long-range structure for the Pt after reaction does not seem to be as well defined as it was before reaction. This can be seen from the poorer definition of minor Pt-Pt peaks in the range 3.5 – 5.5 A in the EXAFS/RSF plot for the after reaction sample.
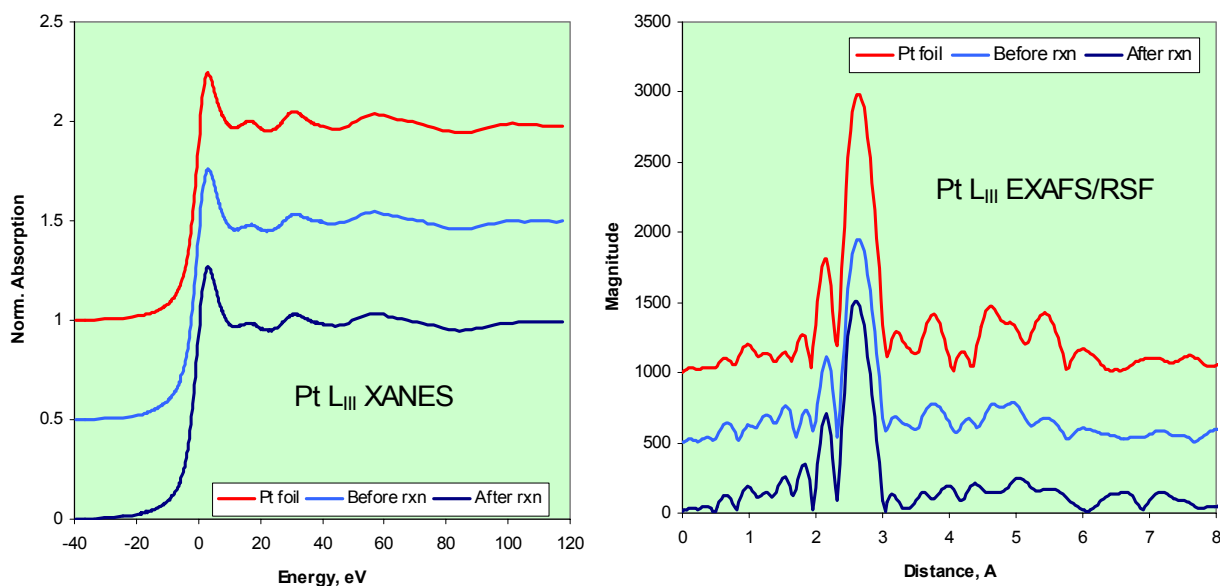


**Figure 3: $L_{III}$-edge XANES (left) and EXAFS/RSF (right) spectra for 1 wt% Pt-4 wt.% Fe supported on alumina catalyst and for Pt foil. Zero-point of energy for the XANES plot occurs at 11,564 eV.**

Similar data collected for the SC-CNT supported Pt catalysts (Figures 4 and 5) show a quite different story. In this case, only a small amount of the Pt is present as metal. This is best seen from the radial structure functions (RSF) in Figure 5. The most prominent peaks occur at approximately 1.6 and 2.2 Å, while a weaker peak occurs at the distance (~2.6 Å) corresponding to the Pt-Pt peak in the RSF for Pt metal. One possibility is that the peak at 1.6 Å corresponds to Pt(IV)-O and that at 2.2 Å to Pt(II)-O. However, high resolution TEM shows the Pt nanoparticles on the SC-CNT support to be very small, ~1-2 nm. Consequently, most of the Pt atoms in the nanoparticles are surface particles and even if the particles are metallic, only a small percentage of the atoms will

have a full complement of Pt nearest neighbors.  It seems quite possible that a significant percentage of the Pt atoms may be interacting with C atoms in the SC-CNT support, in which case the peaks at 1.6 Å and 2.2 A may be related to Pt-C configurations.

In any case, the results are quite interesting and need to be resolved.  We hope to improve our interpretation of these data in upcoming XAFS experiments this summer by examining additional Pt catalysts and Pt standard compounds.
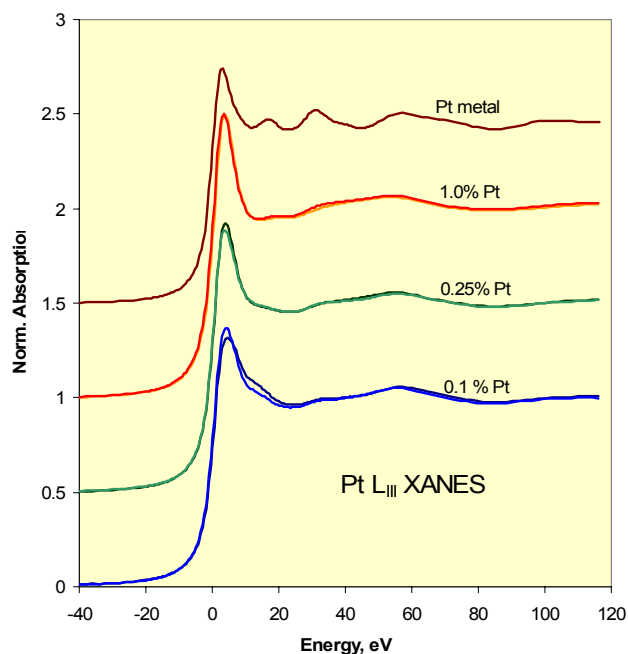


**Figure 4:  Pt L$_{III}$ XANES spectra of Pt impregnated carbon nanotubes.  For the three catalysts, the XANES spectra for the catalyst both before (lighter colors) and after (darker colors) reaction are shown.  However, the two curves overlap significantly for both the 1.0% and 0.25% Pt catalysts.  Zero point of energy corresponds to 11,564 eV.**
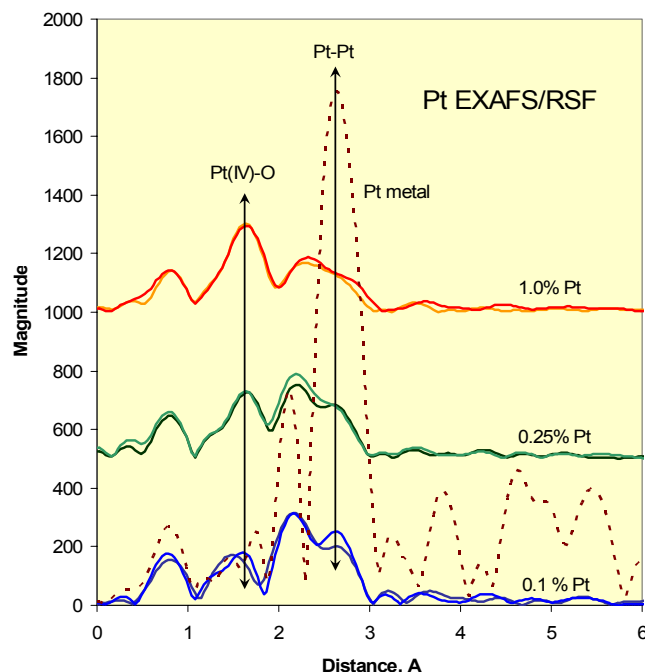
**Figure 5: EXAFS/RSFs for Pt in Pt metal foil and in three CNT-supported catalysts before (light colors) and after (dark colors) reaction**

(c) Investigation of metallocenes and metallocene-doped aerogels (in cooperation with Ernst and Eyring, University of Utah).

At the University of Utah, significant effort is being expended in developing new catalysts for Fischer-Tropsch (FT) synthesis based on silica aerogels doped with metallocene compounds. Typical metallocene or "sandwich" compounds that are proposed for such catalysts include not only ferrocene [bis(eta-5-cyclopentadienyl)iron] and cobaltocene, but also closely related analogues in which one or both of the cyclopentadienyl ligands is/are replaced by the more reactive pentadienyl ligand, which thereby lead to facile attachment to the silica via protonation by surface hydroxyl group. The University of Kentucky is providing XAFS and Mössbauer spectroscopic support for the characterization of these compounds and for the proposed aerogel catalysts prepared from them. Here, we will describe some initial measurements made by XAFS spectroscopy to characterize ferrocene, cobaltocene, and oxidized versions of these compounds.

XAFS spectra of the two metallocenes and their oxidized products were obtained at beam-line X-18B at NSLS. The spectra were collected in absorption geometry at room temperature. The comparison of the XAFS spectral data for ferrocene and the oxidized material is shown in Figure 6. It is clear that the iron XANES spectra of the two materials are very different.
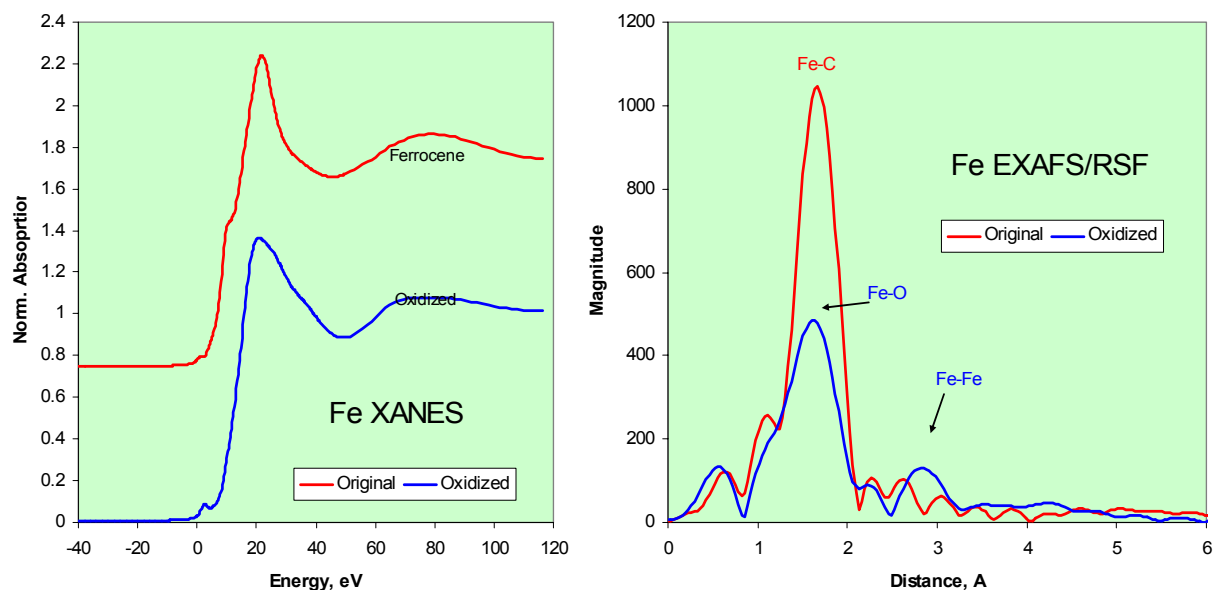
**Figure 6:  Iron XANES and EXAFS/RSF spectra for ferrocene and an oxidized product derived from ferrocene.**

The spectra for the oxidized material are similar to those from ferric iron in various oxides.  However, the small development of the Fe-Fe peak in the EXAFS/RSF spectrum implies that either the particle size is exceedingly fine or it is an amorphous precipitate of an iron oxide.  The Fe XANES spectrum of ferrocene is unlike any other we have seen before because of the combination of the relatively sharp white line and also the prominent inflection point on the edge.  Neither of these features is typically observed in typical ferrous and ferric compounds.  Further, the one main peak in the EXAFS/RSF spectrum is intense and quite narrow; it is clearly consistent with a high symmetry coordination site for the iron, in which all bond-lengths are identical.  Such a site for iron is of course present in ferrocene, in which the Fe is "sandwiched" between upper and lower parallel cyclopentadienyl (cp) rings by pi-bonds that give rise to a 10-fold coordination of the Fe by the carbons of the cp rings, with all ten Fe-C distances the same at ~2.04 A.  Similar EXAFS/RSF data have been reported for ferrocene and derivative compounds [7].

The corresponding Co XAFS spectra for cobaltocene and oxidized cobaltocene are shown in Figure 7.  The Co XANES spectrum of cobaltocene is very similar to the Fe XANES spectrum of ferrocene and indicates that the molecular geometry and electronic structure of the two metallocenes are very similar.
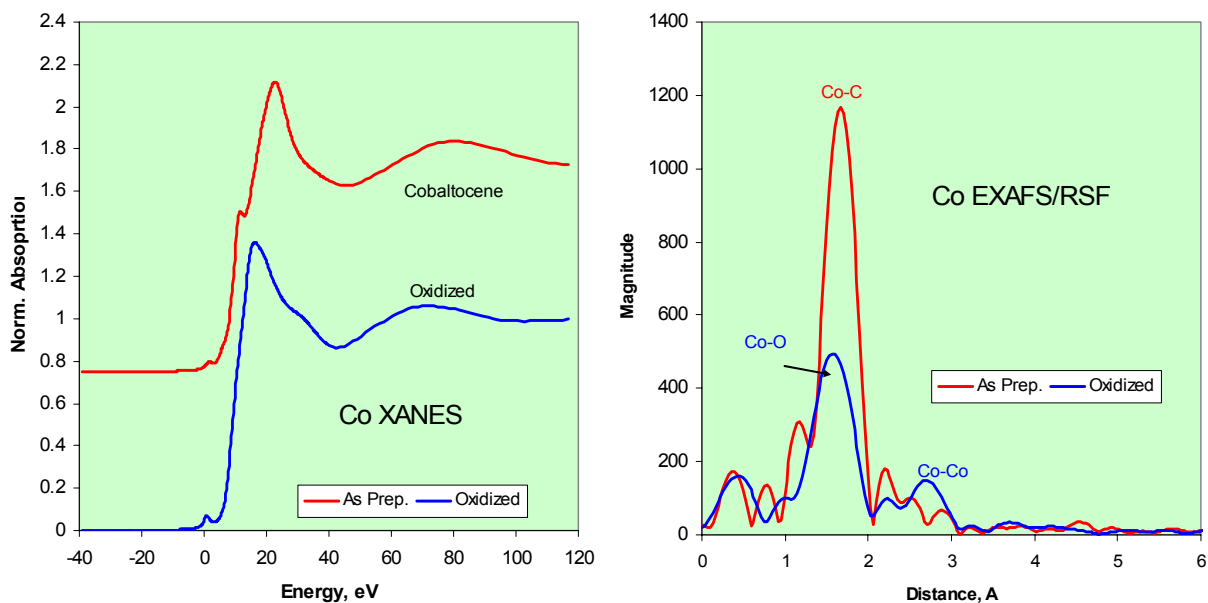
**Figure 7:  Cobalt XANES and EXAFS/RSF spectra for cobaltocene and an oxidized product derived from cobaltocene.  Zero point of energy corresponds to 7,709 eV.**
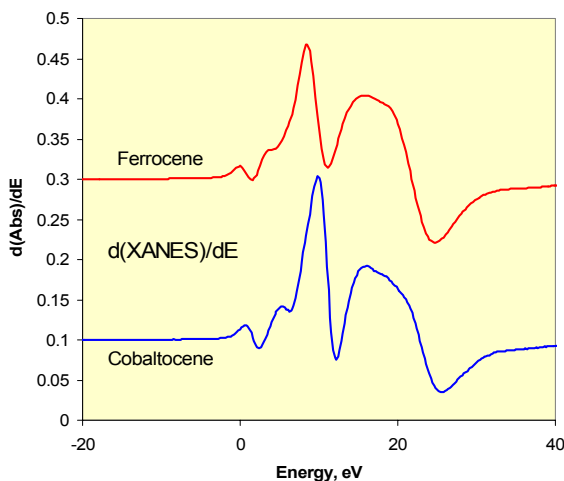


**Figure 8:  Comparison of derivative XANES spectra for ferrocene and cobaltocene.**

This similarity is brought out by comparing the first derivative of the two XANES spectra.  As can be seen from Figure 8, the two derivative spectra are virtually identical. In addition, the EXAFS/RSF spectrum for cobaltocene consists of one sharp, intense peak as was observed for ferrocene.  Analysis of the Co-C bond distance from the EXAFS/RSF spectrum, using the Fe-C bond in ferrocene as the phase-shift standard for

the Co-C phase shift, yielded a bond distance of 2.03 A for the Co-C bond distance. This is significantly shorter than the 2.10 A distance that has been reported for the bond distance in cobaltocene and it is possible that the Co XAFS spectra arise from the cobalt cyclopentadienyl ion, $Co(cp)_2^+$, which is isoelectronic with ferrocene, $Fe(cp)_2$, rather than from $Co(cp)_2$, which has one more electron.

The oxidized cobaltocene formulation shows a typical Co oxide type spectrum. Again, as was observed for iron, the weak development of the Co-Co peak in the EXAFS/RSF spectrum implies that the cobalt oxide is either exceedingly fine or amorphous.


## IV. Conclusions


Mössbauer and XAFS spectroscopic methods have been used successfully to characterize key elements present in various catalyst formulations under development by Consortium researchers for use in C1 or hydrogen-related reactions. Mössbauer investigation of a binary $Fe-Mo/Al_2O_3$ alloy catalyst used in the dehydrogenation of methane emphasizes the importance of the hercynite phase ($FeAl_2O_4$) in determining catalyst activity. With increasing time on stream at 700 ºC, the percentage of iron in hercynite and the hydrogen production decrease, while the percentage of iron in cementite ($Fe_3C$) increases proportionately. This suggests that the reduction of hercynite and the associated formation of cementite are responsible for detachment of the catalyst particles from the alumina support.

Pt XAFS spectroscopy shows that the Pt speciation is quite different in $Pt-Fe/Al_2O_3$ catalysts than in catalysts prepared with Pt supported on stacked-cone carbon nanotubes (SC-CNT), despite the observation that both types of catalyst are very effective in converting cyclohexane to benzene and hydrogen. In the former case, the Pt is entirely metallic, whereas in the latter case the XAFS results indicate that only a fairly small percentage of the Pt atoms in the Pt nanoparticles on the SC-CNT are clearly metallic. Secondary components, which could be due to either Pt-O or Pt-C interactions, dominate the Pt/SC-CNT spectra.

We anticipate also, based on preliminary measurements reported here, that both Mössbauer and XAFS spectroscopies will be useful for understanding the formation of novel catalysts that involve the placement of iron and other metal pentadienyl or cyclopentadienyl compounds inside silica aerogels.


## V. Papers presented or published (include submitted and in-press papers)


Much of the work reported in this project will be incorporated in papers that describe the reactivity and preparation of the catalysts. Two recent publications are listed below:

[a]   N. Shah, S. Pattanaik, F. E. Huggins, D. Panjala, G. P. Huffman, *XAFS and Mössbauer spectroscopy characterization of supported binary catalysts for nonoxidative dehydrogenation of methane*.  Fuel Process. Technol. **83**, 163-173, (2003).


[b]A. Braun, J. Ilavsky, P.E. Jemian, B. Dunn, E.M. Eyring, F.E. Huggins, G.P. Huffman, *Ultra-small angle X-ray scattering of cobalt-doped silica aerogels*. Submitted to J. Appl. Cryst. (2004)**.**


## VI.  Future Work


Similar studies will continue.  To complement the above investigation of binary ferrihydrite catalysts for alkane dehydrogenation with time-on-stream, a suite of catalysts has been prepared at various temperatures between 525 and 700$^{o}$C after a constant time of 10 hours on stream.  These catalysts are currently in the process of being examined by Mössbauer spectroscopy.  Other noble metal catalysts, e.g. Pd, will be investigated for their behavior in alkane dehydrogenation.  Both XAFS and Mössbauer spectroscopy will continue to be used for characterization of the novel metallocene/aerogel catalysts under development at the University of Utah.


## VII. References

1.  N. Shah, D. Panjala, G.P. Huffman, *Hydrogen production by catalytic decomposition of methane.*  Energy & Fuels, **15**, 1528-1534, (2001).

2.  N. Shah, Y. Wang, D. Panjala, G.P. Huffman, *Production of hydrogen and carbon nanostructures by non-oxidative catalytic dehydrogenation of ethane and propane.* Energy & Fuels, **18**, in press, (2004).

3.  Y. Wang, N. Shah, G.P. Huffman, *Pure hydrogen production by partial dehydrogenation of cyclohexane and methylcyclohexane over nanotube supported Pt and Pd catalysts.*  Energy & Fuels, (2004) in press.

4.  Y. Wang, N. Shah, G.P. Huffman, *Hydrogen production by decomposition of propane and cyclohexane over alumina supported binary catalysts.* Submitted to Catalysis Today, (2004).

5.  D.C. Koningsberger, R. Prins, (eds.), X-ray Absorption.  Principles, Applications, Techniques of EXAFS, SEXAFS, and XANES, J. Wiley & Sons, New York, 1988.

6.  N. Shah, S. Pattanaik, FE. Huggins, D. Panjala, G.P. Huffman, *XAFS and Mössbauer spectroscopy characterization of supported binary catalysts for nonoxidative dehydrogenation of methane*.  Fuel Process. Technol. **83**, 163-173, (2003).

7.  V.A. Chernov, S.G. Nikitenko, A.M. Danilenko, *EXAFS study of ferrocene intercalated in fluorographite*.  Nucl. Instrum. Method. A **359**, 248-249, (1995).